EVALUATION OF THE PHOTONIC CONVERSION FINDER FOR THE BaBar EXPERIMENT

By

Zerah Lurie

B. Sc. McGill University, 1999

A THESIS SUBMITTED IN PARTIAL FULFILLMENT OF

THE REQUIREMENTS FOR THE DEGREE OF

MASTER OF SCIENCE

in

THE FACULTY OF GRADUATE STUDIES

DEPARTMENT OF PHYSICS AND ASTRONOMY

We accept this thesis as conforming

to the required standard

. . . .

. . . .

THE UNIVERSITY OF BRITISH COLUMBIA

February 2002

Department of Physics and Astronomy
The University of British Columbia
6224 Agricultural Road
Vancouver, B.C., Canada
V6T 1Z1

Date:

Abstract

A study of the leptonic backgrounds due to unidentified converted photon daughter tracks in semi-leptonic B decays has been conducted. The main tool in identifying converted photons at the BaBar experiment is a Photonic Conversion Finder (PCF) that has only been previously tested on Monte Carlo simulated data. The PCF is tested on a BaBar data sample containing Radiative Bhabha events. It was found that the PCF is able to properly identify two oppositely charged tracks as originating from a Photonic Conversion with a 70-80% isotropic efficiency above a converted photon energy of 0.5 GeV. This efficiency is slightly lower for converted photon energies below 0.5 GeV. The 70-80% efficiency plateau indicates that the PCF has an internal efficiency limit. The overall results of a comprehensive study on the lepton energy spectrum from tracks that were unidentified as originating from converted photons found that for every 2 tracks properly identified as originating from a Photonic Conversion, 2.4 tracks went unidentified. This result is due to both a low energy reconstruction inefficiency of the BaBar detector acting on highly asymmetric Photonic Conversions and to the internal efficiency limit of the PCF. In future studies at the BaBar experiment, users will be able to obtain the energy spectrum of leptons unidentified as originating from converted photons in their analysis by taking the energy spectrum of identified converted photons obtained in this thesis and scaling it to match their energy spectrum of identified converted photons.

Table of Contents

List of Tables

List of Figures

Acknowledgments

I would like to thank my supervisor, Janis McKenna, for all her help, guidance, and especially patience. Thanks to Tom Mattison for answering all my pressing questions and always offering advice. Thanks to Chris Hearty for help with the infinite wonder that is the BaBar computing system and on topics in general. A hearty thank you to Doug Thiessen for helping me with all my problems with coding, since, after all, I had many. A loving thanks to Angie O'Neill for being the most beautiful proofreader I will ever have and putting up with all the long nights where I paid more attention to this thesis than to her. A well written thanks to Katharine Patterson for letting me know what was wrong with my writing and thankfully telling me how to make it gooder. Thanks to mommy and daddy and especially little Joey too. And one last thanks to little Alexander Mattison for sitting through many a long-winded discussion about this thesis...and for making sure it tasted good.

Chapter 1

Introduction

A curious thing happens while I am touching the keyboard to write this thesis: my fingers and the keyboard do not annihilate each other. The same thing is happening while you read this thesis: you and the thesis are not annihilating each other. Why not? Because you, the thesis, the keyboard and I are all made of matter! At first, this statement sounds like a ridiculous thing to consider, but if you think about the ramifications of a universe full of matter you are led into the amazing world of CP violation.

In many Big Bang theories, equal parts of matter and antimatter were present when the universe was created. Suggesting the universe was created otherwise requires unscientific arguments in which the universe is constructed by design. However, since you, the thesis, my keyboard, and I do not annihilate each other it seems that we are all made of only matter. Can we then assume that the universe is primarily composed of matter?

There can be two possible explanations for our current lack of antimatter:

1. The antimatter is gone.

2. The antimatter is somewhere else.

While difficult to imagine, the segregation of matter and antimatter is possible and would also be observable. By itself, antimatter is not directly observable since it has all the same observable characteristics as matter (energy spectra, mass, quantum numbers, etc...). However, since the universe is constantly interacting with itself, matter and antimatter will annihilate wherever they meet. This annihilation is characterized by an intense emission of gamma rays. Although several phenomena are in consideration, no such gamma ray sources have yet been observed.

Other possible evidence of antimatter existence would be from cosmic rays: high-energy particles with extra terrestrial origins that are constantly bombarding the earth. While the majority of cosmic rays originate within our own galaxy, the fact that cosmic rays are predominantly composed of matter suggests that the Milky Way, as well as our local group of galaxies, is also primarily composed of matter. Either the antimatter created in the Big Bang is in some distant corner of the universe or it is all gone.

In order for all the antimatter to be gone, current theory suggests that a phenomenon know as CP violation must be present. CP violation involves a breaking of symmetries within the reactions governing both matter and antimatter. This breaking of symmetries leads to a favouring of matter over antimatter and, when combined with several other phenomena, would account for the current lack of antimatter in our universe. Previous to the BaBar and Belle experiments, only a small amount of CP violation has been observed in the neutral Kaon system; however, this CP violation is not enough to account for the present matter/antimatter asymmetry of our universe. The BaBar and Belle experiments have now measured CP violation in the neutral B system as well [1] [2].

Several of the CP violation measurements at the BaBar experiment involve using B semi-leptonic decays ($B^0 \to \ell^+ \nu X$), a decay in which a B meson decays into a final state that contains a lepton. Within B semi-leptonic events, it is important to measure the decay spectrum of the primary lepton originating from the B meson properly. Unfortunately, there are several background processes that can also produce leptons in B semi-leptonic events and mask the primary lepton's signal. One such process is a Photonic Conversion, where a photon converts into an electron/positron pair.

To detect and remove any converted photons from B semi-leptonic events at the BaBar experiment, a Photonic Conversion Finder(PCF) is used. The PCF attempts to detect and remove converted photons by examining the daughter electron/positron pair. The PCF has only been previously tested on Monte Carlo simulated data.

I will perform a comprehensive analysis of the PCF using real BaBar experimental data. This analysis will involve measuring the direct efficiency of the PCF as well as performing a comprehensive study on the backgrounds that are produced by Photonic Conversion daughter tracks which remain unidentified. The spectrum of unidentified tracks will be correlated to the spectrum of identified tracks to allow future semi-leptonic analyses to determine lepton contamination due to unidentified converted photon daughter tracks simply by using the number of properly identified converted photon found within the study.

Chapter 2 will explain and explore the theoretical framework behind CP violation and will also give a brief introduction on the theory describing CP violation at the BaBar experiment.

Chapter 2

CP Violation

There are, as yet discovered, only four fundamental forces in nature: electromagnetic, strong, weak, and gravitational. Since the coupling of gravity to matter (or antimatter) is many orders of magnitude lower than the coupling of the other three forces, the Standard Model of particle physics only concerns itself with the former three forces. The Standard Model of particle physics is the theoretical model into which all known particle interactions, including the phenomenon of CP violation, are incorporated.

2.1 The Standard Model

Matter (or antimatter for argument's sake) can be differentiated by several of its distinguishing characteristics; for instance, with respect to spin, there are two distinct types of matter: fermions and bosons. Fermions are particles with half integer spins that obey Fermi-Dirac statistics, implying that no two fermion particles may occupy the same quantum state simultaneously. Examples of fermions are fundamental particles such as electrons and quarks. Bosons are particles with integer spins that obey Bose-Einstein statistics, implying that an infinite number of boson particles may occupy the same quantum state simultaneously. Each of the three fundamental forces dealt with in the Standard Model manifests itself through the emission or absorption of a different boson. These bosons, called the gauge bosons, are as yet the only fundamental bosons observed in nature (Table 2.1).

Fermions can be further separated into two distinct groups based on their interactions

	Electromagnetic	Weak	Strong
Force Mediators	γ	W $\pm$, Z^0	gluon (g)

Table 2.1: Fundamental bosons

	First Generation	Second Generation	Third Generation
Quarks	up (u) down (d)	charm (c) strange (s)	top (t) bottom (b)
Leptons (Neutrinos)	electron (e) ν_e	muon (μ) ν_μ	tau (τ) ν_τ

Table 2.2: Fundamental fermions

via the different fundamental forces. Quarks are able to interact via the strong, the weak and the electromagnetic forces. Both electrons and neutrinos, collectively called leptons, are able to interact via the weak force, however, only the electron-type particles (the electron, muon and tau particles) can also interact via the electromagnetic force. Both quarks and leptons exist in three generations, with each successive generation populated by heavier and heavier particles (Table 2.2). This trend may not be true for neutrinos, since even though the SNO experiment has recently shown that they mix, and hence have mass, the individual masses of each neutrino has not yet been determined [3].

It should also be noted that each particle, including all fermions and bosons, has an associated antiparticle (commonly denoted by a bar over the particle symbol). An antiparticle has the same external characteristics as its associated particle, such as mass and spin, however all the internal quantum numbers, such as charge and baryon number, are inverted. This simple definition does not apply to antiparticle conjugates of combinations of particles since the particle combinations are made up of daughter particles while the antiparticle conjugates are made up of daughter antiparticles. Some particles, such as the photon and the Z^0, are even their own antiparticles. Others, such as the electron and b quark, have distinct antiparticles, which in this case are the positron (e^+ or $\overline{e^-}$) and the $\overline{b}$ quark respectively.

Unfortunately I have simplified my previous explanation of the classification of particles with respect to the quarks. The conventional definition of a quark is: The eigenstate (referred to as either mass or flavour eigenstates) that undergoes a strong reaction. The flavour eigenstate is not the same as the eigenstate that undergoes a weak reaction. Instead, the weak eigenstate is a linear combination of all similar quarks across the three generations, i.e., the u,c,t or the d,s,b quarks. The Cabibbo-Kobayashi-Maskawa matrix (CKM) characterizes this “rotation” of eigenstate bases. The CKM matrix is a 3 by 3 unitary matrix ($U^\dagger U = 1$) that describes the mixing of mass or flavour eigenstates into weak eigenstates, as shown below [4]:

$$\begin{pmatrix} d' \\ s' \\ b' \end{pmatrix} = \begin{pmatrix} V_{ud} & V_{us} & V_{ub} \\ V_{cd} & V_{cs} & V_{cb} \\ V_{td} & V_{ts} & V_{tb} \end{pmatrix} \begin{pmatrix} d \\ s \\ b \end{pmatrix} \tag{2.1}$$

where d, s, b are the flavour eigenstates, and d', s', b' are the weak eigenstates.

The u, c, t quarks are commonly chosen to be both the flavour and weak eigenstates by selecting a specific phase convention. The weak eigenstate of a d quark, d' can be expressed as a linear combination of the d, s, b flavour eigenstates:

$$d' = V_{ud}\, d + V_{us}\, s + V_{ub}\, b \tag{2.2}$$

The CKM matrix elements describe the rotation of a particular flavour eigenstate into a particular weak eigenstate.

The magnitudes of the CKM matrix elements, determined to a 90% confidence level are [5]:

$$\begin{pmatrix} 0.9742 \text{ to } 0.9757 & 0.219 \text{ to } 0.226 & 0.002 \text{ to } 0.005 \\ 0.219 \text{ to } 0.225 & 0.9734 \text{ to } 0.9749 & 0.037 \text{ to } 0.043 \\ 0.004 \text{ to } 0.014 & 0.035 \text{ to } 0.043 & 0.9990 \text{ to } 0.9993 \end{pmatrix} \quad (2.3)$$

The near diagonality of the CKM matrix implies that the rotation from flavour to weak eigenstates is small, however, this small rotation is enough to explain why the vast majority of quarks in the universe are either u or d: Without the relative rotation of flavour eigenstates, all quarks would only couple within their own generation. Since the first generation of quarks have lower masses, and because the generations mix in accordance to the CKM matrix, all quarks will eventually decay into first generation quarks.

A popular approximate parameterization of the CKM matrix is:[6]

$$\begin{pmatrix} 1-\lambda/2 & \lambda & A\lambda^3(\rho - i\eta) \\ -\lambda & 1-\lambda/2 & A\lambda^2 \\ A\lambda^3(1-\rho-i\eta) & -A\lambda^2 & 1 \end{pmatrix} \quad (2.4)$$

where A, ρ, η are all real numbers of order unity. The complex phases of the lower left (V_{td}) and upper right (V_{ub}) elements describes the amount of CP violation present in the Standard Model.

2.2 Symmetries and C or P Violations

A property of all gauge (field) theories, the types of theories describing the three fundamental forces in the Standard Model, is that they must collectively obey charge conjugation, parity, and time (CPT) reversal symmetry. The parity transformation transforms a reaction into its mirror image ($F(x, y, z) \rightarrow F(-x, -y, -z)$). Parity invariance implies

Figure 2.1: A righthanded particle's **(a)** spin is in the same direction as its velocity. A lefthanded particle's **(b)** spin is in the opposite direction of its velocity. Only lefthanded neutrinos found in nature, while antineutrinos are only found to be righthanded ([7] 45).

that both the reaction and its mirror image occur at the same rate. Charge conjugation inverts the charges of a particle, or in practical terms, changes a particle into its antiparticle. Charge conjugation invariance is the symmetry between a reaction and a conjugate reaction instead involving all the associated antiparticles. Time reversal invariance is the symmetry of a reaction occurring both forwards and backwards in time. Time reversal invariance implies that if one were to switch parent and daughter products (change $X + Y \rightarrow Z$ into $Z \rightarrow X + Y$), while retaining similar energy considerations, the reaction would be equally likely to occur ([7] 41).

Until 1956 it was thought that the three fundamental forces of the Standard Model (Electromagnetic, Strong and Weak) obeyed each of these three symmetries independently as well as collectively, however, an experiment on the beta decay of cobalt 60 disproved this assumption[8]. In this experiment, it was observed that electrons were always emitted in their direction of spin, or righthanded (Figure 2.1). As the direction of electron spin was coupled with the direction of neutrino spin, this discovery implied that righthanded neutrinos (as well as lefthanded antineutrinos) do not exist in nature. Neutrinos only exist as lefthanded and antineutrinos only exist as righthanded.

The fact that neutrinos may not be both lefthanded and righthanded implies that parity is violated in the weak reaction. Further experiments have shown that parity is maximally violated by the weak force. For this violation to be accommodated in a gauge theory, a similar violation of the C, T or CT symmetries must occur.

Observe a typical weak reaction:

$$\pi^{+} \longrightarrow \mu^{+} + \nu_{\mu} \tag{2.5}$$

in which the anti-muon and neutrino are both lefthanded. The parity transformation of Reaction 2.5, in which both the anti-muon and neutrino are righthanded, does not occur in nature. Similarly the charge conjugate of Reaction 2.5, in which both the muon and anti-neutrino are lefthanded does not occur. Yet, when we apply both a parity transformation and a charge conjugation transformation, we obtain:

$$\pi^{-} \longrightarrow \mu^{-} + \overline{\nu}_{\mu} \tag{2.6}$$

in which the muon and anti-neutrino are both righthanded. Reaction 2.6 does occur in nature, so it was assumed that CP is a good symmetry of the weak force.

2.3 CP Violation in the Kaon System

CP invariance has bizarre implications for the neutral Kaon system: It was noted[9] that if CP is conserved in the weak interaction, a K^0 may spontaneously oscillate into its antiparticle, a $\overline{K}^0$, through a second order weak interaction (Figure 2.2). This oscillation implies that any physically observed particles are not actually a K^0 or $\overline{K}^0$, but instead linear combinations of the two. Because CP was thought to be a good symmetry of the weak force, the linear combinations of the K^0 and $\overline{K}^0$ were then considered to be CP eigenstates since they can undergo weak decays. The two normalized CP eigenstates for neutral Kaons are[9]:

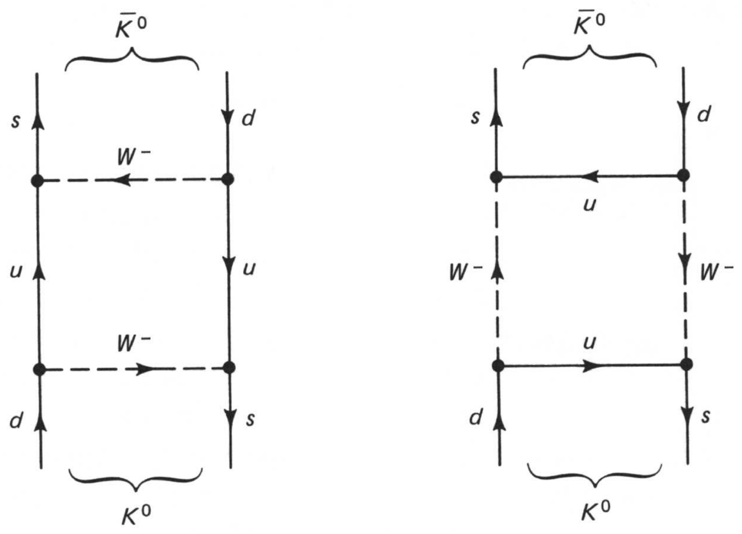

Figure 2.2: Through the two second order weak reactions shown here, a neutral Kaon (K^0) can spontaneously mix into its antiparticle, a neutral antiKaon ($\overline{K}^0$). The reverse is also true for a $\overline{K}^0$ mixing into a K^0. For this diagram and all other Feynman diagrams within this thesis, the time axis is flowing from left to right ([7] 51).

$$\begin{gathered}|K_1>=(\tfrac{1}{\sqrt{2}})(|K^0>-|\overline{K^0}>) \quad \text{and} \quad |K_2>=(\tfrac{1}{\sqrt{2}})(|K^0>+|\overline{K^0}>) \\ \text{so that} \\ CP\,|K_1>=|K_1> \quad \text{and} \quad CP\,|K_2>=-|K_2>\end{gathered} \tag{2.7}$$

If CP is conserved, K_1 can only decay into similar $CP=+1$ final states, and K_2 can only decay into $CP=-1$ final states. Since neutral Kaon systems are seen to decay into either two pion ($CP=+1$) or three pion ($CP=-1$) states, it is reasonable to assume that K_1 decays into the two pion state and K_2 decays into the three pion state. Because of the difference in the density of states (or available phase space) between the decays of the two CP eigenstates, the two pion decay rate is significantly larger than the three pion decay and there are two types of neutral K mesons observed, each with a different lifetime:

$$\begin{aligned} \tau_{K_s} &= 0.89 \times 10^{-10}\ \mathrm{s} \\ \tau_{K_L} &= 5.2 \times 10^{-8}\ \mathrm{s} \end{aligned} \tag{2.8}$$

In a famous 1964 experiment[10], it was found that a beam of K_L, which was thought to consist only of K_2 or CP = -1 final states, will actually decay into the two pion, CP = +1 final state a small percentage of the time ($\sim$ 0.2%). This observation was the first experimental evidence of CP violation. CP violation in the neutral Kaon system is commonly expressed in terms of the CP violating parameter ϵ:

$$\begin{gathered} |K_L >= \frac{1}{\sqrt{1+|\epsilon^2|}}(|K_2 > +\epsilon|K_1 >) \\ \text{and} \\ |K_s >= \frac{1}{\sqrt{1+|\epsilon^2|}}(|K_1 > +\epsilon|K_2 >) \end{gathered} \tag{2.9}$$

where K_L is the long lived Kaon candidate, K_s the short lived, and ϵ is the measure of CP violation ($\epsilon = 1.5 \pm 0.8 \times 10^{-3}$) [5].

K_L, instead of simply being equivalent to K_2, is now considered an admixture of the two CP eigenstates: K_1 and K_2. This evidence of CP violation in the neutral Kaon system was, for over thirty-five years, the only experimental evidence of CP violation and hence the only indication of the imaginary term in Equation 2.4.

2.4 CP Violation in the B System

Theory predicts that the neutral D system will have very little mixing and no neutral D mixing has yet been experimentally observed. On the other hand, the neutral B system has been experimentally observed to exhibit mixing. Because of this similarity with the neutral K system, it is therefore natural to assume that the neutral B system is the next likely place to search for CP violation. Recently, CP violation in the neutral B system has been observed [1]. There is further direct theoretical evidence to suggest that there is a large amount of CP violation in the neutral B system [11].

The unitarity of the CKM matrix gives rise to six relations among its elements. Three of these relations may lead to a better understanding of CP violation in the Standard Model:

$$V_{ud}V_{us}^* + V_{cd}V_{cs}^* + V_{td}V_{ts}^* = 0 \tag{2.10}$$

$$V_{us}V_{ub}^* + V_{cs}V_{cb}^* + V_{ts}V_{tb}^* = 0 \tag{2.11}$$

$$V_{ud}V_{ub}^* + V_{cd}V_{cb}^* + V_{td}V_{tb}^* = 0 \tag{2.12}$$

Each of these relations can be geometrically represented in the complex plane as a triangle (Figure 2.3), each having an equal area. Each triangle, and its corresponding equation, describes the amount of CP violation present in a different physical system. The first triangle describes the CP violation in the Kaon system, while the next two triangles describe CP violation in the B_s and B_d systems, respectively.

In the Kaon and B_s systems, one side of each triangle is so much longer than the other two that the triangles appear almost degenerate (Figure 2.3 (a) and (b)). The openness of the third triangle (Figure 2.3 (c)), which describes the CP violation in the B_d system, implies a large amount of CP violation and non-zero imaginary component in the CKM matrix. This large predicted CP asymmetry in the B_d system is the reason it is a major focus of the BaBar experiment. By choosing a phase convention so that $V_{cd}V_{cb}^*$ from Equation 2.12 is real, and rescaling all of the triangle sides by $\mid V_{cd}V_{cb}^* \mid$, we can easily relate the CP violation in the B_d system to the parameterized CKM matrix in Equation 2.4 (Figure 2.4). In having the real axis of Figure 2.4 scaled to a length of 1, we find that the remaining vertex lies at a coordinate of (ρ,η). This ρ and η are the same CKM matrix parameters that are in Equation 2.4.

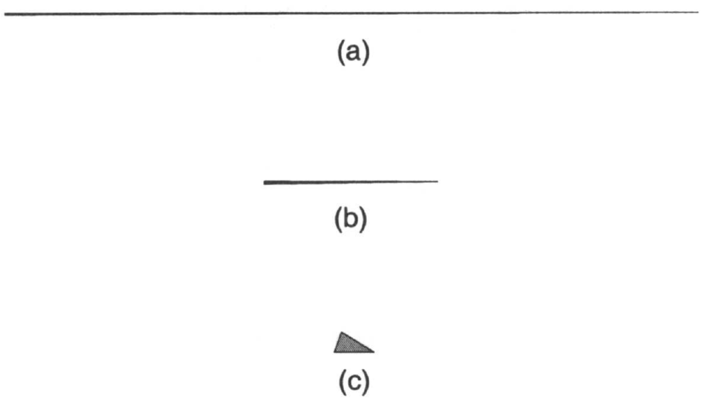

Figure 2.3: Triangle **(a)** represents the CP violation present in the neutral Kaon system (Equation 2.10). Triangle **(b)** represents the CP violation in the B_s system (Equation 2.11), while triangle **(c)** represents CP violation in the B_d system (Equation 2.12). All three triangles have an equal area. CP violation in the neutral Kaon system has already been observed while the CP violation for the B_d system is the focus of the BaBar project ([11] 20).

2.5 The Sakharov Conditions

Now that a brief overview of the terms and ideas surrounding the Standard Model and CP violation have been introduced, we can re-visit the topic left at the end of Chapter 1: something apparently occurred in the early universe to favour matter over antimatter. A.D. Sakharov suggested three criteria that must be satisfied in order to explain the current matter/antimatter asymmetry of the universe [12]:

1. Baryon non-conserving reactions occur
2. CP invariance must be violated
3. The universe may not be in statistical thermal equilibrium when conditions 1 and 2 are met

Free quarks do not exist in nature, or more accurately, a free quark has yet to be observed in nature. Instead, quarks are only observed in composite states known as

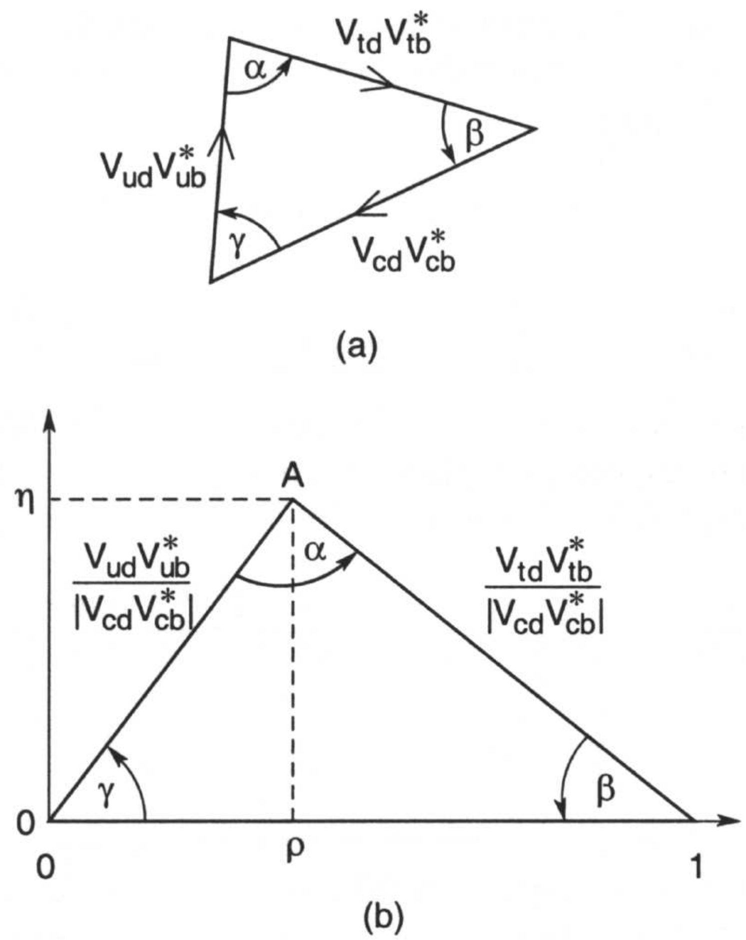

Figure 2.4: We can relate the unitary triangle of the B_d system (Equation 2.10 and Figure 2.3 (c)) to the parameterization of the CKM matrix (Equation 2.4) by scaling all sides by $\mid V_{cd}V_{cb}^* \mid$ and rotating the triangle such that the base sits on the real axis between 0 to 1. The coordinate of the triangle's apex is then denoted by the two CKM matrix parameters ρ and η ([11] 21).

mesons or baryons. A meson is a particle made up of a quark/antiquark pair while a baryon is a three-quark bound state. Baryon number is an internal quantum number. All particles possess a baryon number, although many particles, such as gauge bosons and leptons, have a baryon number of 0. Baryons have a baryon number of 1, while each of the quarks, being one third of a baryon, have a baryon number of $\frac{1}{3}$. Antibaryons have a baryon number of -1 and so antiquarks have a baryon number of $-\frac{1}{3}$. All mesons have a baryon number of 0. Since matter (or baryons) currently dominates the universe, the universe must have a positive baryon number. Since it is assumed that the universe was originally created in the Big Bang with a baryon number of 0, baryon non-conserving reactions must have already occurred (*condition 1*). However, baryon non-conserving reactions do not necessarily favour either matter or antimatter and this is why we require that there be CP violation (*condition 2*). CP violation implies that a reaction has a preference for either matter or antimatter. Since we are made of matter, we must assume that the CP violation in nature favours matter. Together, conditions 1 and 2 could suggest a method for the matter dominance of the universe. However, if conditions 1 and 2 occur in a state of thermal equilibrium, the matter favoured reactions, as well as their reverse reactions, would be equally likely to occur. We require condition 3 to allow the matter favoured reactions to evolve into a non-equilibrium matter predominated universe such as we have today.

2.6 CP Violation at BaBar

The BaBar experiment has been designed with a key goal of exploring the CP violation in the B_d system. The experimental conditions and environment of the BaBar experiment will be discussed in Chapter 3, however, in this section I will quickly explain the theoretical framework surrounding CP violation measurements in the BaBar experiment.

There are three model-independent manifestations of CP violation in the B system ([11] 12):

1. CP Violation in Decay (or Direct CP violation)
2. CP Violation in Mixing
3. CP violation in the interference between decays with and without mixing

2.6.1 CP Violation in Decay

CP Violation in decay occurs in both charged and neutral B meson decays and is the simplest type of CP violation. Given an initial state i, and a final state f, the amplitude of decay for the process $i \to f$ is denoted by A_f. The amplitude of $i \to \overline{f}$, where $\overline{f}$ is the CP conjugate state of f, is denoted by $\overline{A}_{\overline{f}}$. To determine the presence of CP violation in decay, we can observe the ratio of the decay amplitudes ($\left|\frac{\overline{A}_{\overline{f}}}{A_f}\right|$). If CP is a good symmetry of the weak force in the B_d system, this ratio of decay amplitudes would be equal to 1.0 whereas if CP invariance is violated, this ratio would be unequal to 1.0. Any CP violation present in charged B meson decays would be from CP violation in decay. A major goal of the BaBar experiment is to observe charged B meson decays and determine if there is any deviation of $\left|\frac{\overline{A}_{\overline{f}}}{A_f}\right|$ from 1. CP violation in decay can also occur with neutral B mesons however it must compete with the two other manifestations of CP violation mentioned above, both of which are only found in neutral B meson decays.

2.6.2 CP Violation in Mixing

CP Violation in mixing is the type of CP violation that is observed in the neutral Kaon system (Section 2.3). This type of CP violation should also be present in the mixing of neutral B mesons yet with a slight difference: In the Kaon system, the lifetime of the

CP eigenstates is very different, although their masses are similar. In the B system, the masses of both CP eigenstates differ considerably while the decay times are very similar. The Hamiltonian for the neutral B system is given by [13]:

$$\mathcal{H} = \begin{pmatrix} M & M_{12} \\ M_{12}^* & M \end{pmatrix} - \frac{i}{2} \begin{pmatrix} \Gamma & \Gamma_{12} \\ \Gamma_{12}^* & \Gamma \end{pmatrix} \tag{2.13}$$

where the first matrix is the mass matrix and the second matrix is the decay matrix.

The off-diagonal elements of both the mass matrix and the decay matrix are dominated by mixing. However, because the final decay states of neutral B mesons are suppressed, we have: $|\Gamma_{12}| \ll |M_{12}|$. It is this relation that results in the mass eigenstates of the Hamiltonian in the neutral B system being very different, as opposed to the lifetimes as in the neutral Kaon system (Equation 2.8). The mass eigenstates of the neutral B system Hamiltonian (Equation 2.13) are:

$$\begin{aligned} B_{light} &= p|B^0> +q|\overline{B}^0> \\ B_{heavy} &= p|B^0> -q|\overline{B}^0> \end{aligned} \tag{2.14}$$

where p and q are complex numbers.

In measuring CP violation in mixing, a quantity of importance is the ratio:

$$\left|\frac{q}{p}\right|^2 = \left|\frac{M_{12}^* - \frac{i}{2}\Gamma_{12}^*}{M_{12} - \frac{i}{2}\Gamma_{12}}\right| \tag{2.15}$$

If this ratio differs from exactly 1.0, the presence of CP violation is implied. $\left|\frac{q}{p}\right|$ may be measured using the decay amplitudes of semi-leptonic neutral B meson decays (A_{sl}) through the relation:

$$A_{sl} = \frac{1 - |q/p|^4}{1 + |q/p|^4} \tag{2.16}$$

A_{sl} is also directly expressible in terms of the decay rates of semi-leptonic neutral B meson decays:

$$A_{sl} = \frac{\Gamma(\overline{B}^0 \to \ell^- \nu X) - \Gamma(B^0 \to \ell^+ \nu X)}{\Gamma(\overline{B}^0 \to \ell^- \nu X) + \Gamma(B^0 \to \ell^+ \nu X)} \tag{2.17}$$

While accurate measurements of B semi-leptonic decays is of primary importance to determining CP violation in mixing, the measurements can also help in determining both direct CP violation and CP violation in the interference between decays with and without mixing. As mentioned in the Introduction, when analyzing B semi-leptonic decays, it is important to accurately measure the decay spectrum of the primary lepton originating from the B meson. In order to determine the primary lepton's decay spectra, any lepton backgrounds must also be examined. This thesis involves measurements of the backgrounds in semi-leptonic decays due to Photonic Conversions. A more detailed explanation of the analyses involved in this thesis is postponed till Chapter 4.

2.6.3 CP Violation in the Interference Between Decays With and Without Mixing

CP violation in the interference between decays with and without mixing occurs in events containing pairs of neutral B mesons. At the BaBar experiment, pairs of neutral B mesons are created in a coherent state. Due to quantum statistics, at all times after the creation of the B meson pair, the pair consists of exactly one B^0 and one $\overline{B}^0$ even though individually, each B meson could undergo mixing. As soon as one of the B mesons within the pair decays, the remaining B meson will mix accordingly.

The experimental procedure behind the measurement of CP violation in the interference between decays requires that at a time denoted t_f, one of the B mesons from the coherent pair decays into a final CP eigenstate f_{CP}, while at a time denoted t_{tag}, the second B meson decays into a mode which can identify its b-flavour (called a tagging mode). Since the B meson pair was originally in a coherent state, at $t_f = t_{tag}$, if the tag meson is a B^0, the non-tag B meson must be a $\overline{B}^0$ and vice versa. At a time $t_f \neq t_{tag}$, it is possible to predict the probability of the non-tag B meson being in either the B^0 or $\overline{B}^0$ states. This probability is time-evolving and is measured using $t_f - t_{tag}$, the difference between the two B meson decay times, as a reference time (note that this difference can be either positive of negative). The presence of CP violation in the interference between decays is examined by comparing the differences between the time-evolving decay rates for non-tag B^0 and $\overline{B}^0$ states to decay into the same final CP eigenstate f_{CP}:

$$a_{f_{CP}} = \frac{\Gamma(\overline{B}^0(t_f - t_{tag}) \to f_{CP}) - \Gamma(B^0(t_f - t_{tag}) \to f_{CP})}{\Gamma(\overline{B}^0(t_f - t_{tag}) \to f_{CP}) + \Gamma(B^0(t_f - t_{tag}) \to f_{CP})} \tag{2.18}$$

CP violation in the interference between decays is present if $a_{f_{CP}}$ differs from 1.0.

The BaBar detector has been built with the specific focus of measuring CP violation in the B meson system. Any measurement of CP violation in the interference between decays requires the precise measurement of the time difference between the two B mesons' decays and so this requirement has been incorporated into the BaBar detector. Chapter 3 will introduce and explain the experimental environment at the BaBar detector and will also give a in depth description of the BaBar detector itself.

Chapter 3

The BaBar Experiment

This chapter will introduce and explain the environment of the BaBar experiment. The BaBar experiment is housed at the Stanford Linear Accelerator Center (SLAC). SLAC is an e^+e^- accelerator used as an asymmetric B factory allowing the BaBar experiment to study CP violation in the B meson system. The BaBar detector is an assembly of several detector sub-systems, each designed to meet the experimental conditions at SLAC's PEP II storage rings, where the two accelerator means are collided. A brief description of accelerator and detector components used at the BaBar experiment will be given, with emphasis on material relevant to the topic of this thesis.

3.0.4 The Linac, PEP II Storage Rings and the Interaction Region

The SLAC site consists of a two-mile long linear accelerator (Linac) that produces high-energy electron and positron beams. A overview of the SLAC site can be seen in Figure 3.1. Electrons are produced from a heated filament at the beginning of the two-mile long accelerator. To obtain positrons, electrons are accelerated and collided into a tungsten target. Once collected and accelerated to its desired energy, each beam is injected into a separate PEP-II storage ring. The beams collide at a point where the two PEP-II storage rings intersect, designated the interaction point (IP).

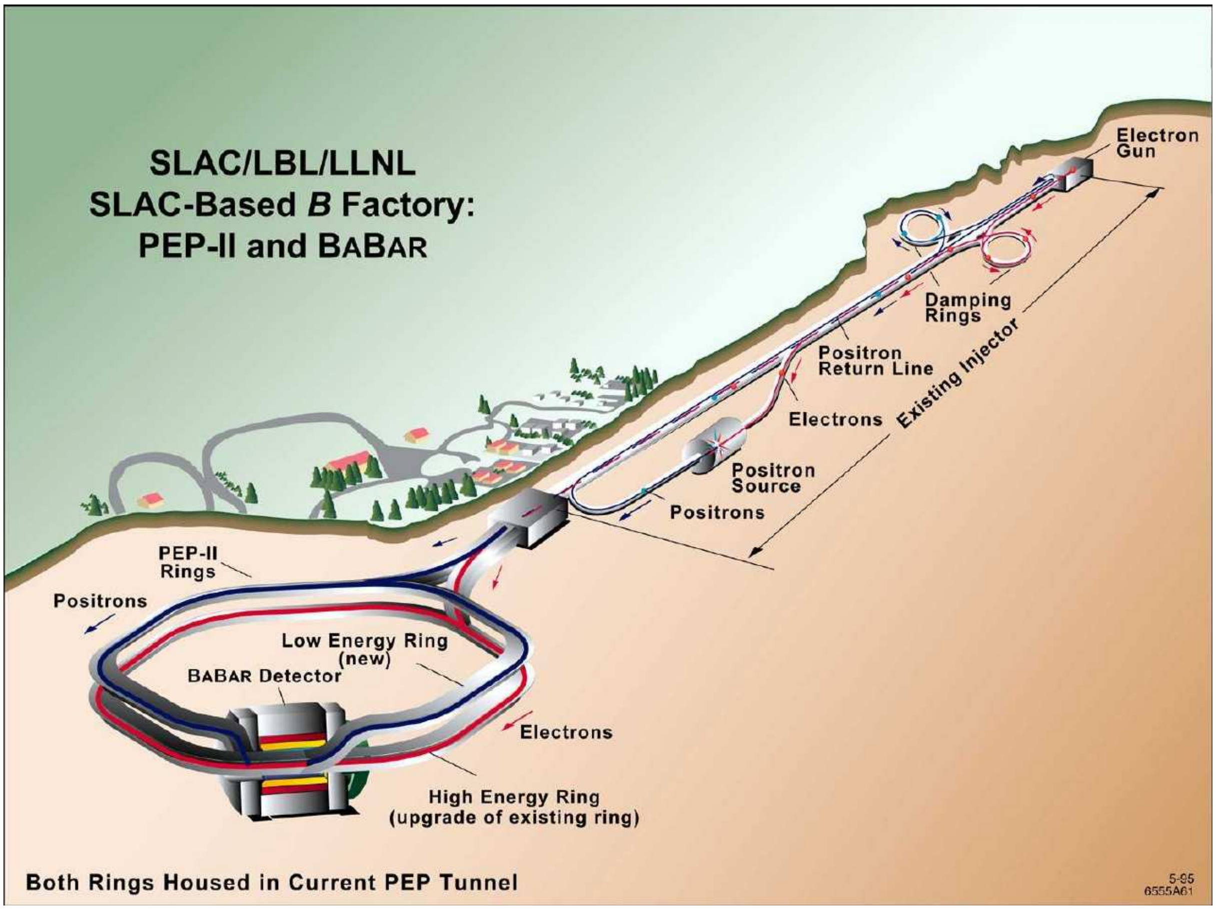

Figure 3.1: Within this picture we can see the 2-mile long Linac, the electron and positron sources, the PEP-II storage rings, and the placement of the BaBar detector with respect to all of these[14].

$e^+e^- \rightarrow$	Cross-section (nb)
$b\overline{b}$	1.05
$c\overline{c}$	1.30
$s\overline{s}$	0.35
$u\overline{u}$	1.39
$d\overline{d}$	0.35
$\tau^+\tau^-$	0.94
$\mu^+\mu^-$	1.16
e^+e^-	$\sim$ 40

Table 3.1: Production cross section for $e^+e^- \rightarrow f\overline{f}$ at the $\Upsilon(4S)$ resonance. Of important note is the comparatively large Bhabha ($e^+e^- \longrightarrow e^+e^-$) cross section.

3.0.5 Overview of the Experimental Setup

The BABAR experiment requires a large number of B mesons for high- efficiency studies. SLAC is required to act as a B factory, producing as many B mesons as possible while at the same time producing few background events. The mass of a B_d meson is 5.279 GeV/c^2 [5] and so the BABAR experiment requires a Center of Mass energy of at least twice this value (10.558 GeV/c^2). To meet these requirements, the SLAC site runs at the Υ (a meson consisting of a b and $\overline{b}$ quark pair) ($4S$) resonance: The $\Upsilon(4S)$ has a mass of 10.580 GeV/c^2, just over twice the mass of a B meson, and hence its dominant ($>$ 96 %) decay products are B-$\overline{B}$ pairs. Because the B-$\overline{B}$ pair is created via the decay of the $\Upsilon(4S)$ state, quantum statistics requires that they are created in a coherent state.

The cross section for fermion pair production with SLAC running at the $\Upsilon(4S)$ resonance is shown in Table 3.1. The comparatively large $e^+e^- \longrightarrow e^+e^-$ cross section (called a Bhabha event) results from the scattering of an electron and positron (one from each beam) at the IP and will be revisited in greater detail in Section 4.2.

The BABAR experiment requires that its Lab frame is not the Center of Mass frame. Running at the $\Upsilon(4S)$ resonance of 10.58 GeV results in the creation of B_d mesons pairs with a maximum 0.02 GeV of kinetic energy in the Center of Mass frame, keeping the velocity(v) of the B mesons $\ll$ c. The limited resolution of detectors makes it impossible to accurately measure the differences in decay times of the very short-lived B mesons ($\tau_B = 1.65 \times 10^{-12}$ s) if both B mesons have been created at the same point. By using a boosted Lab frame, the slow moving B mesons in the Center of Mass frame will have a significant boost in the Lab frame; any difference in decay times will result in a measurable difference in the decay positions. The difference in decay times is essential in the calculation of CP violation parameters mentioned in Section 2.6.3. To produce the boosted Lab frame, the e^+ and e^- beams at SLAC have different energies. The e^- beam has an energy of 9.0 GeV while the e^+ beam has an energy of only 3.1 GeV.

3.1 The BaBar Detector

The BaBar detector has been built to accommodate the experimental conditions at SLAC. Several key detector characteristics are:

- To maximize acceptance, the detector is built to allow for an asymmetry in the lab frame due to the unequal beam energies.
- The vertex resolution must be very precise in order to accurately measure the decay position of particles
- Particle tracking and resolution must be able to function accurately over a wide range of particle types and momenta.

To accomplish these and other detector requirements, the BaBar detector has been built with the following major sub-systems (Figure 3.2):

1. A Silicon Vertex Tracker (SVT)

2. A Drift Chamber (DCH)

3. A Detector of Internally Reflected Cerenkov (DIRC) Light

4. A Cesium Iodide Electromagnetic Calorimeter (EMC)

5. A superconducting coil to provide a magnetic field

6. An Instrumented Flux Return (IFR)

The coordinate system of the BaBar detector is anchored to the DCH since it is the main tracking system ([15] 4). The origin of the BaBar coordinate system is taken as the expected point that the e^+e^- beams would collide if the BaBar magnetic field was turned off. The origin of the BaBar coordinate system may differ in position from the previously mentioned IP, which is where the beams actually collide, by as much as a few millimeters. The z-axis of the BaBar coordinate system corresponds to the principle axis of the cylindrical DCH, offset from its center by 3.7 cm in the backward direction. The z axis is also offset relative to the beam axis by $\sim$ 20 mrad in the horizontal plane. The asymmetric energies of the election and position beams in the PEP-II storage ring gives the Lab frame a Lorentz boost of $\beta\gamma = 0.56$ in the positive z direction (also called the forward direction). The coordinate system is right handed, leaving the positive y-axis to point upwards and the positive x-axis to point outwards from the PEP- II storage rings. There is a 1.5 T magnetic field throughout the BaBar detector along the z axis (or perpendicular to the r-ϕ (x-y) plane). This magnetic field causes charged tracks to curve according to the Lorentz force with a radius of curvature of:

$$\text{Radius of Curvature} = \frac{mv}{eB} \tag{3.1}$$

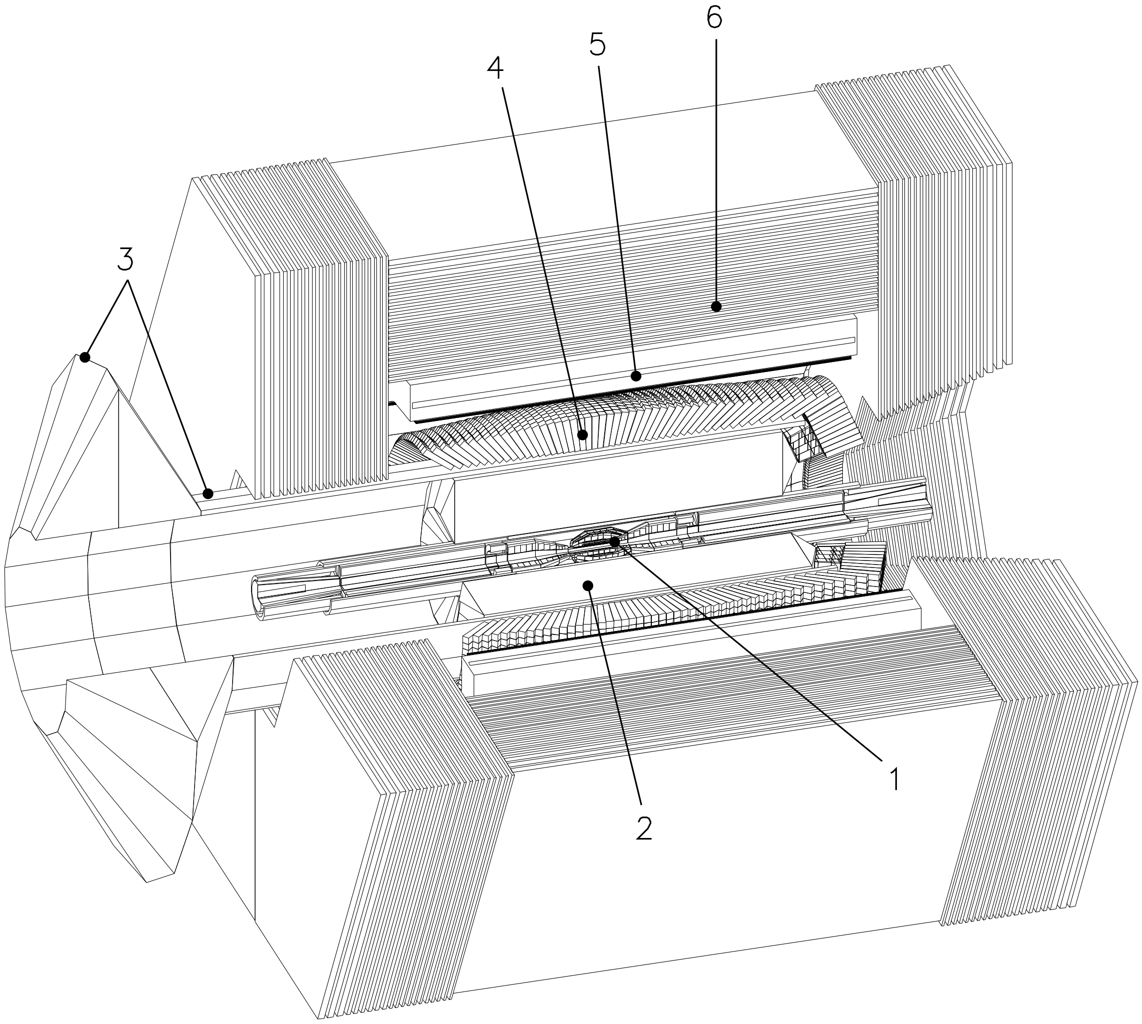

Figure 3.2: The BaBar detector has been built with the 6 major detector sub-systems shown here: 1. The Silicon Vertex Detector (SVT). 2. The Drift Chamber (DCH). 3. The Detector of Internally Reflected Cerenkov (DIRC). light 4. The Electromagnetic Calorimeter (EMC). 5. The superconducting coil which provides the 1.5 T axial magnetic field throughout the BaBar detector. 6. The Instrumented Flux Return (IFR)([11] 79).

where m is the mass of the charged track, v its velocity, e its electric charge and B is the 1.5 T magnetic field. Within the BaBar coordinate system, tracks with a positive charge curve in the direction of negative ϕ while tracks with a negative charge curve in the positive ϕ direction.

3.1.1 The Silicon Vertex Tracker

The main task of the Silicon Vertex Tracker (SVT), also referred to as the vertex detector, is the accurate reconstruction of decay vertices. For $B-\overline{B}$ events, the reconstruction of decay vertices in the boosted Lab Frame can determine the time between decays. This function requires an excellent tracking ability and results in the SVT being one of the primary tracking instruments of the BaBar experiment.

The SVT is built up of many individual silicon strip detectors (SSDs) that measure particle information by detecting an electron/hole pair that is produced whenever a charged particle passes through a silicon strip[16]. The SVT, in tandem with the drift chamber, also provides the momentum measurements for charged tracks based on their curvature within the 1.5 T magnetic field. The SVT can only measure charged particle information and can not measure any neutral particle properties.

The SVT is the first instrument radially outward from the beam pipe. 340 double sided SSDs are arranged in 5 concentric layers between a radius of 3.2 cm and 14.4 cm from the IP (Figure 3.3). The inner three layers are arranged in a "barrel" orientation, where "barrel" signifies that its cylindrical orientation is concentric with the beam pipe. The outer two layers are arranged with their centers in a barrel orientation while the forward and backward regions are placed at an angle to the beam pipe as shown in the side view of Figure 3.3. This angled shape allows for maximal solid angle coverage. Since particular care must be taken to allow for preferential coverage in the forward direction (the direction of the Lorentz boost), the machine components, cooling systems, etc..., are

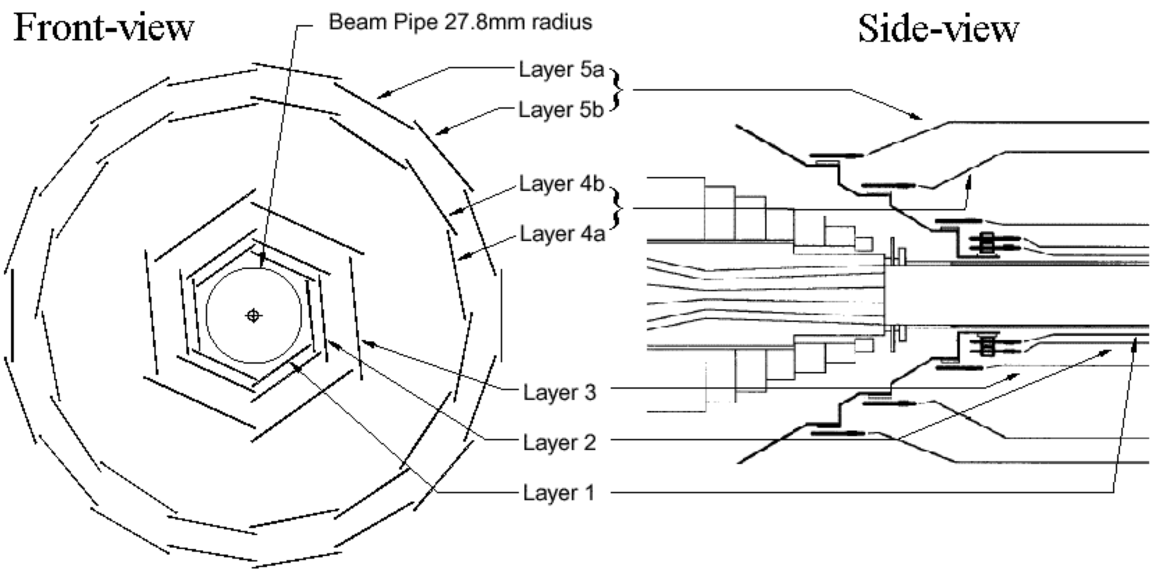

Figure 3.3: The inner three layers of the SVT all have a concentric cylindrical orientation with the beam pipe (a barrel orientation). The outer two layers, each divided into two overlapping sub-layers, have a barrel orientation in the middle region of the detector and are angled with respect to the beam pipe in both the forward and backward regions to allow for maximal solid angle coverage([11] 83-84).

all located in the backward region of the SVT.

The bending magnets, which are used to create the 1.5 T magnetic field, allow a maximum polar angle (θ) coverage with respect to the beam pipe of between 17.2° and 162.8° in the forward direction (or 17.2° in both the forward and backward directions). Allowing for unavoidable dead spaces due to detector support structures, the active areas of the SVT have been made to cover angles in between 20.1° and 150.2° in the forward direction. Also due to the 1.5 T magnetic field, charged particles with less than 100 MeV/c transverse momentum have a curvature too great to reach the Drift Chamber, whose inner wall radius is 20 cm from the IP. For these low-energy particles, the SVT will become the sole source of tracking information. Conversely, particles with less than 40 MeV/c of transverse momentum will not even reach the SVT.

Single charged track hits to the SVT have a z spatial resolution of between 15 and 60 μm depending on the angle of measurement as well as which SVT layer was hit. The SVT's resolution worsens at larger angles with respect to the vertical plane (at $\cos\theta = 0$) of the detector. The inner layers tend to have a better resolution.

3.1.2 The Drift Chamber

The Drift Chamber (DCH) is the main tracking device of the BaBar detector. The DCH is able to measure charged particle tracking information with 40 detector layers, while the silicon vertex tracker has only 5 layers (slightly more where the layers overlap). The DCH also allows for charged particle identification by measuring the energy loss over track length, denoted as $\frac{dE}{dx}$.

The drift chamber is a 280 cm long cylinder with inner and outer radii of 23.6 cm and 80.9 cm respectively. A side-view of the DCH, showing its dimensions, can been seen in Figure 3.4. Since events at the BaBar experiment are boosted in the forward direction with respect to the Center of Mass frame, the DCH, like the SVT, is designed to preferentially favour having active detector areas in the forward end; the forward end-plate is thinner than the backward endplate, and all electronics are mounted in the backward region.

The DCH volume is filled with a helium/isobutane gas mixture of 80%/20%. Ions are created whenever a charged particle interacts with the gas mixture. Powerful field wires create an electric field within the DCH causing the ions to drift towards the nearest sense wire, where an electronic signal is then recorded.

The DCH is sub-divided into ten superlayers consisting of four wire layers each. Within each superlayer, all four wire layers are arranged as either axial (A) or one of two stereo (U,V) possibilities. The axial superlayers run parallel to the beam pipe and provide tracking information in the x-y plane (ϕ-r plane). Each stereo superlayer is

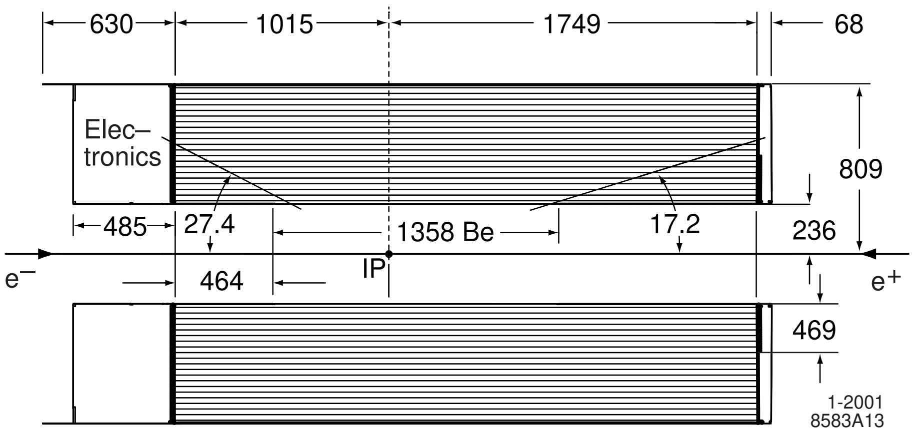

Figure 3.4: A side view of the BaBar Drift Chamber (DCH). The inner radius is at 23.6 cm, limiting the minimum energy required to reach the drift chamber to $\sim$ 100 MeV/c (using Equation 3.1). To preferentially favour the forward end, the center of the drift chamber is offset by 3.7 cm from the IP. The forward and backwards lengths of 101.5 cm and 174.9 cm (as measured from the IP) are chosen so that a particle emitted at an angle of 17.2° in the forward direction, or 27.4° in the backwards direction, will travel through half of the wire layers ([15] 36).

offset by a different small angle to supply z coordinate information. The superlayers are arranged in an alternating pattern of AUVAUV.

Together with the SVT, the DCH provides the complete tracking information for charged tracks in the BaBar detector. Charged tracks can be defined using five parameters ([15] 46):

- The distance of closest approach to the origin in the $x-y$ plane (d_0)
- The distance of closest approach to the origin along the z axis (z_0)
- The azimuthal (x-y or r-ϕ) angle of the track as measured at the distance of closest approach (ϕ_0)
- The dip angle relative to the transverse plane (λ, commonly expressed as tanλ)

Track Parameter	Resolution
d_0	23 μm
z_0	29 μm
ϕ_0	1 mrad
$\tan\lambda$	0.53×10^{-3}
p_t	$0.13\ \% \times p_t + 0.45\%$

Table 3.2: The performance of the SVT and DCH on each of the 5 charged track parameters that are needed to make a consistent curved track ([15] 49).

- The transverse (x-y) momentum of the track p_t, or its curvature $\omega = \frac{1}{p_t}$ in the x-y plane.

The combined tracking performance of the SVT and DCH can be viewed in Table 3.2 and are well within the BaBar experimental requirements.

3.1.3 The Detector of Internally Reflected Cerenkov Light

Whenever a particle travels faster than the local speed of light of a material, an electromagnetic shock wave is produced. This shock wave radiation is called Cerenkov radiation. The angle at which the shock wave propagates depends on both the medium and the velocity of the particle. If we are able to determine the momentum of the particle from the SVT and the DCH, and we are able to determine the velocity of the particle from its Cerenkov radiation, we can calculate its mass. Using this mass, BaBar's Detection of Internally Reflected Cerenkov (light) detector (or DIRC) is the main detector component for charged particle identification.

The DIRC consists of 144 long, straight bars of synthetic fused silica arranged in a 12-sided polygonal barrel placed radially just after the outside wall of the DCH (Figure 3.5). A Cerenkov light cone is created when a particle exceeding the speed of light in quartz passes through the polygonal quartz barrel. The Cerenkov radiation is reflected

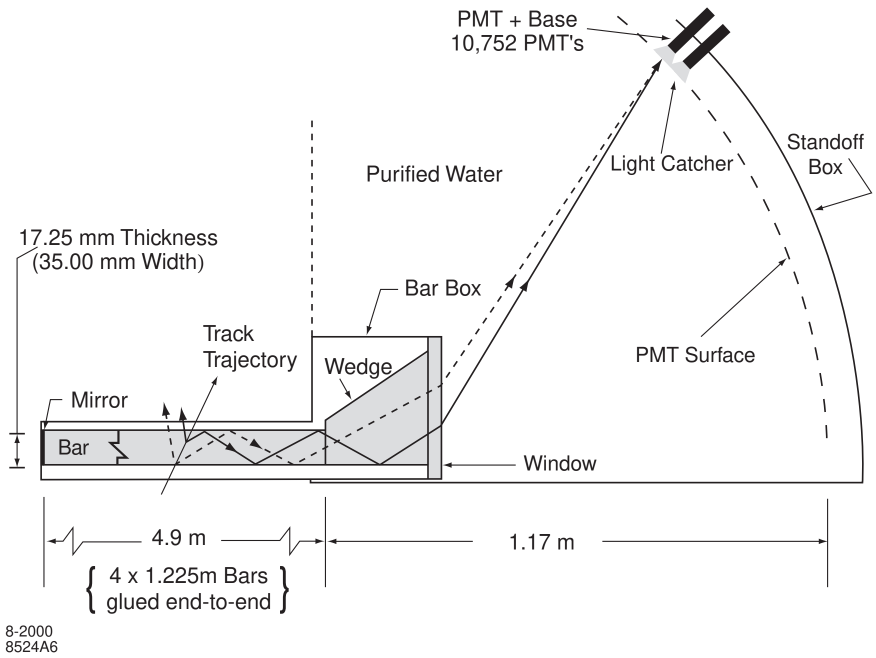

Figure 3.5: The BaBar Detector of Internally Reflected Cerenkov (DIRC) light. The Cerenkov radiation cone is directed towards the forward direction, to the right in this figure. There, an array of 11,000 photomultiplier tubes (PMTs) is placed around the exterior of a huge purified water tank to measure the Cerenkov radiation. By reconstructing the angle of the Cerenkov radiation, and by using the momentum of the particle, the particle's mass, and therefore its identity, can be obtained([15] 52).

along the length of a quartz bar to the backward direction—a mirror is placed in the forward direction—where it enters a huge tank filled with purified water. Purified water is chosen to preserve the original angular information because its refractive index is similar to that of the quartz. Within the purified water, the Cerenkov radiation is measured by an array of 11,000 photomultiplier tubes (PMTs) placed around the exterior of the tank.

The DIRC is primarily used in identifying hadron species while leptons are identified using the EMC, DCH, IFR, and SVT. The DIRC is primarily used for charged particle identification above a momentum of 700 MeV/c. Under 700 MeV/c, the primary source of particle identification is the $\frac{dE}{dx}$ of the DCH.

3.1.4 The Electromagnetic Calorimeter

The primary purpose of the BaBar experiment's Electromagnetic Calorimeter (EMC) is the measurement of photon, neutral and electron energies. Within the BaBar detector, photons are produced directly, such as in a Radiative Bhabha event ($e^+e^- \longrightarrow e^+e^-\gamma$), or via the decay of a neutral pion into two photons. The EMC is also used for lepton identification through the ratio of the lepton's measured energy and momentum. Even though the full momenta of all three electron-type particles can be measured by the DCH and SVT, only electron's deposit virtually all of their energy within the EMC while muons and taus tend to deposit only a fraction. By comparing the energy deposited in the EMC to the momentum as measured by the DCH and SVT, (referred to as E over p, or $\frac{E}{p}$) electrons may be identified by the fact that their $\frac{E}{p}$ will be close to 1.

The BaBar calorimeter is separated into two main components, both of which are cylindrically symmetric. The barrel region contains 5760 thallium doped cesium iodide (CsI(Tl)) crystals arranged in 48 θ rings. The CsI(Tl) crystals function as scintillators, emitting light whenever an incident particle interacts with them. The emitted light is then measured by silicon PIN photodiodes. The magnitude of the observed photodiode pulse is directly proportional to the energy of the incident particle. The barrel region covers a solid angle of $(\pi - 684m)r \leq \theta \leq 470mr$ or $-0.775 \leq \cos\theta \leq 0.892$. The second main component of the calorimeter is the forward endcap. A backward endcap was deemed unnecessary due to the high cost and the forward asymmetry of the BaBar experiment's boosted Lab Frame. The forward endcap is conical with tilted front and back surfaces. It is composed of 820 CsI(Tl) crystals in 8 θ rings and covers a solid angle of $486mr \leq \theta \leq 275mr$ or $0.892 \leq \cos\theta \leq 0.962$ (Figure 3.6).

For the EMC to function well, it must be able to accurately measure the energy of any incident electromagnetically interacting particles. When a particle interacts with matter

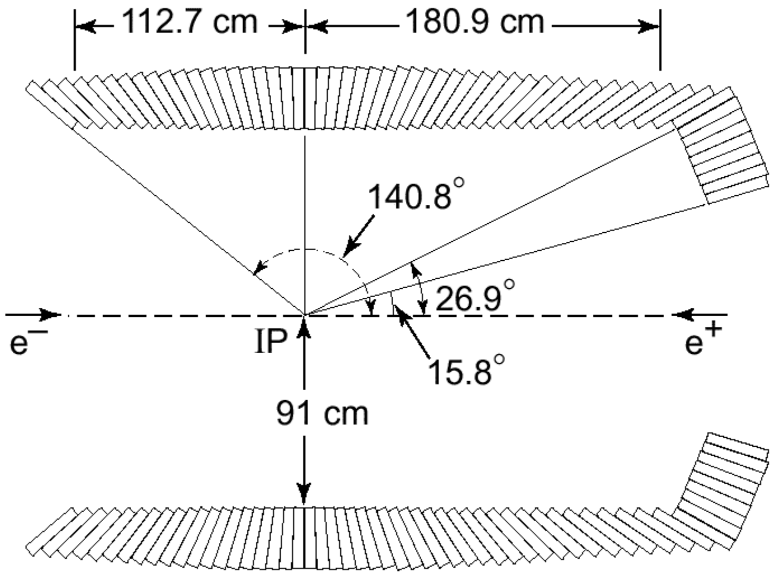

Figure 3.6: A longitudinal view of the Electromagnetic Calorimeter (EMC) for the BaBar detector (the EMC is cylindrically symmetric). The forward endcap of the EMC is tilted with respect to the barrel region to allow for maximal solid angle coverage. The EMC is divided into 56 θ rings, with 8 lying in the forward endcap. The fiducial region of the EMC does not include the 3 forward-most θ rings because there is an excess of material between them and the IP—3.0 X_o compared with 0.3 to 0.6 X_o for the remainder of the EMC ([11] 98)

it can lose some of its energy, so it is desirable to minimize the mass in between the IP and the EMC. For this reason, the forward regions of all inner BaBar detectors have been kept as low in mass as possible, placing any detector components in the backward region whenever feasible. However, a small amount of material in the forward region is always unavoidable and the three forward most θ rings of the forward endcap are shadowed by SVT support structure as well as a beam focusing magnet. This excess material results in up to 3 radiation lengths (X_o—the length required to reduce a particle's energy to 1/e of its initial value) before these three θ rings. In contrast, the other 5 θ rings of the forward endcap as well as the barrel region only have between 0.3 and 0.6 X_o in front of them ([15] 63). The fiducial, or well-measured region of the EMC, is limited to the areas with lower radiation lengths between the IP and the EMC. The fiducial region therefore covers an angle of $-0.78 \leq cos\theta \leq 0.92$, thereby excluding the three forward most θ rings of the EMC's forward endcap. This coverage represents a Center of Mass angle of $-0.92 \leq \cos\theta \leq 0.80$

3.1.5 The Muon and Neutral Hadron Detectors

A large iron structure is the outermost component of the BaBar detector. It is needed as a flux return path for the 1.5 T magnetic field throughout the BaBar detector. This structure has been segmented and instrumented with $\sim$ 100 Resistive Plate Counters (RPC) to provide muon identification and to aid in neutral hadron detection. This detector component is called the Instrumented Flux Return (IFR) (Figure 3.7).

The iron plates of the IFR consist of a barrel section with endcaps at both ends. This structure provides solid angle coverage from between 300 mr in the forward direction to 400 mr in the backward direction. The RPCs's function is similar to that of the DCH: whenever a charged particle passes through the chamber of an RPC, it ionizes the gas mixture. External electrodes then measure the ions to provide tracking information.

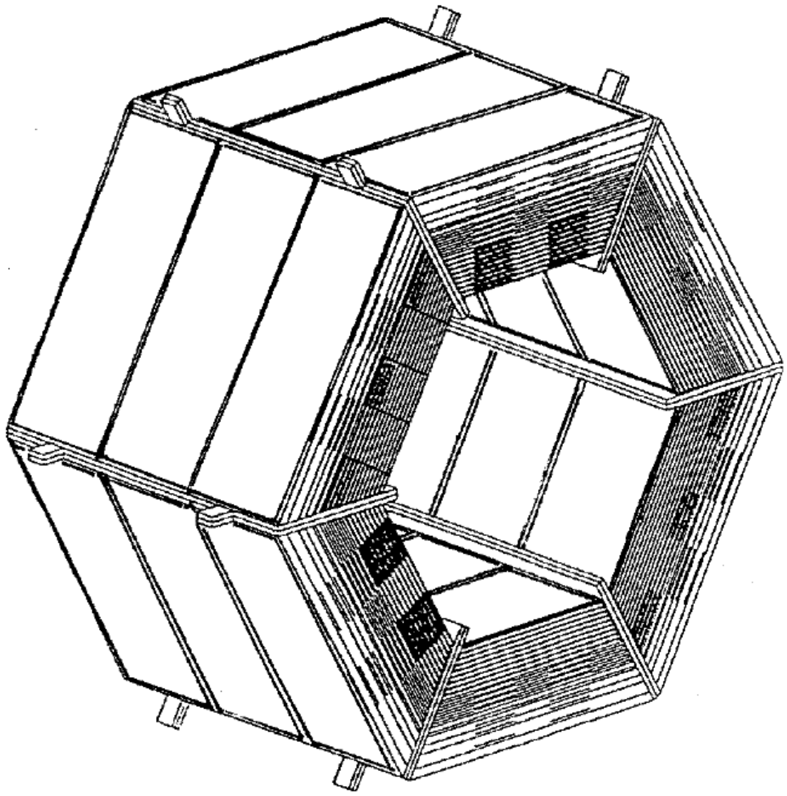

Figure 3.7: The barrel region of the Instrumented Flux Return (IFR). Resistive Plate Counters (RPCs) are interspersed in between 19 layers.

Neutral hadrons are detected by observing the characteristic length of hadron showers produced in the IFR.

Chapter 4

Introduction to the Analysis

As stated in the preceding chapters, one of the main goals of the BaBar experiment is to study CP violation in the B_d system. As explained in Section 2.6.2, one possible manifestation of CP violation in the B_d system is that of CP violation in mixing. The study of CP violation in mixing, as well as several other measurements being conducted at the BaBar experiment, requires an accurate understanding of the semi-leptonic decays of neutral B mesons ($B^0 \to \ell^+ \nu X$). One difficulty in the measurement of semi-leptonic B decay spectra arises from lepton contamination, i.e., lepton candidates in the event that do not originate from the decay of the original B meson. One such source of lepton contamination is from converted photons—in which a photon, in the presence of an external electromagnetic field, changes into an electron/positron pair ($\gamma \to e^+e^-$).

Many photons in the BaBar experiment originate from the decay of neutral pions ($\pi^\circ \to \gamma\gamma$) or from the radiation of high energy particles ($X^* \to X\gamma$). Whenever a photon converts, it creates an additional electron/positron pair in an event. Since for semi-leptonic B decays, measuring the properties of the lepton that originated from the primary decay of the B meson is important, it is necessary to eliminate any electrons/positrons due to converted photons from the lepton sample.

The elimination of converted photons is a challenging and complicated task because it relies primarily on an ability to reconstruct the converted photon from its two daughter tracks. However, an accurate reconstruction is not always possible since reconstruction efficiencies are not perfect. A "Photonic Conversion Finder" (PCF) algorithm has been written for the express purpose of reconstructing a converted photon candidate from its two daughter tracks. The efficiency of the PCF lies in its ability to properly identify a converted photon candidate while simultaneously rejecting fake background candidates, in which the reconstructed photon is the result of two unrelated tracks.

While a number of Monte Carlo studies have been conducted using the PCF, a comprehensive analysis of its performance on the BaBar experiment's data has not yet been done.

The primary goal of this thesis is to perform efficiency studies of the PCF using the BaBar data. These studies will examine:

- The ability of the PCF to properly identify a converted photon candidate if the two daughter tracks have been reconstructed by the BaBar detector,
- How often the BaBar detector does not reconstruct both converted photon's daughter tracks. Hence, a measure of the how many single converted photon daughter track backgrounds are in the lepton sample.

A detailed analysis will be conducted to determine the contamination within a lepton sample from the unidentified converted photon's daughter tracks. Both unidentified converted photon candidates—in which the PCF has failed to properly identify a converted photon candidate—and partially reconstructed converted photons—in which one daughter track was not reconstructed by the BaBar detector—will be considered in this analysis. Because future semi-leptonic studies will not be able to determine the number of unidentified converted photon daughter tracks within their own lepton samples, this study's background contamination will be correlated to the number of identified converted photon candidates. This correlation will enable future semi-leptonic analyses to determine lepton contamination due to unidentified converted photons simply by using the number of properly identified converted photon candidates found within the study.

4.1 The Photonic Conversion Finder

Essentially, the PCF algorithm attempts to reconstruct a converted photon candidate from any two oppositely charged tracks. The likelihood that the two charged tracks actually originated from the converted photon candidate is then examined by testing the candidate's properties against a set of predefined cuts. If a candidate passes the cuts, the candidate is considered as a reconstructed converted photon and the two daughter tracks are considered identified as originating from that converted photon. If the candidate fails the cuts, the converted photon candidate is considered the result of two tracks that are not from a converted photon. In the next section I will introduce and explain the PCF algorithm as well as several previously conducted studies thereof.

4.1.1 Principle of the Algorithm

Electron/positron tracks are reconstructed within the BaBar detector based on tracking information from both the DCH and SVT. In the SVT, charged particles are detected by a charge flow in the SSDs, while in the DCH, charged tracks register as ions that have been produced in the gas mixture and subsequently detected in the forty layers of sense wires. A charged track is then reconstructed based on a track-fitting algorithm that combines detector hits from both the DCH and SVT. Since a charged particle will have approximately the same momentum within the SVT and the DCH, it will also have the same curvature due to the BaBar experiment's magnetic field (as per Equation 3.1). Therefore, the track-fitting algorithm attempts to join individual detector hits in order to form a consistent helical particle trajectory. It should be noted that it is possible for a track to originate from different points within the BaBar detector system and not just from the IP. For instance, if a conversion were to occur at the inner wall of the drift chamber, the resultant tracks would only be detected by the DCH.

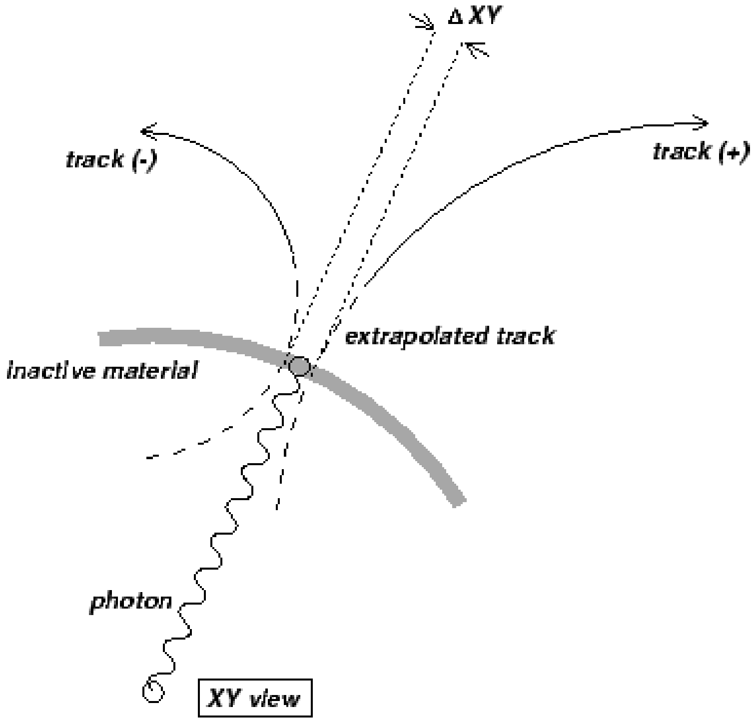

Figure 4.1: A photon converts in some inactive material of the BaBar detector into an electron and positron that curve in opposite directions. By extrapolating each track's path back towards the point at which they are tangent to one another in their plane of curvature (the x-y plane), a Photonic Conversion can be reconstructed[18].

The most widely used BaBar PCF algorithm [17] makes use of the (E, p) four-vectors and the position information of the two reconstructed charged tracks. In the x-y plane, oppositely charged tracks curve in opposite directions and so each set of oppositely charged tracks can be extrapolated (or swum) backward to their point of closest approach. At this point, the two tracks are (re)constructed into a converted photon candidate as shown in Figure 4.1. The point of closest approach is taken where the slopes of two charged tracks are tangent to one another in the x-y or r-ϕ plane.

In order to test the identity of a converted photon candidate, the PCF algorithm calculates several of the candidate's properties:

- The distance of closest approach for the two charged tracks in the x-y plane (Δ_{xy}).
- The distance of closest approach for the two charged tracks along the z axis (Δ_z).
- The converted photon candidate's mass (m_γ).
- The Distance of Closest Approach (abbreviated DOCA) between the trajectory of the converted photon candidate and the interaction point (D_γ).

When extrapolated and projected onto the x-y plane, each track traces a circle (or a spiral due to energy loss) whose radius is determined by the track's momentum (Equation 3.1). The point of closest approach for each pair of tracks can be joined by a line segment, denoted by M in Figure 4.2. The PCF algorithm calculates Δ_{xy} and Δ_z from M. Because it is possible for two charged tracks to have overlapping paths, it is possible that the point of closest approach be inside of the two traced circles (Figure 4.3) and so Δ_{xy} is a signed quantity. Δ_z is positive definite since it does not matter which of the charged tracks is above or below the other (Figure 4.4). The mass of the converted photon candidate (m_γ) is calculated using the trajectories and momenta of the two daughter tracks as taken at their point of "point of conversion". The "point of conversion" of a converted photon candidate is taken as the midpoint of the closest approach line segment M—this point is represented by the small line at the middle of M in Figures 4.3 and 4.4. The fourth converted photon property, D_γ, has been included into the PCF algorithm specifically for semi-leptonic analyses [19]. The DOCA of the converted photon (D_γ) is calculated by extrapolating the constructed photon's trajectory backwards from its point of conversion and determining its minimum distance to the IP.

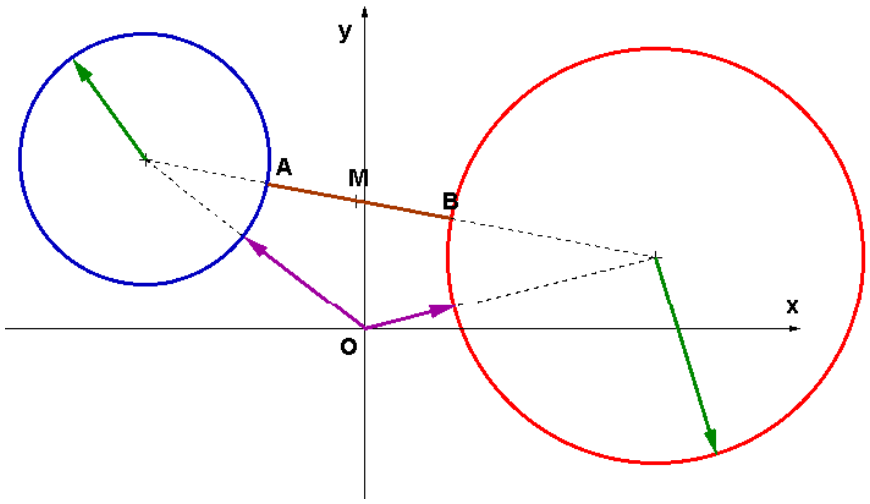

Figure 4.2: Each extrapolated track forms a circle when projected onto the x-y plane. The points of closest approach for each track is where the two tracks are tangent to each other—points A and B. The line segment M joins points A and B. The mid-point of M (the small vertical line) is considered the "point of conversion"[17].

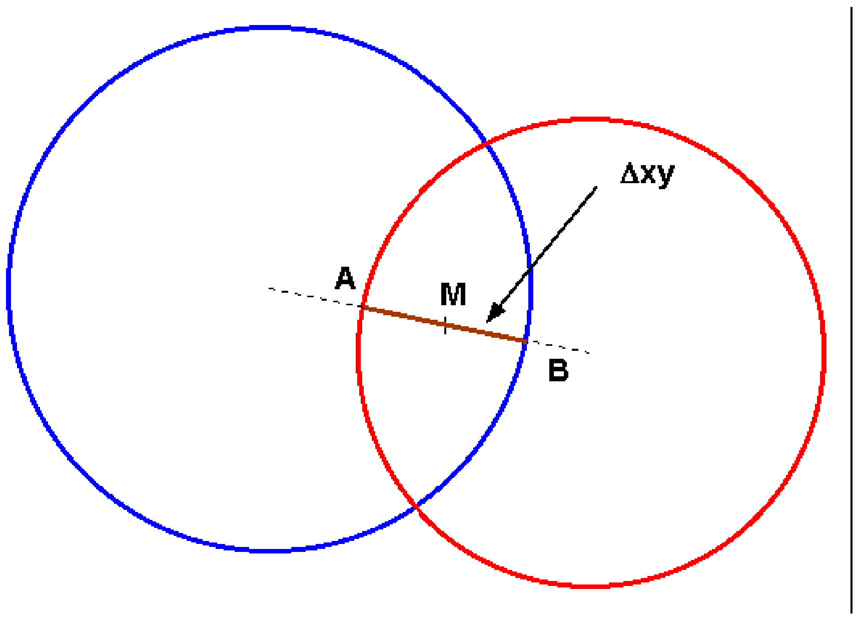

Figure 4.3: It is possible for the two extrapolated track paths to overlap in the x-y plane. In this case, Δ_{xy} is negative whereas in Figure 4.2, Δ_{xy} would be positive [17].

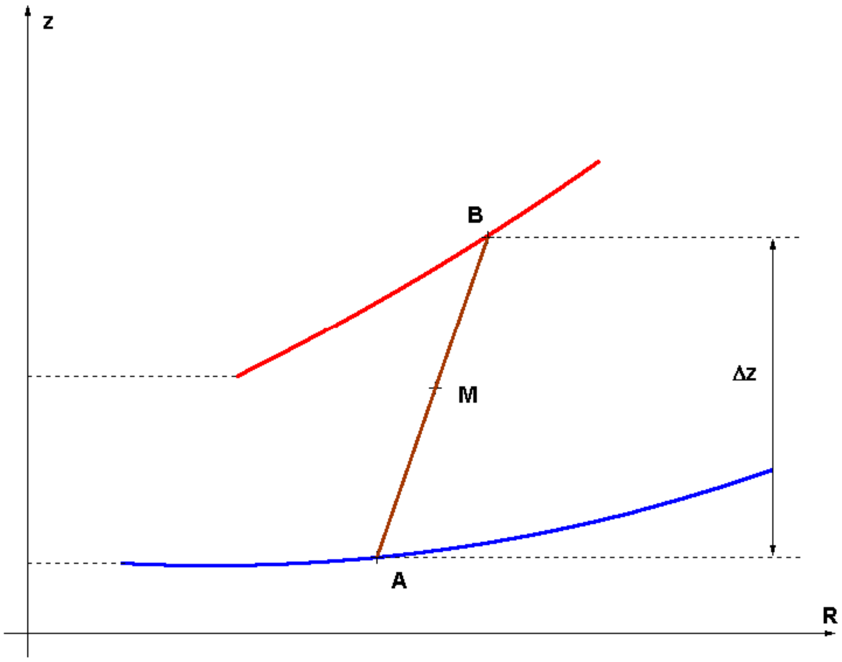

Figure 4.4: Δ_z is the distance between points A and B on the z axis. It is the length of the z component of the line segment M[17].

The BaBar experiment's reconstruction code assigns different masses to charged particles based on several particle identification properties. The most basic BaBar list of reconstructed charged tracks assumes that every charged particle is a pion since they are the most abundantly produced final state particles in hadronic reactions. Regardless of the reconstruction code's mass assignment it is always necessary to set the mass of each particle used in the PCF algorithm to that of an electron or positron because the particles resulting from a Photonic Conversion are almost exclusively electron/positron pairs.

4.1.2 Testing of the Algorithm: Past Monte Carlo Study

The results of the PCF algorithm were originally studied using several of the BaBar experiment's data sets containing samples of converted photons[17]. These studies were conducted in order to obtain cuts for a converted photon candidate's four calculated parameters that were described in Section 4.1.1: Δ_{xy}, Δ_z, m_γ, and D_γ. The cuts for these parameters are chosen in order to obtain a high acceptance of real Photonic Conversions while rejecting most background events in which a converted photon candidate has been reconstructed from two oppositely charged tracks that are not from a converted photon. Further comprehensive efficiency studies were done with simulated Monte Carlo generic B events in order to obtain appropriate parameter cuts specific to semi-leptonic analyses [19]. As this project is also concerned with obtaining the efficiencies of the PCF with respect to semi-leptonic B-decay analysis, I will focus on the cuts obtained from these Monte Carlo studies.

The Monte Carlo studies were conducted on approximately five-hundred thousand generic $B - \overline{B}$ events (BaBar runs 230175-243188 for generic $B\pm$, and run 240265-243300 for generic B^0). Converted photon candidates were reconstructed and their four calculated parameter distributions were compared to those contained in the Monte Carlo truth table. The Monte Carlo truth table contains a list of the generated tracks within an event as well as the Monte Carlo simulated data that contains the results of the BaBar reconstruction code acting on that same list of generated tracks. The appropriate cuts for each variable were determined in order to maximize the correlation between identified candidates in the reconstructed Monte Carlo data and the Monte Carlo truth.

The criteria for reconstructing a converted photon within the Monte Carlo study required that within each event, a single electron/positron candidate would be selected if it passed the following cuts:

- It satisfied the BaBar Particle ID very tight electron cuts found in [20]
- The track's polar angle distribution was restricted to -0.717 $\leq \cos\theta \leq$ 0.92
- The Lab frame momentum must be $\geq$ 0.5 GeV/c
- The Center of Mass frame Momentum must be $\geq$ 0.6 GeV/c

The PCF was used with the electron/positron passing the above cuts and every other oppositely charged track within the event regardless of its particle ID, being sure to set each charged track's mass to that of an electron. Whenever an event had more than one reconstructed conversion candidate, only the one with the smallest mass (since the mass of a photon is zero) was selected. This Monte Carlo study is concerned about the efficiencies of the PCF in identifying both converted photons and Dalitz pairs. A Dalitz pair is the name given to an electron/positron pair created through the internal (within a particle reaction) conversion of a virtual photon. Dalitz pairs are most commonly created in pion decays ($\pi^0 \rightarrow e^+e^-\gamma$). Since this thesis is only concerned with Photonic Conversions, all results obtained for Dalitz pairs will be ignored. The plots for each of the candidate's four parameters form both the Monte Carlo data and the Monte Carlo truth can be seen in Figures 4.5 and 4.6. From an examination of these distributions, the following cuts were chosen as best identifying Photonic Conversions within this Monte Carlo study:

- $m_\gamma \leq 0.01$ GeV/c^2
- $\Delta_{xy} \leq \pm$ 0.2 cm
- $\Delta_z \leq 1.0$ cm
- $D_\gamma \leq 2.5$ cm

As a result of further studies on the PCF, two different sets of cuts were obtained in order to maximize the acceptance of real Photonic Conversions. A "loose" conversion candidate is now considered to have:

- $m_\gamma \leq 0.03$ GeV/c^2
- $\Delta_{xy} \leq \pm$ 0.5 cm
- $\Delta_z \leq 1.5$ cm
- $D_\gamma \leq 3.5$ cm

A "tight" conversion candidate is now consider to have:

- $m_\gamma \leq 0.02$ GeV/c^2
- $\Delta_{xy} \leq \pm$ 0.2 cm
- $\Delta_z \leq 1.0$ cm
- $D_\gamma \leq 3.0$ cm

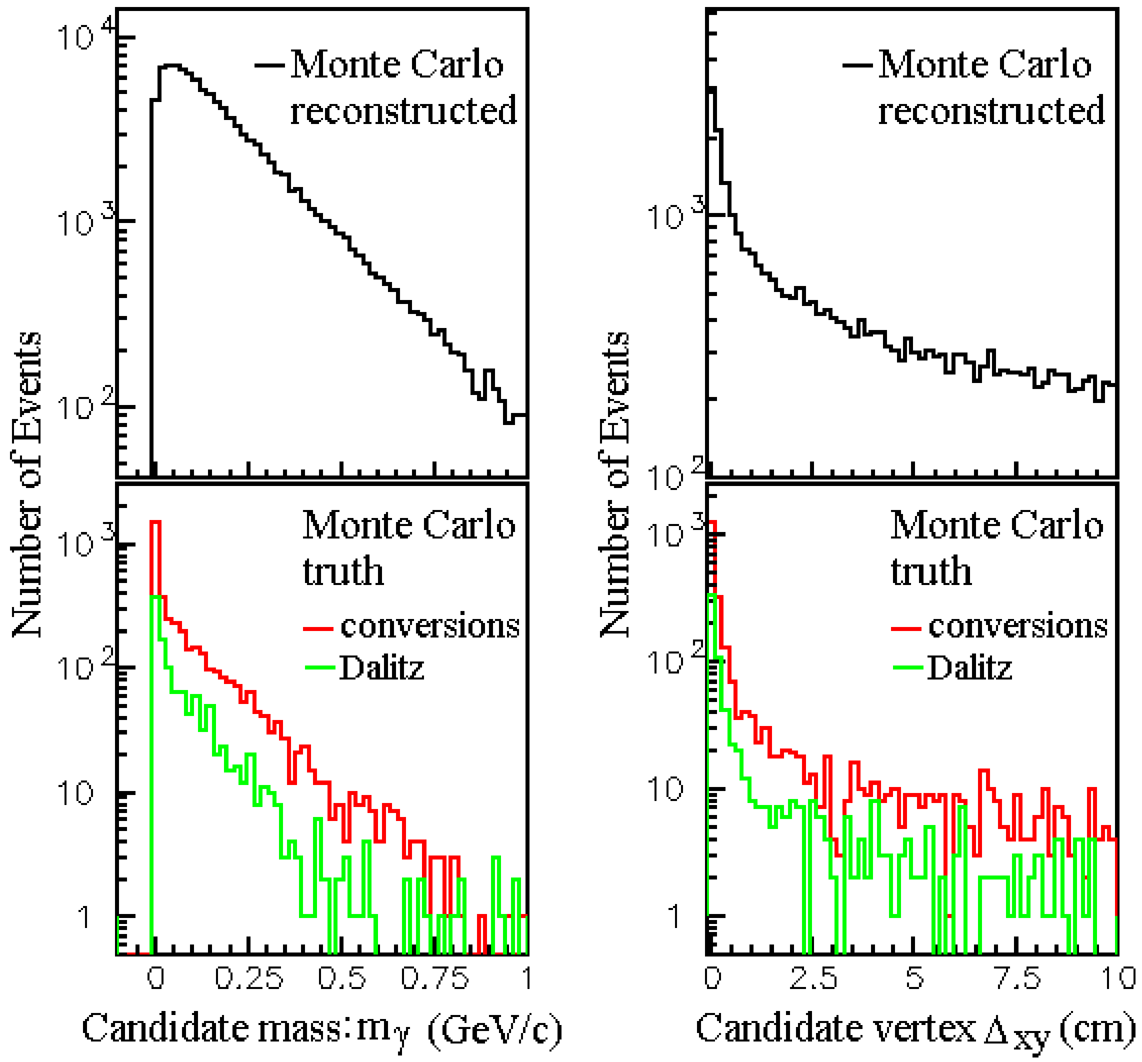

Figure 4.5: Plots of m_γ and Δ_{xy} for all converted photon candidates in the Monte Carlo simulated data are shown on the top. Plots of these variables from actual Photonic Conversions and Dalitz pairs, as determined by the Monte Carlo truth table, are shown on the bottom[19].

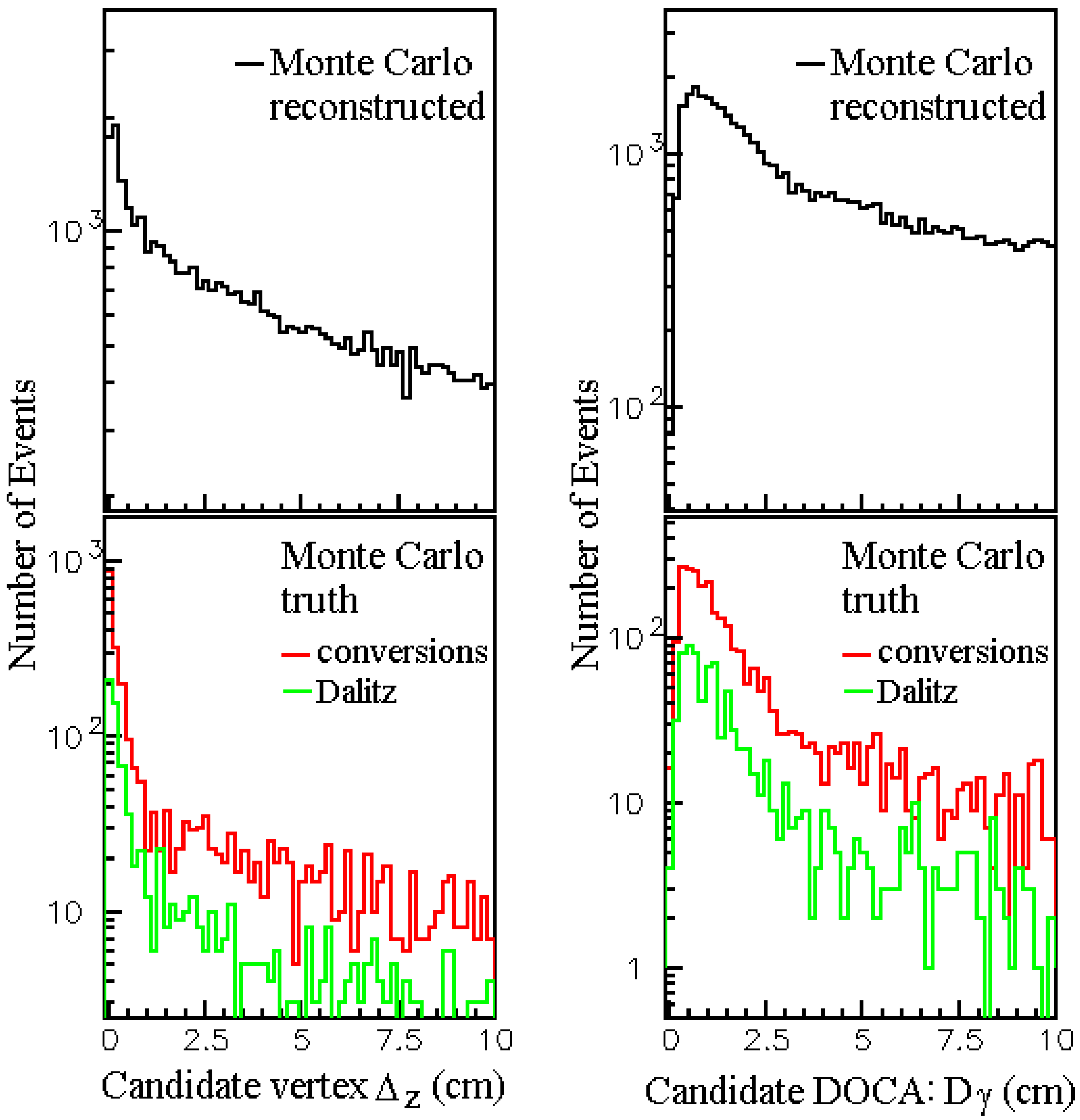

Figure 4.6: Plots of Δ_z and D_γ for all converted photon candidates in the Monte Carlo simulated data are shown on the top. Plots of these variables from actual Photonic Conversions and Dalitz pairs, as determined by the Monte Carlo truth table, are shown on the bottom[19].

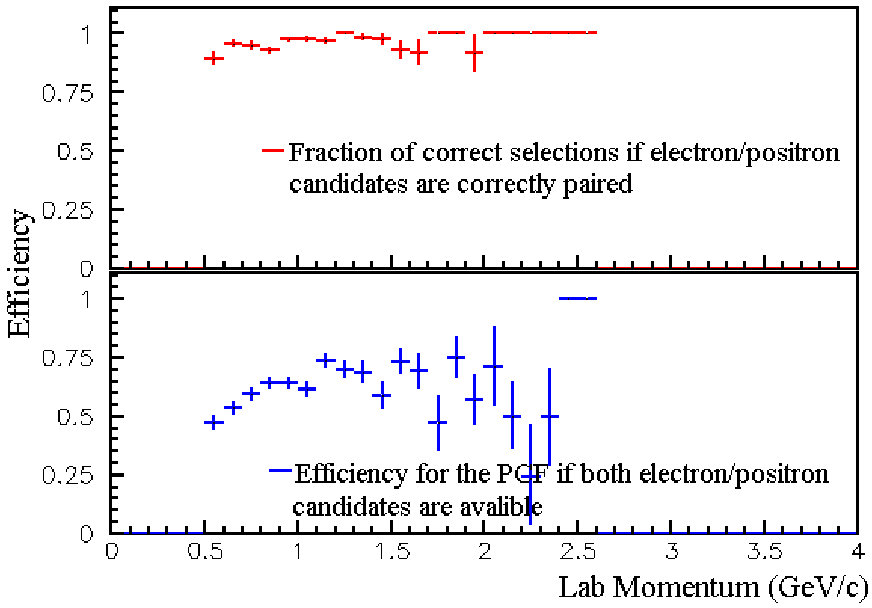

Figure 4.7: The efficiencies of the PCF versus energy be divided in two classes: The top graph shows the efficiency of the PCF in correctly identifying two charged tracks as originating from a converted photon when those tracks have been labeled in the Monte Carlo truth as originating from a converted photon. The bottom graph shows the efficiency of the PCF in correctly selecting out two charged tracks within a sample of leptons when those two tracks have been labeled in the Monte Carlo truth as originating from a converted photon [19].

The label "loose" and "tight" are used to imply the level of restrictions placed on a converted photon candidate's four parameters. By looking at Figures 4.5 and 4.6, one expects a higher percentage of backgrounds in events passing the loose cuts than in events passing the tight cuts. Even though the Monte Carlo study referred to in this section uses a different set of cuts, both the loose and tight cuts that have been determined after further study are used for the efficiency studies of this thesis. The loose and tight cuts are collectively referred to as the quality cuts of the PCF. For my efficiency studies of the PCF, I will only use the loose quality cuts.

The results obtained for the efficiency of the PCF using the Monte Carlo study referred to in this section are shown in Figure 4.7.

Since the efficiency studies referred to in Figure 4.7 only consider events in which the two daughter tracks of the converted photon were actually reconstructed by the BaBar detector, the results do not contain all the identification and background errors that may be present in my efficiency studies. Therefore, regardless of the differences in the cuts used, these results are expected to be slightly different than those obtained in this thesis.

Within the efficiency studies using the Monte Carlo simulated data, the largest source of unreconstructed or unidentified conversions was due to unreconstructed electron/positron daughter tracks within the BaBar detector. This result is because of both the lower momentum reconstruction limit and the low-momentum track reconstruction inefficiencies of the BaBar detector. Plots of the electron/positron momentum distributions for reconstructed but unidentified converted photons can be seen in Figure 4.8. In most events in which a reconstructed converted photon/Dalitz pair failed the PCF cuts, one of the electron/positron tracks usually had a moderately lower energy than the other (~ 0.5 GeV) and also usually had a momentum below 0.5 GeV/c. These findings imply a PCF efficiency bias against conversions with either highly asymmetric electron/positron pairs or conversions having a daughter electron/positron track with a low energy.

The PCF efficiency results obtained in this study are slightly dependent on the types of events (Generic B events) used for the Monte Carlo data and truth tables; therefore, regardless of the differences in the cuts used, a slight variation is expected between this Monte Carlo study's results and those obtained in this thesis' efficiency studies as I am utilizing a different type of event input for this thesis, namely radiative Bhabha events (see Section 4.2 for explanation) as opposed to generic B events.

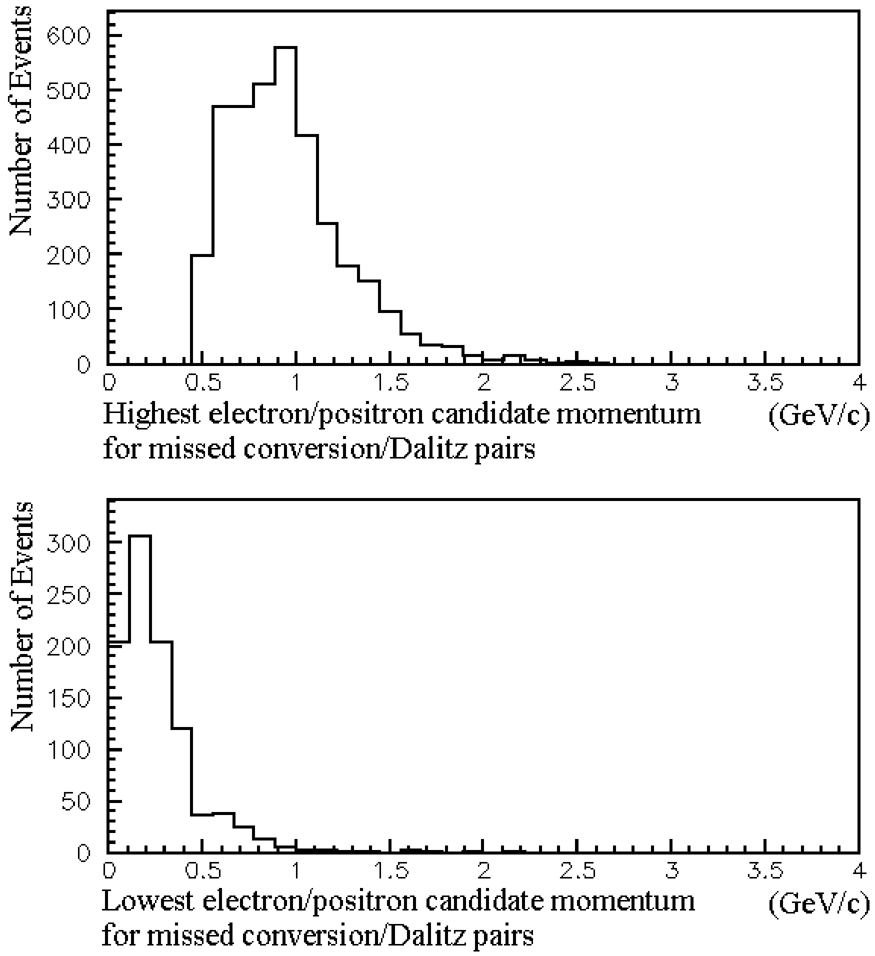

Figure 4.8: Plots of the electron/positron momentum for reconstructed but unidentified converted photons/Dalitz pairs. Unidentified implies that the converted photon candidate had failed the PCF quality cuts even though the Monte Carlo truth indicates that the candidate is indeed a converted photon/Dalitz pair. The higher momentum electron/positron track of the pair is shown in the top graph while its lower energy partner is shown in the bottom graph[19].

4.2 Experimental Environment of this Analysis

As described in Section 4.1.1, the BaBar PCF attempts to reconstruct a converted photon candidate from its two daughter tracks. I want to test the PCF's efficiency in correctly identifying reconstructed converted photons (in which the converted photon candidate is actually a converted photon) as well as the PCF's inability to detect any partially reconstructed converted photons (in which the BaBar detector has only reconstructed one of the two electron/positron daughter tracks from the conversion). The combined results of the efficiency studies will be used to obtain the background spectrum for unidentified electron/positron tracks originating from Photonic Conversions. In order to test the efficiency of the BaBar PCF, I require a data sample to have the following characteristics:

- Large numbers of converted photons and their daughter tracks
- The possibility of having partially reconstructed converted photons or unconverted photons
- Small numbers of final state tracks not resulting from converted photons
- Low Background contamination from tracks not part of the original event
- As few as possible tracks that are not part of the Photonic Conversion so as to minimize errors and possible backgrounds.

Multi-hadron events are unsuitable for this study because they usually contain a large number of tracks and are therefore difficult to understand. Radiative Bhabha events ($e^+e^- \longrightarrow e^+e^-\gamma$) are well understood, have a minimum number of backgrounds, and best satisfy all the other experimental requirements. For events with a well-measured photon, Radiative Bhabha events have the following experimentally favourable conditions:

- They contain large numbers of photons and converted photons
- They are easily identifiable, and so there is little chance of backgrounds
- There are typically only two charged tracks in the event (the primary e^+e^- pair in all Bhabha events), and thus additional tracks in the event are likely to be either background or from converted photons

Radiative Bhabha events have been chosen for conducting the efficiency studies of the PCF. Bhabha events are to be used for testing purposes since they are similar to Radiative Bhabha events except that they do not contain any photons or Photonic Conversions. Radiative Muon and Tau events are also suitable for the efficiency studies, although Tau events have a undesirably large missing energy. It would be possible to use Radiative Muon events for experimental verification since they are not considered in this thesis.

4.2.1 Bhabhas

The BaBar experiment is running at the PEP-II e^+e^- collider where the electron and positron beams pass each other at the IP, interacting in only a fraction of beam crossings. Significant proportions of reactions occurring within the BaBar detector are from the scattering of an electron and a positron from within the beams (Table 3.1). Such a reaction is called a Bhabha event ($e^+e^- \longrightarrow e^+e^-$). Bhabha events are among the simplest of all leptonic reactions occurring at the BaBar experiment. There are two leading order Feynman diagrams for Bhabha events (Figure 4.9). In the Annihilation Channel (Figure 4.9 **(a)**), the electron and positron annihilate into a virtual photon which then decays back into an electron/positron pair. In the Exchange Channel (Figure 4.9 **(b)**), the electron and positron exhcnage a virtual photon. Exchange Channel Bhabha events will tend to have a low scattering angle with respect to the incident particles

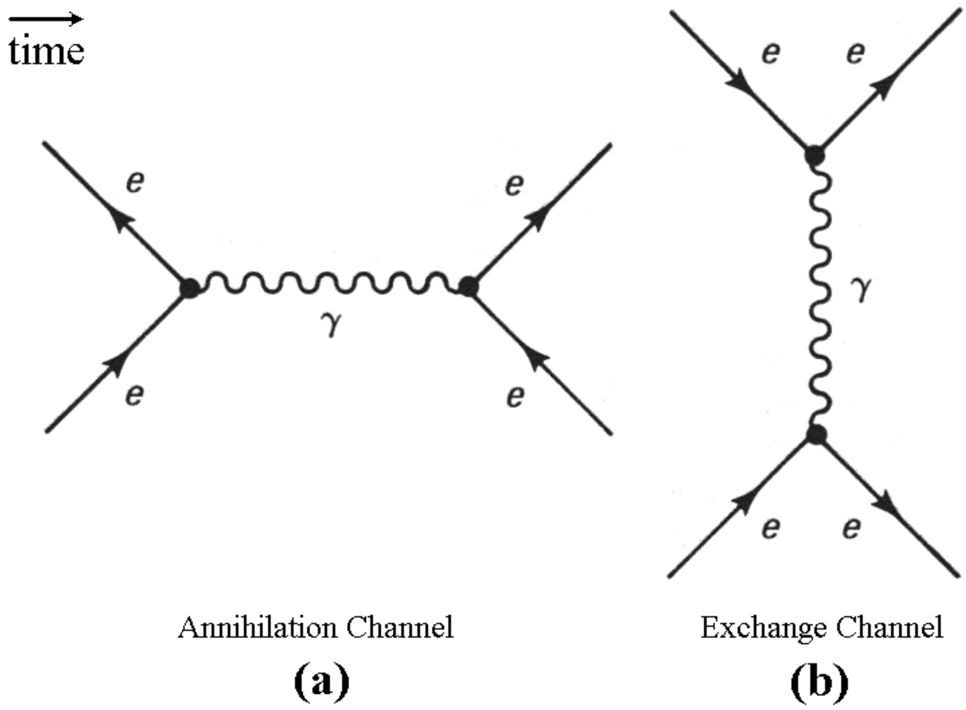

Figure 4.9: **(a)** is the Annihilation Channel for a Bhabha reaction in which an electron and a positron annihilate into an intermediate virtual photon which then decays back into an electron/positron pair. **(b)** represents the Exchange Channel for a Bhabha reaction in which the electron and positron interact by exchanging a virtual photon.

($\cos\theta_{e^-}$ in Figure 4.10). The Exchange Channel contributes a much larger differential cross section than the Annihilation Channel since an Exchange Channel Bhabha event can occur even if the electron and positron only exchange a very low energy photon. Therefore, most Bhabha and Radiative Bhabha events at BaBar will be low angle scatters in which the electron/positron pair approximately retain their beam energies.

The differential cross section for Bhabha events in which the electron and positron are considered "Ultra relativistic" (they have momentum $\gg \mathrm{m}_e$) is given in Equation 4.1. Equation 4.1 is a minimum at an angle of π ($\cos\theta = -1$) and blows up at an angle of 0 ($\cos\theta = 1$)— this result is expected for events dominated by an Exchange channel. A

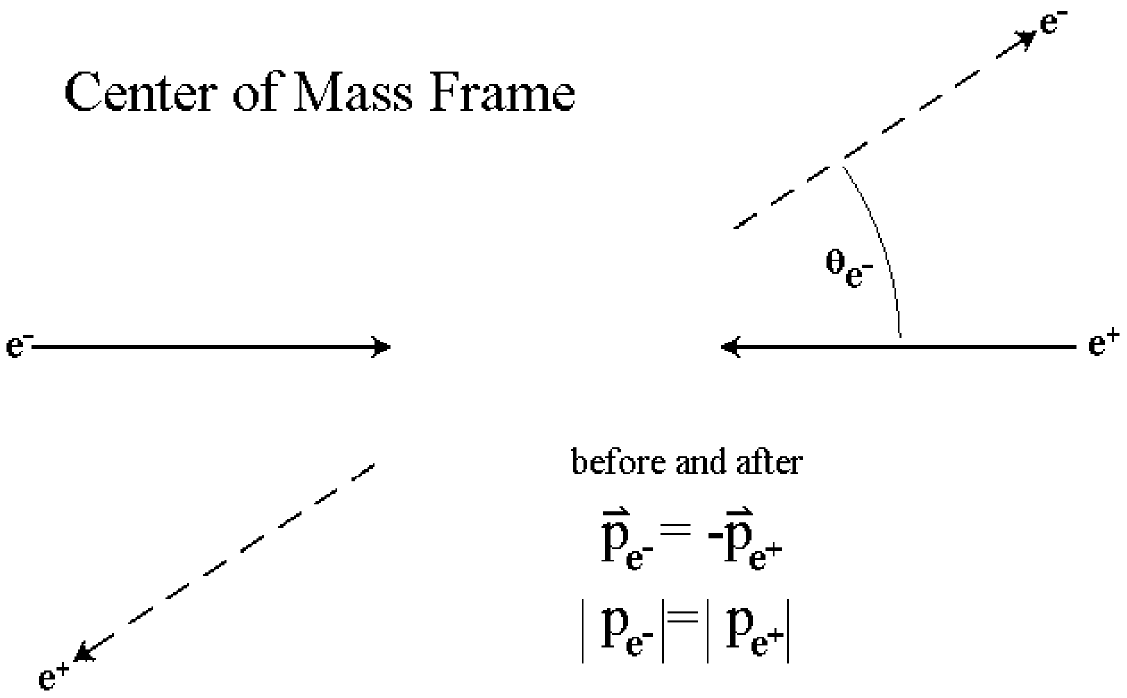

Figure 4.10: A Bhabha event in the Center of Mass frame has the electron and positron momenta back to back and with equal magnitudes. The scattering angle of the electron (θ_{e^-}) is given by Equation 4.1 and is plotted with respect to $\cos\theta$ in Figure 4.11.

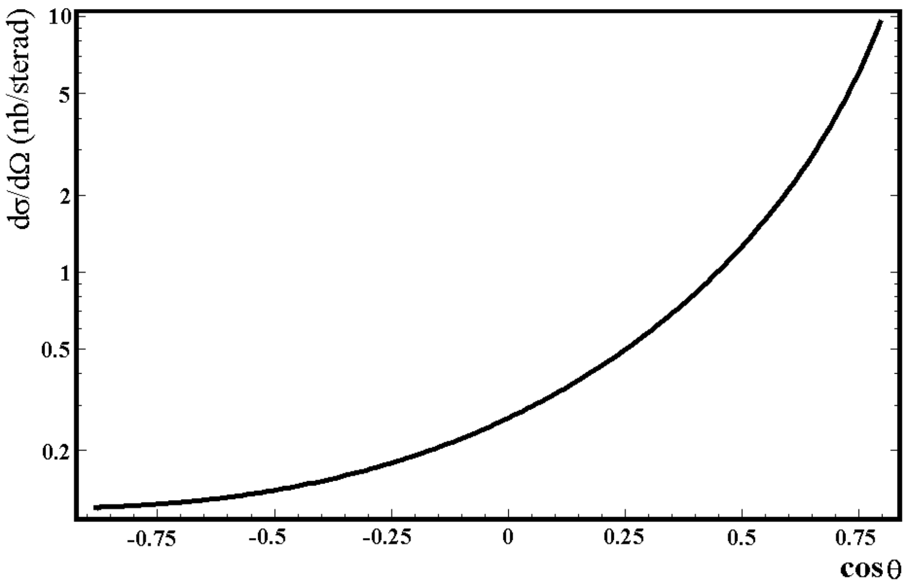

Figure 4.11: The differential cross section of a bhabha event versus $\cos\theta$. Plotted results are for the Center of Mass angles that are covered by the BaBar detector.

plot of the differential cross section for Bhabha reactions (Equation 4.1) versus the Center of Mass angles that are covered by the BaBar detector is shown in Figure 4.11 for the case in which the Center of Mass energy is 10.58 GeV—that of the BaBar experiment.

$$\frac{d\sigma}{d\Omega} = \frac{\alpha}{8E_{CM}}\left(\frac{1+\cos^4\frac{\theta}{2}}{\sin^4\frac{\theta}{2}} + \frac{1+\cos^2\theta}{2} - \frac{2\cos^4\frac{\theta}{2}}{\sin^2\frac{\theta}{2}}\right) \tag{4.1}$$

where α is the fine structure constant and equals $\sim 1/137$.

4.2.2 Radiative Bhabhas

A Radiative Bhabha event is simply a Bhabha event in which either track in the electron/positron pair has undergone radiation ($e^+e^- \longrightarrow e^+e^-\gamma$). A small percentage of radiated photons will subsequently convert to form another e^+e^-pair. Most photons will simply travel through the detector until striking the EMC, being measured as an energy deposit. For a photon to be included within my efficiency studies, it must not only be recorded within the EMC but it must pass several other tracking and reconstruction criteria that were determined by the particle ID group. These criteria, which allows a photon candidate to pass into a reconstructed track list called GoodPhotonsLoose, are[21]:

- Each candidate must be a single EMC deposit that is not matched with any charged track path.
- Each candidate must have a minimum energy deposit inside the EMC of 0.030 GeV
- The maximum lateral moment for each candidate is 0.8, where the lateral moment is a measure for the spread of the EMC cluster.

Only photons passing these criteria will be used in determining whether or not an event is a Radiative Bhabha event instead of simply a Bhabha event.

There are several different classes of radiation that a high-energy track may undergo, not all of which will result in the same photon reconstruction efficiency: Initial State Radiation, Final State Radiation, and Bremsstrahlung.

Initial state radiation events are those in which a photon is radiated before any other interaction takes place. Most initial state radiation events will radiate along the beam pipe direction and so the photon in such events will often be unobserved.

Bremsstrahlung radiation is a type of electromagnetic radiation caused by the change in velocity of an electromagnetic particle, such as when an electron collides with material. Final state radiation is the name given to the situation in which one of the final state particles, produced after the primary interaction, has undergone radiation. In Radiative Bhabha events, the final state radiation and Bremsstrahlung events are similar in that both result in a high correlation between the direction of the radiation and the direction of the radiating track (Figure 4.12). This high correlation between the radiation and the radiating track will sometimes result in an overlap, or merging, of their associated EMC

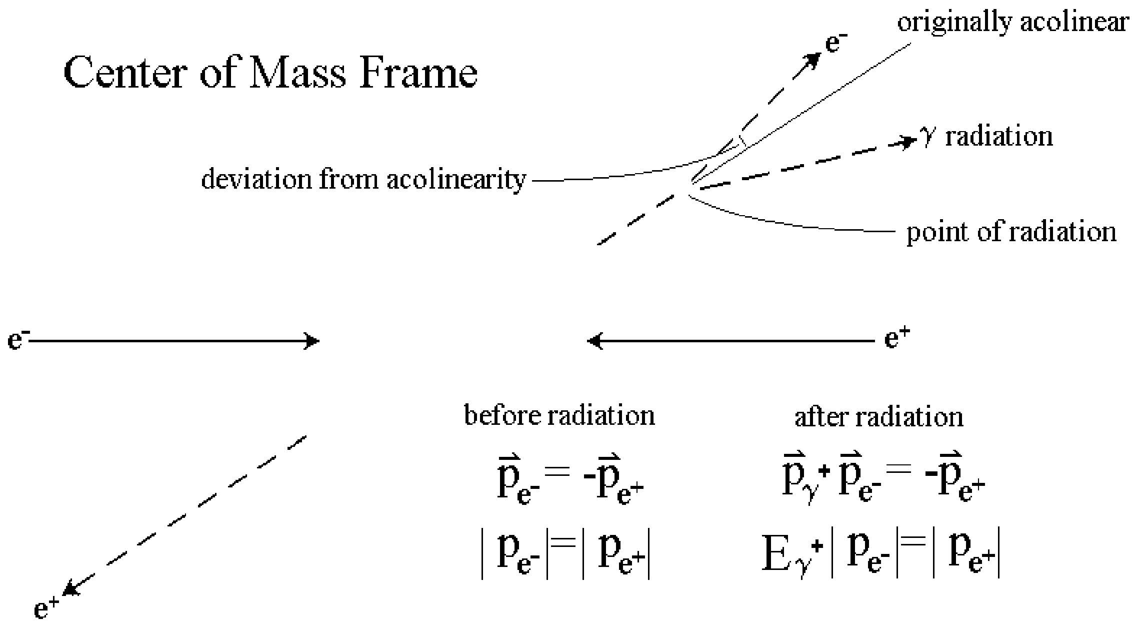

Figure 4.12: In a Bremsstrahlung or final state radiation event, one member of the original electron/positron pair subsequently emits a photon (in this case, the electron). The emission of the photon results in a change of direction for the original track that also results in a deviation from perfect acolinearity. The magnitude of this deviation depends on the point of radiation in relation to the IP and the EMC, the energy of the photon (E_γ), and the angle between the photon and the radiating track.

signals. Because photons are only measured by the EMC, while the radiating track can be measured by the SVT, the DCH, and the EMC, the two EMC clusters could be merged, which would result in the radiated photon being unmeasured. Because the radiating track is already pointing to the merged EMC cluster, the track-fitting algorithms will often assign the whole merged EMC cluster's energy, including the photon's, to the radiating track. Further discussion of this problem is left until Section 5.2.5.

4.2.3 Photonic Conversions

Photons with an energy greater than twice the mass of the electron ($E_\gamma > 1.02\mathrm{MeV/c^2}$) have a finite probability to convert into a electron/positron pair when they are in the presence of an electromagnetic field. This probability of conversion is directly related to the intensity of the electromagnetic field encountered by the photons. The electron/positron produced in a Photonic Conversion will hereby be referred to as the "conversion daughter track(s)".

For the BaBar experiment, the probability of conversion is dictated by the amount of inactive material present in the BaBar detector. Since the electromagnetic field in matter (due to the Coulomb field of the nuclei in the material) is much larger than the electromagnetic field in air, the probability of conversion sharply increases when a photon travels through the matter. The "point of conversion" distributions of Photonic Conversions with the BaBar detector will roughly mimic its matter density distribution.

Whenever a photon converts, the resultant electron/positron pair must share the available energy. Since the BaBar detector has a reconstruction bias towards higher-energy tracks, this energy sharing is of direct interest to my efficiency studies. The fraction of an electron's energy to the converted photon's energy for various photon energies can be seen in Figure 4.13. Since electrons and positrons have identical masses, they will also have identical energy distributions with respect to the converted photon. Within Figure 4.13, events in which (E_{e^-}/E_γ) is close to 0 or 1 have either the electron or the positron with a very low energy. The low-energy track in these events will likely be unreconstructed because of the BaBar detector's low-energy reconstruction inefficiencies.

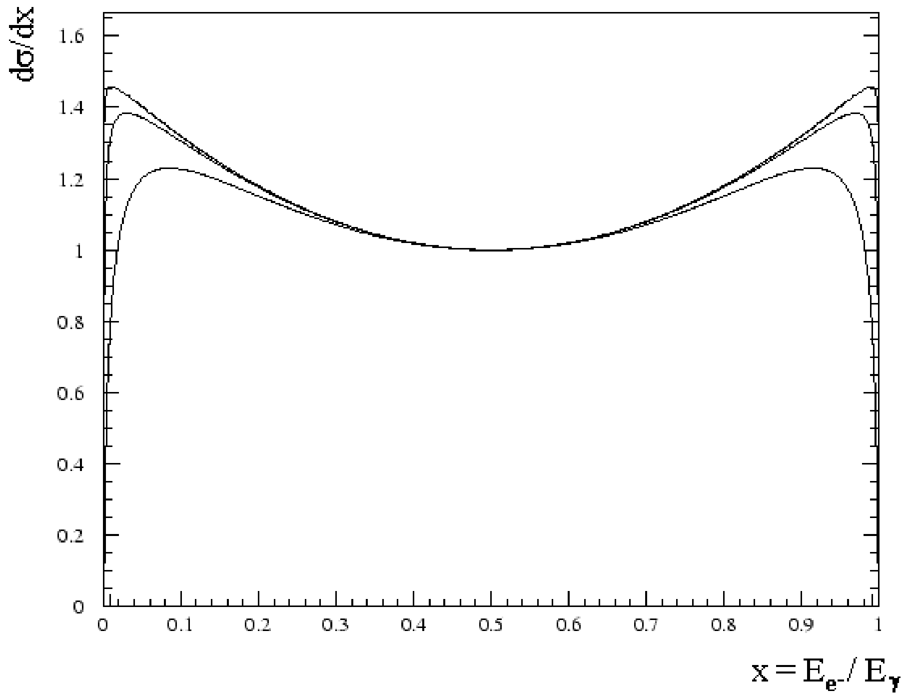

Figure 4.13: The energy sharing distribution (E_{e^-}/E_γ) between a converted photon and its daughter electron at photon energies of 0.1 (bottom), 1, and 10 (top) GeV. All cross sections have been normalized to 1 at a value of x = 0.5. These distributions are made by assuming that the conversion has occurred in aluminum, yet because the energy sharing shows very little material dependence, these distributions also represent the energy sharing for most materials [22] [23].

Chapter 5

Obtaining the Data Sample

As explained in Section 4.2, I have chosen to use Bhabha and Radiative Bhabha events for my efficiency studies of the BaBar PCF. Bhabha and Radiative Bhabha events are produced in large numbers within the BaBar experiment as it is running at an e^+e^- collider (Table 3.1). Because there is a very high event rate in the BaBar detector, in order to reduce computer storage space and dead-time, the BaBar experiment must be very selective with respect to which events it will retain. Since the BaBar experiment is primarily interested in $B - \overline{B}$ events and various other hadronic reactions, triggering and recording a large number of Bhabha events is experimentally undesirable.

The BaBar Trigger system utilizes a two-level trigger to select experimentally significant events (such as $B - \overline{B}$ events) with a high efficiency while simultaneously rejecting as many background events (such as cosmic rays and beam-induced backgrounds) as possible. The BaBar Trigger system is also used to reduce the number of experimentally insignificant events (such as Bhabha events), while at the same time retaining a sufficient number of these events for calibration and diagnostic purposes.

The first level of the BaBar Trigger system, the "Level 1 Trigger", is implemented in hardware to identify and classify relevant events. The second level of the BaBar Trigger system, the "Level 3 Trigger", subsequently analyzes all events that pass the Level 1 Trigger. The Level 3 Trigger is implemented in software to perform further event classification and to then reduce or alter several specific event classes, such as Bhabhas and Radiative Bhabhas. In this chapter, I will examine the BaBar Trigger system and reconcile this project's specific requirements in order to obtain an unbiased data sample of Bhabha and Radiative Bhabhas.

Depending on its results within the BaBar Trigger system, an event could be output into different data streams. Every event passing certain levels of the BaBar Trigger system (Level 1, Level 3, and various sub-levels), including Bhabha and Radiative Bhabhas, is stored in several global data streams containing all types of event classes. Experimentally significant event classes, such as $B - \overline{B}$ events, are also separated into specific data streams. Since Bhabha and Radiative Bhabha events are mainly used for diagnostic and calibration purposes, they are not separated from the global data streams. In order to obtain an appropriate data sample of Bhabha and Radiative Bhabha events for my efficiency studies, I must separate them from all other types of events in the global data streams. Therefore, I have written a "Bhabha Selector", a computer algorithm used to determine if an event is either a Bhabha or Radiative Bhabha event that is suitable for this project's analysis. In this chapter, I will examine and explain my Bhabha Selector and its relevance to this project. Once an appropriate sample of Bhabha and Radiative Bhabha events have been selected, the efficiency studies of the PCF can then be performed.

5.1 The BaBar Trigger System

During normal operation of the BaBar experiment, the vast majority of events triggered by the BaBar detector system have very little physics of interest. Typical production rates for experimentally significant physics processes can be seen in the third column of Table 5.1. There is a combined production rate of less than 200 Hz whereas the total event production rate at the BaBar experiment is $\sim$ 20000 Hz. The BaBar Trigger system is primarily designed to eliminate a significant percentage of backgrounds while retaining

Event Type	Cross section (nb)	Production Rate (Hz)	Level 1 Trigger Rate (Hz)
$b\overline{b}$	1.1	3.2	3.2
other $q\overline{q}$	3.4	10.2	10.1
e^+e^-	$\sim$ 53	159	156
$\mu^+\mu^-$	1.2	3.5	3.1
$\tau^+\tau^-$	0.9	2.8	2.4

Table 5.1: The expected cross section at the PEP-II e^+e^- collider, the actual production rate in the BaBar detector, and the rate at which each type passes the Level 1 Trigger([15] 83).

most experimentally significant physics processes. The Level 1 Trigger is designed to have an output rate of less than 2 kHz while the Level 3 Trigger then reduces the total trigger output to $\sim$ 120 Hz.

5.1.1 The Level 1 Trigger

The Level 1 Trigger uses data from three detector subsystems in order to reject backgrounds: the DCH, EMC and IFR. The DCH is used to reject tracks with a low transverse momentum (relative to the beam direction, or p_{xy}). The EMC trigger compares the measured calorimeter energy to expected thresholds for each desired physical process and records the timing distributions for later analysis by the Level 3 Trigger. The IFR trigger is used to select cosmic rays or events with muons using both the IFR's hit pattern and timing information. By associating the three detector trigger responses with values expected for physically significant events, the Level 1 Trigger decides if an event is aborted or is passed on to be analyzed by further reconstruction software, such as the Level 3 Trigger. The output rate of the Level 1 Trigger is shown in the last column of Table 5.1. More than 99.9% of all $B-\overline{B}$ events pass the Level 1 Trigger, while many other physics processes, including Bhabha events, also pass with very high efficiencies.

5.1.2 The Level 3 Trigger

The Level 3 Trigger system responds to the entire output of the Level 1 Trigger and performs a reduction and flagging of events needed for calibration purposes as well as a second stage rate reduction on background processes. The output rate of the Level 3 Trigger is designed to be $\sim$ 90 Hz for important physics processes and $\sim$ 30 Hz for calibration and diagnostic purposes. The Level 3 Trigger is a software filter that is run over the complete data from each event; it uses more complete information than the Level 1 Trigger, which is based only on hardware. The Level 3 Trigger is run in three stages:

- First, events are classified from data received by the Level 1 Trigger and its associated trigger systems.
- Second, each event is then tested using a series of scripts which are dependent on the event classification and that construct parameters of interest from the available event data, such as the Total EMC Energy.
- Third, an event is classified by its constructed parameters and any required filtering is then performed by the Level 3 filters.

The Level 3 Trigger filters perform event classification and background reduction. There are two orthogonal filters, one based on the DCH data and one based on the EMC data. Both filters are dominated by Bhabha events since they are the most common physical processes that are not considered a background. The acceptance of Bhabha events is reduced in favour of other more experimentally significant physical processes, such as $B\overline{B}$ events. This rate reduction of Bhabha events is accomplished by a Bhabha veto filter that relates an event's track parameters to those of expected Bhabha and Radiative Bhabha events. The output rates of Bhabha and Radiative Bhabha events are adjusted to generate an approximately flat distribution in the polar angle (θ). Since

Event Type	Rate (Hz)
Hadrons, $\tau^+\tau^-$, and $\mu^+\mu^-$	16
Other QED, 2-photon events	13
Unidentified Bhabha backgrounds	18
Beam-induced backgrounds	26
Total experimentally relevant	73
Calibration Bhabhas (e^+e^-)	30
$\gamma\gamma$, Radiative Bhabhas ($e^+e^-\gamma$)	10
Random triggers and cosmic rays	2
L1, L3 pass through diagnostics	7
Total calibration/diagnostics	49

Table 5.2: The rate of different event types after passing the Level 3 Trigger. L1, L3 pass through diagnostics are also known as "Prescale" collections, which will be discussed in Section 5.1.3([15] 92).

the unaltered distributions are largely forward peaked (Equation 4.1 and Figure 4.11), this adjustment favours high-angle scatters that have a lower probability of occurrence. Typical Level 3 Trigger output rates are shown in Table 5.2. Comparing the rates shown in Table 5.2 to those in Table 5.1, we see that the Level 3 Trigger greatly reduces the Bhabha event rate yet retains almost all hadronic, $\tau^+\tau^-$, and $\mu^+\mu^-$ event

5.1.3 Usage of Prescale Data Samples

An accurate efficiency study of the BaBar PCF requires an unbiased data sample. Performing an analysis on the Level 3 Trigger output events, with the Bhabha and Radiative Bhabha event θ distributions flattened, is undesirable because it will produce biased results. An unbiased sample must therefore be obtained by choosing events that have not gone through the Bhabha veto filter. The Level 1 Trigger flags and passes Bhabha events but does not adjust their distributions since it is only performing an overall background reduction. Therefore, the data sample for this analysis is obtained from two prescale data streams to be described below, which are created before the Level 3 Trigger output yet after the Level 1 Trigger output.

At different stages in each of the trigger systems, a set percentage of all events are marked for calibration and diagnostic purposes regardless of the overall Level 1 Trigger or Level 3 Trigger decisions. These events are marked and stored in "Prescale" collections and represent collections of events unbiased by certain trigger selections. As the output rates of the first few levels of the BaBar Trigger systems are many times the available analytical power of the BaBar experiment (hence the usage of the Trigger system) and because the majority of prescaled events are inconsequential to the BaBar experiment, the percentage of events that are prescaled is kept small. The list of available Prescale collections along with their prescale factor (the fraction of events prescaled) can be found in [24].

The "L3OutL1Open" Prescale collection consists of output from the Level 1 Trigger with the Level 3 Trigger turned off (or open) and has a prescale factor of 200. The "L3OutDchEmcPreVeto" Prescale collection is taken from events that have passed the two orthogonal DCH and EMC filters, yet have not undergone the Bhabha veto and have a prescale factor of 50. Since the Bhabha veto filter is the point along the BaBar Trigger system at which Bhabha event distributions are altered, any Prescale collection that is made before this point is appropriate for my efficiency studies of the BaBar PCF.

The data sample used for my efficiency studies consists of events from the following two prescale collections:

- The Level 1 Trigger output collection with the Level 3 Trigger left open: 'L3OutL1Open'
- The Level 3 DCH and EMC filter output collection taken before the Bhabha Veto filter: 'L3OutDchEmcPreVeto'

The combined production rate for these two Prescale collections is 2.5 % of the total data collected during a BaBar experimental run. My Bhabha Selector has been used on events from these two Prescale collections. All events are taken from the lists of "good runs" with measured integrated luminosities of 452, 20212, and 21329 pb^{-1} for the 1999, 2000, and 2001 BaBar experimental data runs respectively[25].

5.2 Bhabha Selector Code

The Prescale collections mentioned in the previous section are global data streams that contain a full spectrum of events created at the PEP-II e^+e^- collider. I have written a "Bhabha Selector" in order to obtain a Bhabha and Radiative Bhabha data sample needed to perform my efficiency studies on the BaBar PCF. This Bhabha Selector employs increasingly specific cuts on an event's data in hopes of eliminating from the data sample as much background contamination as possible while simultaneously retaining a large percentage of suitable Bhabha events. The data sample created by the Bhabha Selector should contain Bhabha events with the possibility of radiation and subsequent conversions. The possibility of a Photonic Conversion being either reconstructed or undetected by the BaBar detector must be taken into consideration when choosing the selection criteria. Events without photons or in which a photon has not converted are used for the testing of the Bhabha Selector while events with Photonic conversions are used for my efficiency studies of the BaBar PCF.

5.2.1 Global Event Cuts

In this and the next few sections, the Bhabha Selector cuts developed for this analysis are introduced and justified. The Bhabha Selector's first level of cuts are global in the sense that they are simply a very loose check on whether or not an event has the general characteristics of a Bhabha or Radiative Bhabha event, yet they do not determine if the event actually is one.

A Bhabha event contains two, and only two, high-energy charged tracks, each at approximately half the Center of Mass beam energy, in the Center of Mass frame. A Radiative Bhabha event also contains two high-energy charged tracks, however, at least one of the tracks must be below half the Center of Mass beam energy since it has undergone a radiation. If one of the radiated photons subsequently converts into an electron/positron pair, a Radiative Bhabha event could also contain an extra two charged tracks if both of the conversion daughter tracks were reconstructed. To reduce the errors in my efficiency studies, I have chosen to exclude events that contain more than one Photonic Conversion. This exclusion results in a upper limit of four on the number of charged tracks in an event within my data sample. Since I must allow for the possibility of a single conversion being only partially reconstructed, I also select into my data sample events with three charged tracks. For calibration purposes, I will also retain many two charged track events such as Bhabha events and Radiative Bhabha events without conversions. By simply restricting the number of charged tracks within an event to between two and four, I am able to eliminate a large portion of non-Bhabha events.

All the cuts used in my Bhabha selector are described as below:

Cut 1 *There must be between two and four charged tracks in the event.*

This cut allows for the possibility of:

- A radiated photon that does not convert, or which converts and neither conversion daughter track is reconstructed (two charged track event)
- If a photon converts and only one conversion daughter track is reconstructed (three charged-track event)

- If a photon converts and both conversion daughter tracks are reconstructed (four charged-track event)

Within each Bhabha event, partially reconstructed conversions will carry an excess total charge of $\pm 1e$. Each electron/positron pair, either from the primary Bhabha interaction or from a Photonic conversion, will be electrically neutral. It is thereby reasonable to assume that I can eliminate from my data sample any events with a charge more than $\pm 1e$. However, after examining the background contamination in my data sample, I found that there are a small number of events containing both a single track originating from a Photonic Conversion and a single background track having the same charge. Therefore, to include all relevant Radiative Bhabha events within the data sample, I can only impose the cut that all charged tracks within an event can not have the same charge, since the primary electron/position pair from all Bhabha events must always be oppositely charged.

Cut 2 *All tracks within an event cannot have the same charge.*

An essential characteristic of Bhabha events is that they produce two high-energy tracks originating near the IP. These tracks will be further labeled as the "Bhabha-tracks" since any other tracks in an event should be either from background processes or the result of a converted photon that was radiated from either of these Bhabha-tracks.

The BaBar experiments track reconstruction software classifies events by the "quality" of their measurements. If a track satisfies a certain specific set of requirements, it can be classified as a "very loose" track, a "loose" track, etc... or, if the track is very well measured, a "very tight" track. Since the two Bhabha-tracks must be high-energy tracks, my Bhabha selector requires that they satisfy at least one set of the reconstruction quality cuts. In order to keep the data sample requirements relatively open, the quality cuts for "loose" tracks have been chosen.

Cut 3 *At least two tracks within the event must satisfy the following BaBar tracking requirements for "loose" tracks[21]:*

- *The minimum transverse momentum (or momentum in the x-y plane) is 0.1 GeV/c.*
- *The maximum momentum is 10 GeV/c.*
- *More than 12 DCH Hits must be used to reconstruct the track.*
- *There is no minimum cut on the likelihood of the track-fitting algorithms.*
- *The maximum DOCA in the x-y plane is 1.5 cm.*
- *The minimum DOCA along the z axis is -10 cm.*
- *The maximum DOCA along the z axis is 10 cm.*

where DOCA stands for the Distance of Closest Approach to the IP.
Only charged tracks satisfying the tracking requirements in **Cut 3** may be considered to be Bhabha-tracks in an event.

5.2.2 Bhabha Cuts

The BaBar detector utilizes various forms of particle identification. Since a Bhabha event is an $e^+e^- \longrightarrow e^+e^-$ event, I require that my data sample specifically contain a high-energy electron/positron pair. All that is needed to determine the charge of a track is its direction of curvature within the magnetic field of the BaBar detector (Equation 3.1). As a Bhabha event requires both an electron and a positron, I can impose the simple requirement that the two Bhabha-tracks must be oppositely charged.

Cut 4 *The two Bhabha-tracks must be oppositely charged.*

Determining the particle identity of a track is considerably more complicated than determining the particle's charge. Typically, several detector systems are utilized in particle

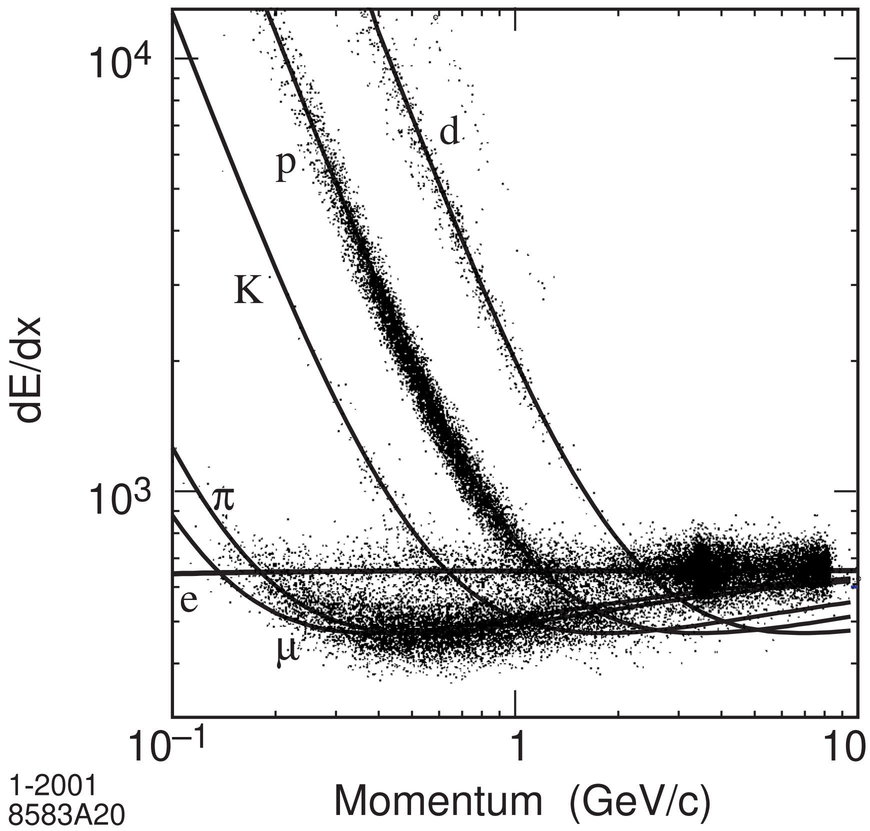

Figure 5.1: The $\frac{dE}{dx}$ distributions of the DCH versus different particle momenta for several different particle species. Each dot represents an experimental measurement while the solid lines represent the fitted distributions for each particle species.

identification, each specialized for different particle species in different energy ranges. As mentioned in Section 3.1, both the DCH (through $\frac{dE}{dx}$) and the EMC used in tandem with the DCH and SVT (through $\frac{E}{p}$) are used in electron identification. Unfortunately, the $\frac{dE}{dx}$ of the DCH is not very useful for electrons at high energies (Figure 5.1). In Bhabha events, the two Bhabha-tracks can have a momentum of up to 5.3 GeV/c. Near this momentum, the electron's $\frac{dE}{dx}$ distribution is nearly the same as the $\frac{dE}{dx}$ of pions. Therefore, I do not cut on a Bhabha-track's $\frac{dE}{dx}$ and the two high-energy Bhabha-tracks in this analysis are instead identified using their $\frac{E}{p}$.

An electron is expected to deposit all of its energy within the EMC. Because of the electron's low mass relative to its expected energy in the Bhabha events at the BaBar experiment, this energy deposited within the EMC is expected to equal the momentum of the electron as measured by the DCH and SVT. Therefore, the $\frac{E}{p}$ of an electron, or the energy deposited in the calorimeter divided by the momentum measured from the DCH and SVT, should ideally be one. In contrast to an electron, a muon will only deposit a fraction of its energy within the EMC, yet the DCH and SVT will still measure its full momentum. The $\frac{E}{p}$ of a muon is expected to be well under 0.5.

To assure that the two Bhabha-tracks are an electron/position pair, I will place a cut on their $\frac{E}{p}$. The value of this cut is decided by inspecting Figure 5.2, which shows the $\frac{E}{p}$ distribution of Bhabha-tracks passing **Cuts 1-4**. In Figure 5.2, the large peak centered at 1 contains the electron signal while the peak near zero contains μ, π, K or p. Based on Figure 5.2, a minimum $\frac{E}{p}$ cut of 0.8 is used to ensure that all Bhabha-tracks are electrons/positrons.

Cut 5 *The two Bhabha-tracks must have a minimum* $\frac{E}{p}$ *of 0.8, with no upper* $\frac{E}{p}$ *limit.*

5.2.3 Center of Mass Cuts

The Lab frame of the BaBar experiment is boosted with respect to the Center of Mass frame by a $\beta\gamma = 0.56$ to allow for precision measurements of the differences in B meson decay times. When interpreting a physical process, it is sometimes advantageous to work within the Center of Mass frame instead of the boosted Lab frame.

The two highest-energy tracks in the Center of Mass frame that have satisfied **Cuts 3**, **4** and **5** are chosen to be the two Bhabha-track candidates and are the focus of all "Center of Mass cuts". The Center of Mass cuts are used to ensure that an event in question is indeed a $e^+e^- \longrightarrow e^+e^- + \gamma$ event and not a similar physics process that

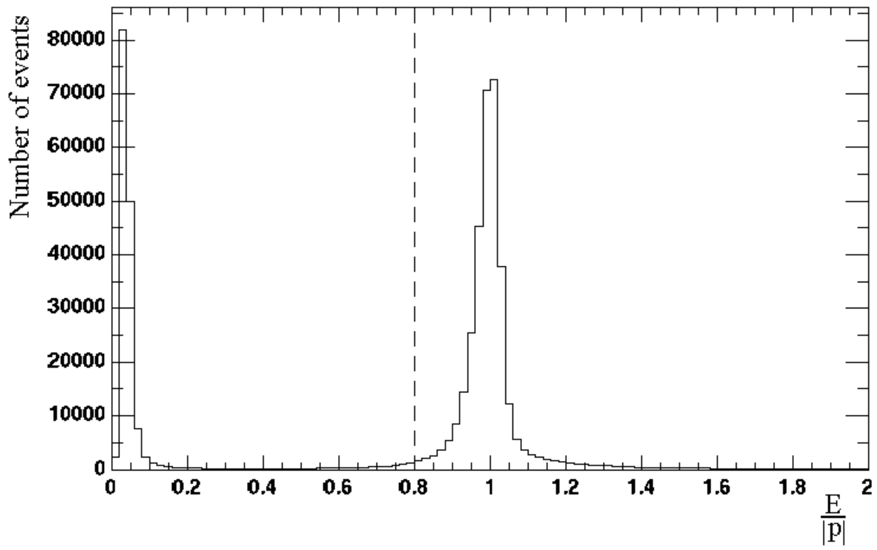

Figure 5.2: The Energy of tracks, as measured by the EMC, divided by the magnitude of the track's momentum, as measured by the DCH and SVT, for both Bhabha-tracks in all events passing **Cuts 1** to **4**. To ensure that all Bhabha-tracks are electrons/positrons, a minimum $\frac{E}{p}$ cut of 0.8 is used and is denoted with the dashed line.

could also satisfy the first five Bhabha Selector cuts. Any other charged tracks within an event will be ignored until later cuts as they are assumed to be the result of either converted photons or background processes.

In the Center of Mass frame, both the electron and positron beams have the same energy: half that of the $\Upsilon(4S)$ resonance or approximately 5.3 GeV each. Because the net momentum of the Center of Mass frame is zero, in a Bhabha event, the electron/positron pair produced after a collision of the beams must be back-to-back, or acollinear. A typical Bhabha event can be viewed in Figure 4.10, while a Radiative Bhabha event is shown in Figure 4.12. Only allowing for a small to medium degree of radiation requires that the two Bhabha-tracks remain approximately acollinear even after one of them has radiated. Figure 5.3 is a plot of the difference between the two Bhabha-track angles for all events passing **Cuts 1-5**. In Figure 5.3, the large peak at zero suggests a predominance of either non-radiative or slightly radiative Bhabha events. To retain all these events, a loose cut

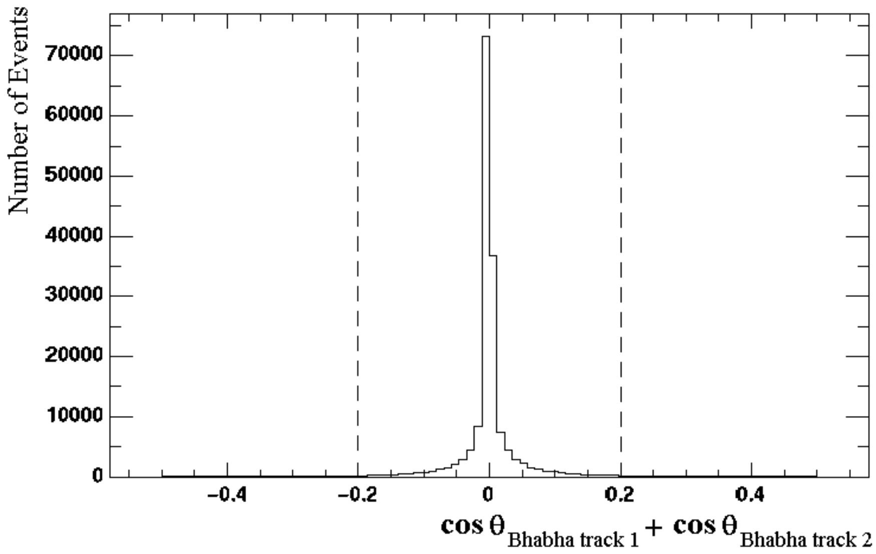

Figure 5.3: $\cos\theta$ of one Bhabha- track plus $\cos\theta$ of the other Bhabha-track for all events passing **Cuts 1** to **5** in my Bhabha Selector. The dashed lines denote $\pm$ 0.2, which have been chosen as maximum values for events in my Bhabha Selector.

requiring a $|\cos\theta_{\text{track1}} - \cos\theta_{\text{track2}}|$ of below 0.2 has been chosen for the acolinearity of Bhabha-tracks for events in this project's data sample.

Cut 6 *The two Bhabha-tracks must have a* $|\cos\theta_{\text{track1}} - \cos\theta_{\text{track2}}|$ *of below 0.2 in the Center of Mass frame.*

As mentioned for **Cut 1**, I have chosen to exclude events with multiple conversions from this data sample. One method of ensuring that there are not multiple conversions in an event is to ensure that only one and not both of the Bhabha-tracks radiate. Working within the Center of Mass frame, it is possible to distinguish a Radiative and Non-Radiative Bhabha-track: The Non-Radiative track will retain approximately half the total available Center of Mass energy, or $\sim$ 5.3 GeV/c, while the Radiative track will have a continuous energy distribution that is peaked at 5.3 GeV/c and extends down to 0 GeV/c. To maximize the acceptance of Bhabha events, while simultaneously minimizing

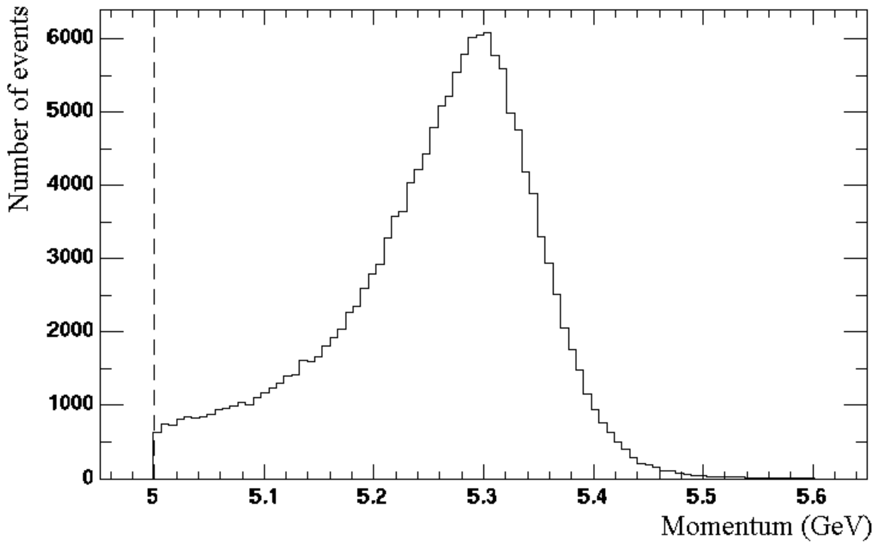

Figure 5.4: The momentum distribution of the highest momentum Bhabha-track in the Center of Mass for all events passing **Cuts 1** to **6**. A 5 GeV/c minimum cut, represented by the dashed line, has been placed on the momentum of the highest Center of Mass Frame track to ensures that at least one Bhabha-track is either non or only slightly radiative.

the allowable radiation from the Bhabha-tracks, I require a minimum momentum of 5 GeV/c for the highest momentum Bhabha-track in the Center of Mass frame (Figure 5.4 and 5.5).

Cut 7 *At least one Bhabha-track must have a momentum greater than 5 GeV/c in the Center of Mass frame.*

This cut is to ensure that at least one of the two Bhabha- tracks in each Bhabha event does not significantly radiate as this would unnecessarily over complicate the data sample. This cut also helps to ensure that the event could be a Bhabha event by forcing at least one of the two Bhabha-tracks to retain almost half the Center of Mass energy.

The charged track with the second highest momentum in the Center of Mass frame, even if it is also above 5 GeV, is hereby considered the “Radiative Bhabha-track” since

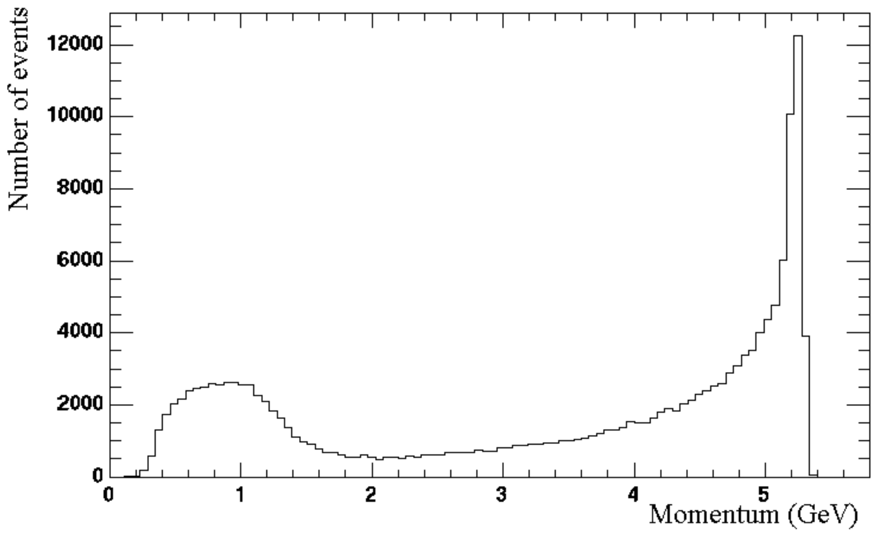

Figure 5.5: The momentum distribution of the second highest momentum Bhabha-track in the Center of Mass frame for all events passing **Cuts 1** to **6**. The momentum distribution peaks at 5.3 GeV/c (half the Center of Mass energy) and extends down to 0 GeV/c. The low-energy peak is from backgrounds.

it is the more likely of the two Bhabha-tracks to have radiated. Similarly the highest energy charged track, which must specifically satisfy **Cut 7**, is hereby considered the "Non-Radiative Bhabha-track".

5.2.4 Lab Frame Cuts

In a Radiative Bhabha event, the energy distribution of the Radiative Bhabha-track should decrease exponentially from its maximum Non-Radiative energy of 5.3 GeV. However, because of background contamination, the Radiative Bhabha-track's energy spectrum rises at low energies (Figure 5.5). Therefore, even at the cost of sacrificing any significantly radiating events, I require a minimum energy cut on the Radiative Bhabha-track in order to reduce backgrounds.

In order to obtain the minimum energy cut on the Radiative Bhabha-track, I must further examine the types of radiation (see Section 4.2.2) contained within my data sample. Specifically, events with a Bremsstrahlung radiation (Bremsstrahlung events) might require special attention as the radiation is usually both high energy and highly correlated to the direction of the radiative track. While it is not necessary to eliminate Bremsstrahlung events from the data sample, it is important to include them when defining the cuts on the Radiative Bhabha-track.

In order to detect Bremsstrahlung events, I compare the direction of any radiated photons in an event to the direction of the Radiating Bhabha-track (Figure 5.6). In Figure 5.6, only the θ direction is shown as the ϕ direction of the Radiative Bhabha-track is affected by the magnetic field of the BaBar detector. The peak centered on zero in Figure 5.6 signifies the presence of Bremsstrahlung events while the flat distribution underneath this peak is likely due to final state radiation events. Because Bremsstrahlung radiation tends to be higher energy than final state radiation, this peak can be isolated from the events underneath by requiring the highest energy photon in an event to be above 0.5 GeV. Figure 5.7 **(a)** shows the photon energy spectrum of the highest-energy photons in an event (recalling that all photons must pass the cuts mentioned in Section 4.1.2 also) for events that are inside the peak of Figure 5.6, while Figure 5.7 **(b)** shows this same photon energy spectrum for the events that are outside the peak of Figure 5.6. The photon energy spectrum in Figure 5.6 **(b)** is what might be expected for simple radiative events while the photon energy spectrum of Figure 5.7 **(a)** and above a momentum of 0.5 GeV/c is what might be expected for Bremsstrahlung events. Therefore, I have specifically defined a Bremsstrahlung event as an event which has $|\theta_{Rad\,Track} - \theta_\gamma| < 0.02$ and a photon momentum above 0.5 GeV/c.

An examination of the momentum spectrum for the Radiative Bhabha-track in the Lab frame (Figure 5.8 **(a)**) indicates that I should impose a low momentum cut of 2.5

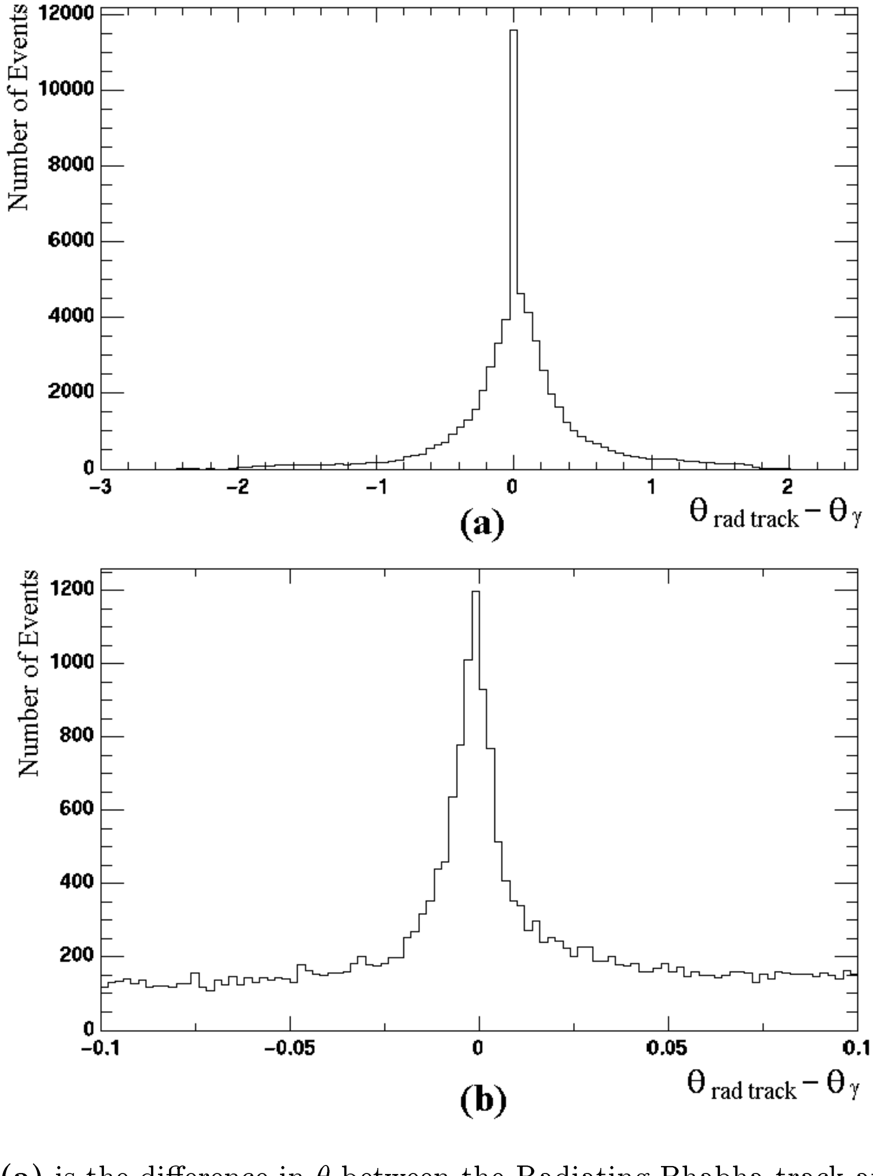

Figure 5.6: **(a)** is the difference in θ between the Radiating Bhabha-track and the highest-energy photon for all events passing **Cuts 1** to **7**. **(b)** shows a blow-up of **(a)** for $|\theta_{Rad\,Track} - \theta_\gamma| < 0.05$ rad.

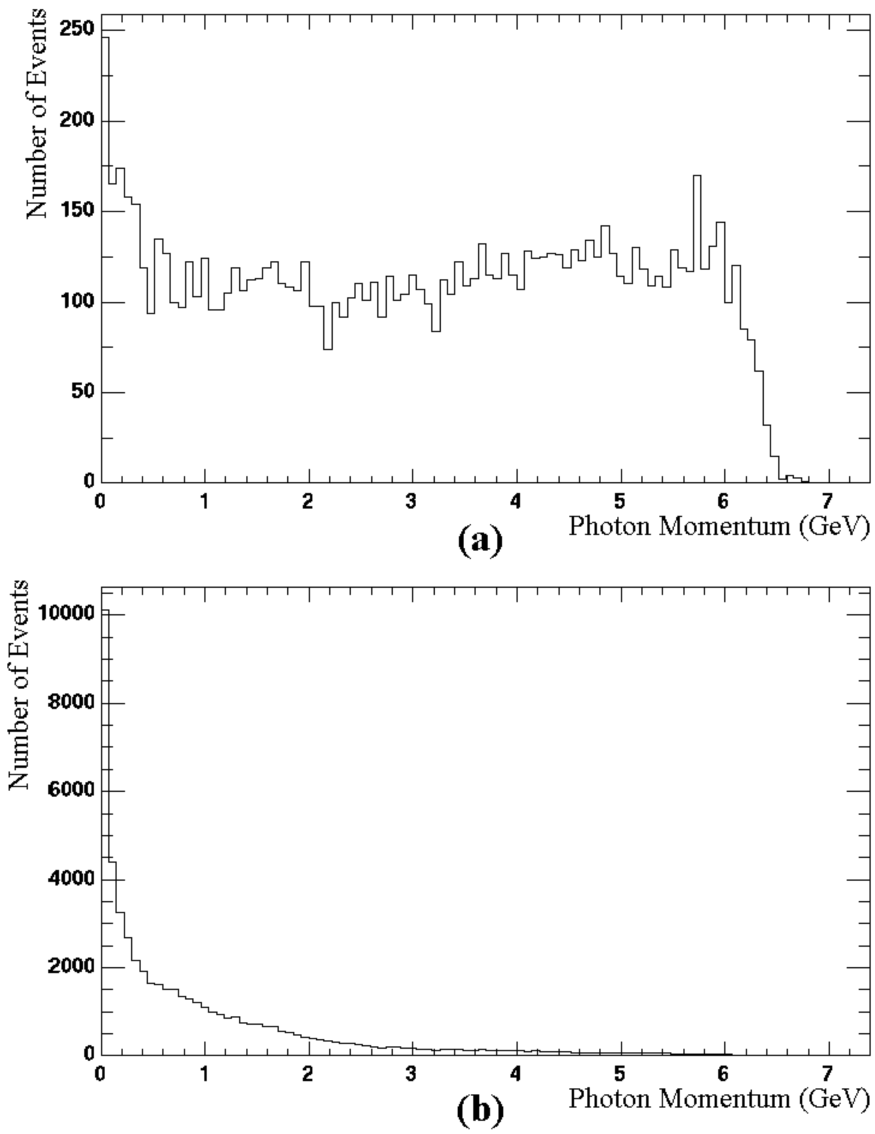

Figure 5.7: **(a)** is the energy spectrum of the highest-energy photon for events passing **Cuts 1** to **7** and that have a $|\theta_{Rad\,Track} - \theta_\gamma| < 0.02\,\mathrm{rad}$. **(b)** shows the energy spectrum of the highest-energy photon for events that have a $|\theta_{Rad\,Track} - \theta_\gamma| > 0.02$ rad.

GeV/c. However, if I take Figure 5.8 **(a)** and exclude all events for which the Radiating Bhabha-track has also undergone Bremsstrahlung radiation (that are Bremsstrahlung events), I obtain Figure 5.8 **(b)**. Figure 5.8 **(b)** indicates that I can use a low momentum cut of only 1 GeV/c on the Lab frame momentum of the Radiative Bhabha-track. It is more desirable to use this lower cut because I would be able to retain many more significantly radiative events in my data sample

Cut 8 *The Radiative Bhabha-track must have a momentum of more than 1 GeV/c in the Lab frame.*

5.2.5 Quality Cuts

After passing **Cuts 1-8** of my Bhabha Selector, the events of my data sample should be almost entirely made up of Bhabha and Radiative Bhabha events with a low percentage of background contamination. All further Bhabha Selector cuts will now focus on ensuring that an event can be useful to my efficiency studies.

As I require the events within my data sample to allow for the possibility of a Photonic Conversion, particular care must be taken to ensure my ability to measure all possible Photonic Conversion daughter tracks. The BaBar detector will never be able to reconstruct a charged track if it has a momentum too low to reach the SVT, or if the track is directed down the beam pipe. However, if a charged track has neither of these characteristics, there are several possible cuts on an event's parameters that will allow me to increase the reconstruction efficiency of the BaBar detector.

The BaBar detector's EMC is separated into two parts: the barrel region and the forward endcap. As mentioned in Section 3.1.4, the forward-most region of the forward endcap has a lower reconstruction efficiency than the rest of the forward endcap and the

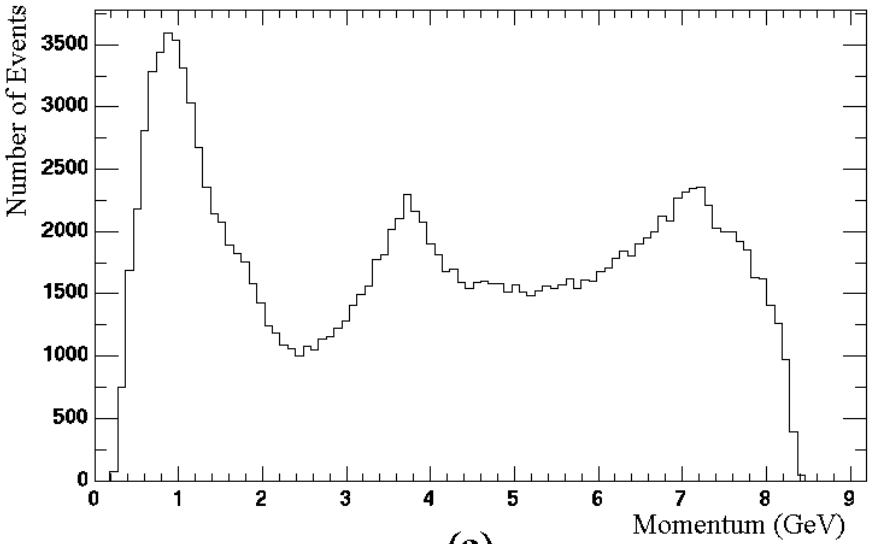

(a)

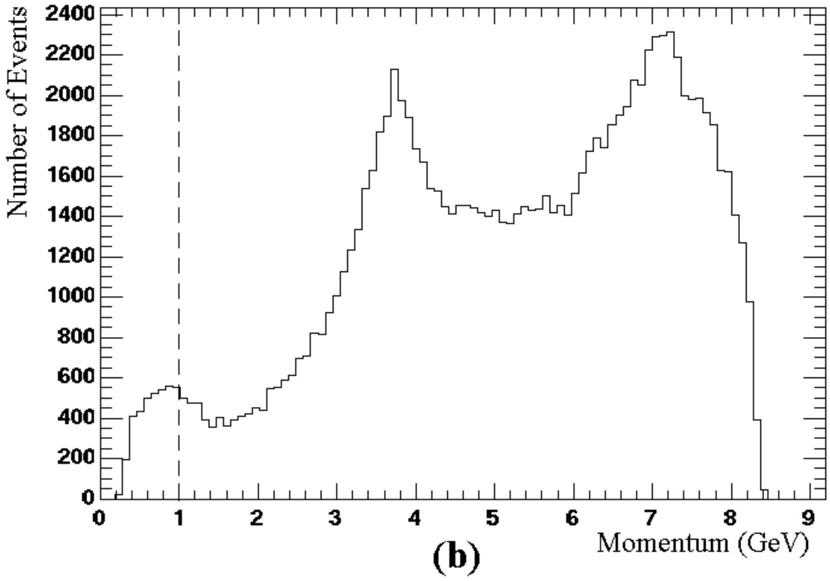

(b)

Figure 5.8: **(a)** is the momentum of the Radiating Bhabha-track in the Lab frame for all events passing **Cuts 1** to **7**. **(b)** shows this same momentum distribution with the added requirement that the Radiating Bhabha-track has not undergone any Bremsstrahlung radiation (or is not a Bremsstrahlung event). The dotted line in **(b)** shows the 1 GeV/c low momentum cut that is used to eliminate background from my data sample.

barrel region, collectively called the fiducial region. This difference in reconstruction efficiencies is mainly because some of the SVT electronics are placed in front and at the same angle with respect to the IP as is the forward most part of the forward endcap. Since the rate of conversion is so highly correlated to the matter density of the BaBar detector (Section 4.2.3), the SVT electronics cause a large forward dominated peak in the conversion distributions. Therefore, I have chosen to completely disregard any measurements outside the fiducial region of the EMC, or outside $-0.78 \leq cos(\theta) \leq 0.92$.

Cut 9 *All tracks in an event must be within the fiducial region of the EMC.*

It is easy to ensure that no charged track strike outside the fiducial region of the EMC by simply restricting its angular distribution. However, since I also allow for the possibility of partially reconstructed Photonic Conversions within my data sample, I must also place an angular restriction on the direction of all Photonic Conversions, reconstructed or otherwise, to ensure that no conversion daughter tracks can strike outside the fiducial region of the EMC. By calculating a direction of radiation using the primary electron/positron pair in each Bhabha event, it is possible to determine the direction of any radiated and subsequently converted photons regardless of their being measured. Using this calculated direction of radiating, it is possible to restrict the radiation's angular distributions to inside the fiducial region.

In calculating this direction of radiation, I will examine the type of events within my data sample. A simple Radiative Bhabha event contains at least 3 tracks: The two charged Bhabha-tracks and a radiated photon. Since the photon is not electrically charged, it will not curve within the BaBar magnetic field and so it will travel in a straight line after having been radiated. By subtracting the four-vectors of the two Bhabha-tracks—which is completely determined by the SVT and DCH detector systems (the tracking systems)—from the Center of Mass four-vector (Equation 5.1), I can predict the direction of any single photon radiation or subsequent conversions thereof. This calculation does not rely on anything beyond the measurement of the two Bhabha-tracks and so leaves open the possibility of the conversion going undetected.

$$\text{Calculated Radiation}^{\mu} = \text{CoM}^{\mu} - (\text{BT1}^{\mu} + \text{BT2}^{\mu}) \tag{5.1}$$

Where

- "Calculated Radiation$^{\mu}$" refers to the calculated radiation's four- vector
- CoM$^{\mu}$ refers to the Center of Mass frame's four-vector
- BT1$^{\mu}$ refers to the four-vector for the non-Radiative Bhabha-track
- BT2$^{\mu}$ refers to the four-vector for the Radiative Bhabha-track

Cut 10 *The calculated direction of radiation as determined by equation 5.1 must be within the fiducial region of the EMC.*

Since the direction of radiation is highly correlated to the direction of the Radiative Bhabha-track, while slightly redundant, it is prudent to also require that the directions of all Bhabha-tracks before radiation be within the fiducial region of the EMC. Since the act of radiating will affect the momentum and direction of the Radiative Bhabha-track (Figure 4.12), I will calculate its direction before radiation using the direction of the non-radiative Bhabha-track: In the Center of Mass frame, two originally non-radiative Bhabha-tracks are back-to-back. As only one of the two Bhabha-tracks in this data sample is allowed to significantly radiate (due to **Cut 7**), the direction opposite the non-radiative Bhabha-track should be equal to the direction of the Radiative Bhabha-track before it underwent radiation. The calculation for the original direction of the Radiative Bhabha-track is done by performing a parity inversion of the non-radiating Bhabha-track in the Center of Mass frame and subsequently boosting it to the Lab frame (Equation 5.2). I then restrict the angular distribution in Equation 5.2 to the fiducial region of the EMC.

$$\text{Original direction}^{\mu} = \text{Boost}(\text{CoM} \longrightarrow \text{Lab})\text{Parity}\ (\text{nRBT}^{\mu}) \tag{5.2}$$

Where

- "Original direction$^{\mu}$" refers to the direction of the Radiative Bhabha-track before it radiated
- "Boost(CoM $\longrightarrow$ Lab)" is a Lorentz Boost from the Center of Mass frame to the Lab frame
- "Parity" is a parity transformation that transforms a track's four-vector from (t,x,y,z) to (t,-x,-y,-z)
- "nRBT$^{\mu}$" refers to the elements of non-Radiative Bhabha-track's four-vector

Cut 11 *The original direction of the Radiative Bhabha-track as calculated in Equation 5.2 must be within the fiducial region of the EMC.*

In Equation 5.1, I calculated the direction of radiation assuming the most simple type of Radiative Bhabha event in which the radiative Bhabha-track radiates only a single photon. Another portion of unsuitable events for this project's data sample are events in which there are multiple radiations where a few photons have been radiated into poorly instrumented regions of the detector. Kinematically, many of these events will pass **Cut 9** and since I have already decided to include many Bremsstrahlung events in the data sample, I must also include all measured photons into Equation 5.1, giving Equation 5.3.

By including all measured photons into Equation 5.1, I am now calculating the direction of any unmeasured radiation within an event.

$$\text{Unmeasured Radiation}^{\mu} = \text{CoM}^{\mu} - (\text{BT1}^{\mu} + \text{BT2}^{\mu} - \gamma^{\mu}) \tag{5.3}$$

Where

- "Unmeasured Radiation$^{\mu}$" refers to any unmeasured radiation's four-vector
- CoM$^{\mu}$ refers to the Center of Mass frame's four-vector
- BT1$^{\mu}$ refers to the four-vector for the non-Radiative Bhabha-track
- BT2$^{\mu}$ refers to the four-vector for the Radiative Bhabha- track
- γ^{μ} refers to the four-vector sum of all measured photons in an event

If there are measured radiated photons in an event, I require that the calculated direction of unmeasured radiation as given by Equation 5.3 be within the fiducial region of the EMC. If a photon has converted, it will be undetected by the EMC and not included into Equation 5.3, hence it will be considered part of the unmeasured radiation. Assuming that there is a high EMC photon measurement efficiency leaving no unmeasured photons in an event except for the ones that converted, Equation 5.3 becomes the calculated direction of the Photon Conversion. Therefore, cutting on the direction of Equation 5.3 helps to ensure an accurate reconstruction of any conversion daughter tracks in an event.

Cut 12 *The calculated direction of unmeasured radiation in Equation 5.3 must be within the fiducial region of the EMC.*

If I assume that all radiated and unconverted photons of relevant energy were measured by the EMC, Equation 5.3 in Section 5.2.5 can be considered the four-vector of any converted photon within an event. From here on, the four-vector that is calculated in Equation 5.3 is referred to as the calculated converted photon. Any subsidiary value derived from the four-vector of the calculated converted photon, such as the mass or direction, would be referred to as the calculated mass or direction of the converted photon. This value will be used extensively within Chapter 6, which covers the analysis of the data sample.

If a radiated photon has not been well measured, there could be some discrepancies in the overall event data. Because the angular distribution of radiation in Bremsstrahlung events is so highly correlated with the angle of the Radiative Bhabha-track (Figure 5.6), the EMC signals of a radiated photon and the radiating electron/positron will sometimes get merged into a single EMC signal. The EMC has an angular resolution of $\sigma_\theta = \sigma_\phi = (3.87 \pm 0.07/\sqrt{E\ (GeV)}) \pm 0.00 \pm 0.04$ mrad ([15] 73). If both a charged track and a photon strike the EMC within this angle of each other, the EMC reconstruction algorithms will consider the two EMC signals as being from a single signal cluster, originating from only one track. Since the charged track is already detected by other detector systems (the DCH and the SVT) and is directed towards the merged cluster, the EMC reconstruction algorithms will assign the merged EMC cluster to the charged track and leave the photon unreconstructed. To resolve the problem of merged EMC clusters, I will use the inconsistencies in the tracking information of the charged track between the momentum measurements by the DCH and SVT and the energy measurements by the EMC.

A charged track can never deposit more energy into the EMC than the magnitude of its momentum. Furthermore, if the charged track is an electron/positron, the energy of the EMC energy deposit should be very close to the magnitude of its momentum (as discussed in Section 5.2.2). Therefore, a combined electron and photon EMC signal should have an energy equal to the sum of the electron's and photon's energies. It is therefore reasonable to assume that in a Bhabha event, the photon energy within a merged EMC cluster is equal to the $Energy - |Momentum|$ or $E - pc$ of the Radiative Bhabha-track. However, the $E - pc$ of the Radiative Bhabha-track does not show a clear distinction between events with merged EMC signals and events with poorly measured momenta and/or energy. As well, because of the asymmetry of the electron and positron beam energies, a 9 GeV electron having an $E - pc$ of 0.5 GeV is less likely to be the result of a merged EMC signal in comparison to a 3.1 GeV positron with a $E - pc$ of 0.5 GeV. To differentiate between events with poorly measured track parameters and events with merged EMC clusters, I will compare the merged EMC photon energy from the $E - pc$ of a charged track to the calculated energy of radiation as obtained by Equation 5.1 (Equation 5.4). Inside Equation 5.4, Equation 5.3 can also be used in place of Equation 5.1, but, since Bremsstrahlung radiation is usually high-energy, the subsequent analysis produces the same results with either equation.

Whenever a charged track has little to no radiation merged into its EMC signal, the numerator of Equation 5.4 tends towards 0 while the denominator varies between zero and several GeV because the event may still be radiative. This situation will cause the value of Equation 5.4 to be centered on zero. Conversely, Bhabha events with a single radiated photon that has its EMC signal merged with the EMC signal of the Radiative Bhabha-track gives both the numerator and denominator of Equation 5.4 a value near the photon energy (any discrepancies are due to measurement errors), resulting in values centered on 1.

A plot of Equation 5.4 can be seen in Figure 5.9 while, for comparison, a similar plot of Equation 5.4 for the non-Radiative Bhabha-track is shown in Figure 5.10. In Figures 5.9 and 5.10, a peak centered on 1 would contain events in which a radiated photon's EMC signal has been merged with the EMC signal of the radiating charged track. A peak centered on 0 would contain events in which the charged track did not significantly radiate. The events outside either of these peaks are the result of poorly measured track parameters. The fact that there is no peak centered on 1 in Figure 5.10 indicates that, as expected, no photons have been merged with the charged track's EMC signal for the non-Radiative Bhabha-track.

$$\text{Excess Ratio} = \frac{(\mathrm{E} \; - \; \mathrm{p}\;)_{\mathrm{RBT}}}{\mathrm{E}_{\mathrm{calc}}} \tag{5.4}$$

Where

- "Excess Ratio" is the ratio of the excess energy in the Radiative Bhabha-track with the calculated energy of radiation.
- "E" refers to the energy of the Radiative Bhabha-track
- "p" refers to the momentum of the Radiative Bhabha-track
- "RBT" refers to the Radiative Bhabha-track
- $\mathrm{E}_{\mathrm{calc}}$ refers to the energy of the Calculated Radiation four-vector from Equation 5.1

By examining Figure 5.9 and its resulting implications, I have chosen to remove events for which Equation 5.4 has a value near 1. To reduce the possibility of eliminating events in which the track parameters are poorly measured, I also required that the calculated energy of radiation from Equation 5.1 be larger than 0.5 GeV. The resultant plot of Equation 5.4 with this added restriction can be seen in Figure 5.11. This added restriction removes a large fraction of non-radiating and normally radiating events from the graph, emphasizing the peak of centered on 1. I have decided to cut out events with a value of Equation 5.4 in between 0.35 and 1.65. In examining Figure 5.11, the upper value cut of 1.65 is taken from the maximum value of the peak centered on 1 while the lower value cut

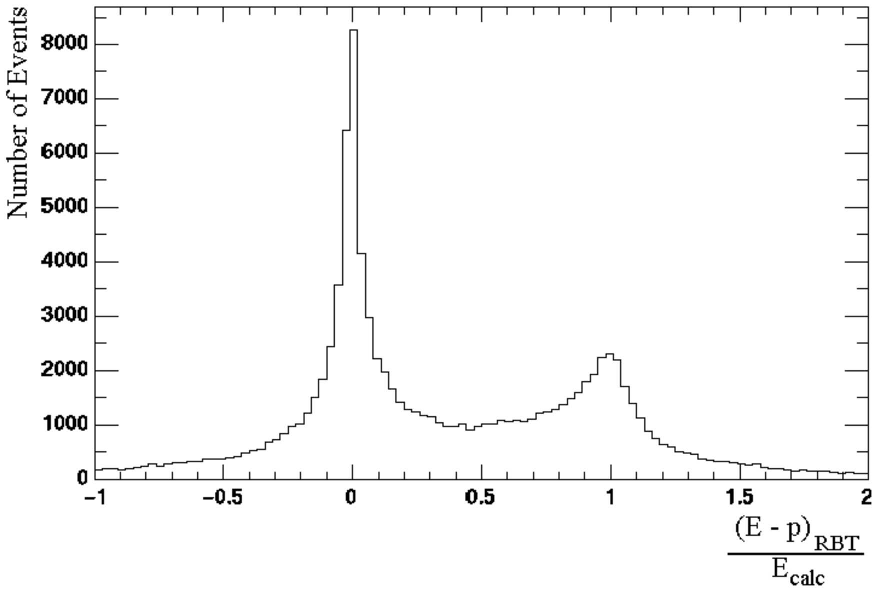

Figure 5.9: A histogram of Equation 5.4 for events having passed **Cuts 1** to **8**.

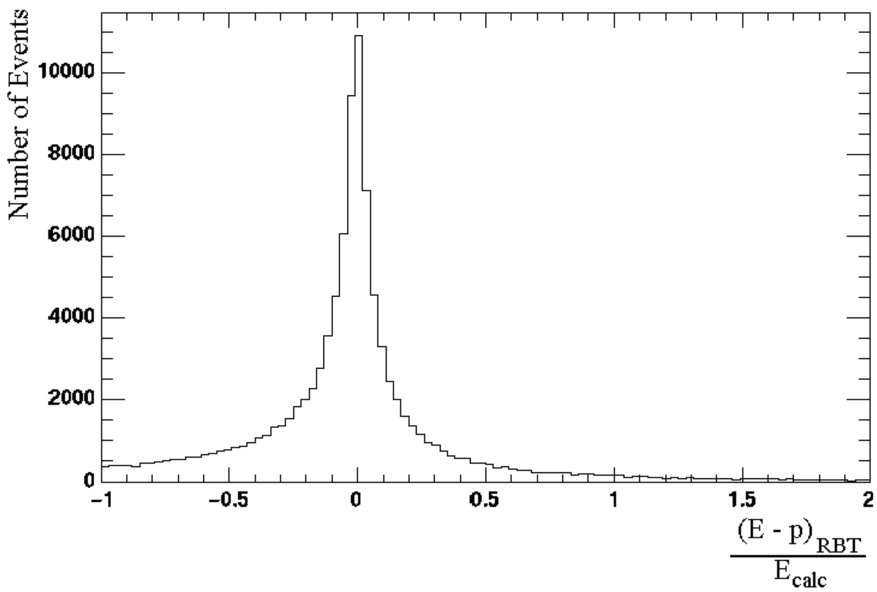

Figure 5.10: A histogram of Equation 5.4 with the non-Radiative Bhabha-track in place of the Radiative Bhabha-track, for events having passed **Cut 1** to **8**.

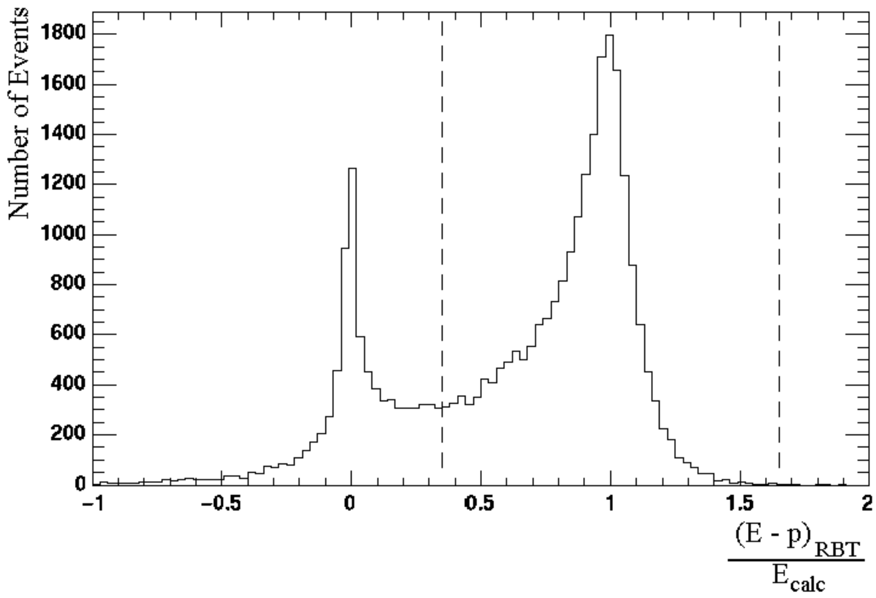

Figure 5.11: A plot of Figure 5.9 with the added requirement that the calculated energy of radiation from Equation 5.1 is greater than 0.5 GeV. The dashed lines indicate the cuts on Equation 5.4 of between 1.65 and 0.35 that are used to eliminate events with merged EMC signals.

of 0.35 is taken as the approximate point where the peak centered on 1 becomes larger than the peak centered on 0.

Cut 13 *The value of Equation 5.4 must be less than 0.35, or more than 1.65, when the calculated energy of radiation as per Equation 5.1 is greater than 0.5 GeV.*

Chapter 6

Analysis

As discussed in Section 5.2, I have written and manipulated a data sample of Bhabha and Radiative Bhabha events in order to study the efficiencies of the BaBar PCF. Within this data sample, I have used cuts on an event's parameters to ensure that each event is indeed a Bhabha or Radiative Bhabha event that is suitable for my efficiency studies. Most events within the data sample will only contain the primary electron/positron pair present in every Bhabha event, which have been labeled the Bhabha-tracks. I primarily used these "two charged-track events" to determine the value of the cuts used in my Bhabha Selector, which was described in Section 5.2. For my efficiency studies of the BaBar PCF, I cannot use any two charged-track events since they can never contain any reconstructed conversion daughter tracks. The events with more than two charged-tracks, or with an excess of charged-tracks after including the two Bhabha-tracks, are the events that may possibly contain one or both conversion daughter tracks. In analyzing these events, I must consider other physics processes and detector intricacies that could also produce extra charged-tracks in the events of my data sample. Because I am specifically focusing on the possibility of converted photons within an event, the specifics of my efficiency studies will depend on whether only one or both of the conversion daughter tracks might have been reconstructed. Therefore, I have chosen to separate the data sample into three distinct classes based on the number and charge of the charged-tracks within each event:

- Events with three charged-tracks—these are Bhabha events in which only one conversion daughter track may have been reconstructed
- Events with four charged-tracks and with no net charge—these are Bhabha events in which both conversion daughter tracks may have been reconstructed.
- Events with four charged-tracks and with a net charge of ± 2e—these are Bhabha events in which only one conversion daughter track may have been reconstructed yet a background track with the same charge would also be present.

From here on, all charged-tracks that are not one of the two Bhabha-tracks will be further referred to as the "candidate-tracks". One purpose of this chapter is to describe how I determine if a candidate-track is either a conversion daughter track or a background track. In order to reduce the presence of candidate-tracks that are due to backgrounds from my data sample, I will compare the directions of all candidate-tracks to the calculated direction of the converted photon by taking their normalized dot product. The normalized dot product is equivalent to the cosine of the angle between two tracks. I can use this angular comparison to eliminate any background contamination as the two directions should be uncorrelated if the candidate-track is background. This lack of correlation is because the angular distribution of converted photons is mostly determined by the matter distribution of the BaBar detector and is restricted by the kinematics of the event while the angular distribution of backgrounds is determined by other factors.

6.1 Efficiency Studies

My efficiency studies of the BaBar PCF can be divided into two parts:

- A "background study" measuring the energy spectrum of conversion daughter tracks which are not unidentified.

- An "efficiency study of the PCF" measuring the ability of the PCF to correctly identify a converted photon candidate.

In the background study, measuring the spectrum of unidentified conversion daughter tracks will involve using both the four charged-track event classes regardless of their net charged and the three charged track event class. The efficiency studies of the PCF will use only four charged-track events with no net charge as a converted photon candidate can only be constructed in those events.

Within my background study, I will correlate the energy spectrum of all unidentified conversion daughter tracks to the energy spectrum of identified converted photon candidates. In future studies at the BaBar experiment, users will be able to obtain the spectrum of unidentified conversion daughter tracks in their analysis by taking the spectrum of identified converted photon candidates obtained in this thesis and scaling it to match their spectrum of identified converted photon candidates. The spectrum of unidentified conversion daughter tracks obtained in this study can then be used to estimate the unidentified conversion daughter track spectrum in other analyses. The analysis involved in my efficiency study of the PCF requires a comprehensive analysis of four charged-track events with no net charge. Since the background study will include such an analysis, I will postpone my discussion on the efficiency study of the PCF until Section 6.3. Within my efficiency studies, I have also conducted a small Monte Carlo study to ensure the validity of my results and to observe the Monte Carlo truth for events passing my Bhabha Selector. This study will be presented in Section 7.4.

6.1.1 Background Study

The explicit goal of my background study is to obtain the unidentified conversion daughter track energy spectrum per energy bin of identified converted photon candidates. This goal involves correlating the energy of a candidate-track to the energy of its possible parent converted photon that would be present within the same event. For this study, I want to include candidate-tracks that are from either partially reconstructed converted photons (three charged-track events and four charged-track events with a net charge of $\pm$ 2e) or fully reconstructed yet unidentified converted photons (four charged-track events with no net charge). Therefore, I must choose a method of correlating the energies that does not differentiate between the number of candidate-tracks within an event. The PCF algorithm calculates a converted photon candidate's momentum for events in which two oppositely charged candidate-tracks were input into the PCF. However, I cannot use this method to obtain a converted photon's momentum for events in which only one candidate-track has been reconstructed nor for events in which both candidate-tracks are of the same charge. Yet, because I am using kinematically simple Bhabha and Radiative Bhabha events in my data sample, I can instead use the calculated energy of the converted photon from Equation 5.3. Equation 5.3 uses information from the two Bhabha-tracks, the Center of Mass Frame, and any photon's measured in the EMC, but does not use any information from the candidate-tracks within an event. Equation 5.3 can be used for all event classes within my background study regardless of the reconstruction and identification status of a converted photon candidate. Therefore, I will use Equation 5.3 to correlate the energy spectrum of the unidentified conversion daughter tracks to the energy spectrum of their parent converted photons within my background study. In deriving the equations for my background study, we start with the ratio of the leptons unidentified as originating from a converted photon to the number of identified converted photon candidates binned in energy, as shown in Equation 6.1:

$$ratio_j = \frac{Nl_j}{N\gamma c_j} \tag{6.1}$$

where

- the index j refers to the energy bins of the calculated converted photon in each event.
- $ratio_j$ is the ratio of leptons that are unidentified as originating from converted photons to the number of identified converted photons candidates in energy bin j.
- Nl_j is the number of leptons unidentified as originating from converted photons in energy bin j.
- $N\gamma c_j$ is the number of identified converted photon candidates in energy bin j.

As a further refinement of Equation 6.1, the number of leptons in energy bin j is split into different lepton energy bins, which will be denoted by the index i. This splitting will now give the energy spectra per lepton energy bin, for each energy bin of identified converted photon candidate, as desired. Also, The energy spectra of the candidate-tracks that are used to obtain the element Nl of Equation 6.1 can be subdivided into a signal and background component. Incorporating these changes into Equation 6.1 gives Equation 6.2.

$$ratio_{ij} = \frac{Nsl_{ij} - Bl_{ij}}{N\gamma c_j} \tag{6.2}$$

where

- the index i refers to the energy bin of the leptons that are unidentified as originating from a converted photon.
- the index j refers to the energy bin of the calculated converted photon in each event.

- $ratio_{ij}$ is the ratio of leptons that are unidentified as originating from converted photons in energy bin i, to the number of identified converted photon candidates in energy bin j.

- Nsl_{ij} is the number of leptons within the candidate-track energy spectrum, in energy bins i,j.

- Bl_{ij} is the number of background leptons within the candidate-track energy spectrum, in energy bins i,j.

- $N\gamma c_j$ is the number of identified converted photon candidates in energy bin j.

Each of the three event classes mentioned in Section 6 contributes a single term to both Nsl_{ij} and Bl_{ij} from Equation 6.2. With every element written out explicitly, the equation used to obtain the results of my background study is Equation 6.3:

$$ratio_{ij} = \frac{N3_{ij} + N4fail_{ij} + N4sc_{ij} - B3_{ij} - B4fail_{ij} - B4sc_{ij}}{N\gamma c_j} \tag{6.3}$$

where

- the index i refers to the energy bin of the leptons that are unidentified as originating from a converted photon.

- the index j refers to the energy bin of the calculated converted photon in each event.

- $ratio_{ij}$ is the ratio of leptons that are unidentified as originating from a converted photon in the energy bin i, to the number of identified converted photon candidates in the energy bin j.

- $N3_{ij}$ is the number of leptons in energy bin i, for each identified converted photon candidate in energy bin j, for three charged-track events.

- $N4fail_{ij}$ is the number of leptons in energy bin i, for each identified converted photon candidate in energy bin j, for four charged-track events with no net charge and in which the converted photon candidate has failed the PCF quality cuts. Since there are two candidate-tracks in each event, there are always two $N4fail_{ij}$ entries per event, which are not necessarily in the same energy bins.

- $N4sc_{ij}$ is the number of leptons in energy bin i, for each identified converted photon candidate in energy bin j, for four charged-track events with a net charge of $\pm$ 2e. Since only one of the two candidate-tracks in each event can be a conversion daughter track, there is only one $N4sc_{ij}$ entry per event.

- $B3_{ij}$ is the background contamination present in energy bin i, for each identified converted photon candidate in energy bin j, for three charged-track events.

- $B4fail_{ij}$ is the background contamination present in energy bin i, for each identified converted photon candidate in energy bin j, for four charged-track events with no net charge and in which the converted photon candidate has failed the quality cuts of the PCF. There are always two $B4fail_{ij}$ entries per event that are not necessarily in the same energy bins.

- $B4sc_{ij}$ is the background contamination present in energy bin i, for each identified converted photon candidate in energy bin j, for four charged-track events with a net charge of $\pm$ 2e. Since each event already has at least one background track that will not be included into $N4sc_{ij}$, there is only one $B4sc_{ij}$ entry per event.

- $N\gamma c_j$ is the number of identified converted photon candidates per energy bin j.

The error on the $ratio_{ij}$ in Equation 6.3 is a multinomial distribution with an entry for each j and i bin. As this multinomial distribution involves 240 possible permutations, it is impractical to calculate the errors using this method. Instead of using the multinomial distribution, the error is determined by treating each element of Equation 6.3 as uncorrelated. Since each element is a bin in a two-dimensional histogram, the individual errors are $\sqrt{n}$, the Poisson error of a bin with n entries. The resulting error for $ratio_{ij}$ of Equation 6.3 then becomes:

$$\sigma_{ratioij} = \sqrt{\begin{array}{c}\frac{N3_{ij}+N4fail_{ij}+N4sc_{ij}+B3_{ij}+B4fail_{ij}+B4sc_{ij}}{(N\gamma c_j)^2} \\ + \\ \frac{(N3_{ij}+N4fail_{ij}+N4sc_{ij}-B3_{ij}-B4fail_{ij}-B4sc_{ij})^2}{(N\gamma c_j)^3}\end{array}} \tag{6.4}$$

The numerator of Equation 6.3 can be thought of as the number of leptons per bin originating from converted photons but that are unidentified as such. Treating each element as uncorrelated, the error for the numerator becomes:

$$\sigma_{Nlij} = \sqrt{N3_{ij} + N4fail_{ij} + N4sc_{ij} + B3_{ij} + B4fail_{ij} + B4sc_{ij}} \tag{6.5}$$

The errors for the denominator of Equation 6.3 is simply $\sqrt{n}$, the Poisson errors for a bin with n entries:

$$\sigma_{N\gamma cj} = \sqrt{N\gamma c_j} \tag{6.6}$$

Note that using Poisson errors, if a bin has zero entries, the error of the bin is $\pm$ 2.3. Also note that for this thesis I am using the BaBar convention for displaying the results: The number of significant figures is determined by the error. If the last two significant figures of an entry are above 35, it is rounded. However, if the last two significant figures of an enrty are below 35, it is not rounded. As mentioned above, the j energy bins in Equation 6.3 are the energy bins of the calculated converted photon in each event. I determine the minimum width of the j energy bins by observing the resolution of the calculated converted photon energy with respect to a converted photon candidate's energy as determined by the PCF, in the events in which the converted photon candidate passed the PCF quality cuts (was identified). The converted photon candidate's energy, as determined by the PCF, is assumed to be the more accurate of the two energies as it relies only on direct information from the candidate-tracks whereas the calculated energy of the converted photon relies on information from all other tracks in an event except for the candidate-tracks. The minimum width of the i energy bins in Equation 6.3 is determined by the BaBar detector's lepton energy measurement resolution, given as $\frac{\sigma_E}{E} = \frac{(2.32\pm0.30)\%}{\sqrt[4]{E(GeV)}} \bigoplus (1.85 \pm 0.12)\%$ ([15] 73). This formula gives a 0.042 GeV energy resolution for a lepton energy of 1 GeV. Since this energy resolution is quite precise, the limiting factor for the i bin width in Equation 6.3 will instead be statistical.

6.2 Treatment of the Data Sample

6.2.1 Three Charged-Track Events

After passing my Bhabha Selector, the two most likely possibilities for the candidate-track (the track not identified as a Bhabha-track) in a three charged-track event is either background contamination or a single reconstructed conversion daughter track. There are several possible sources of background contamination, only several being separable from the distributions of conversion daughter tracks. False tracks, whether they are reconstructed from stray hits in the BaBar detector or the result of poorly fit real detector hits, are undetectable in any large-scale data study and must be included as systematic errors. In order to minimize these systematic errors, each candidate-track has been required to be within the fiducial region of the EMC (**Cut 9** of my Bhabha Selector). Beam-induced backgrounds are backgrounds resulting from the high-energy electron/positron beams. The dominant source of beam-induced backgrounds in the BaBar detector is from stray

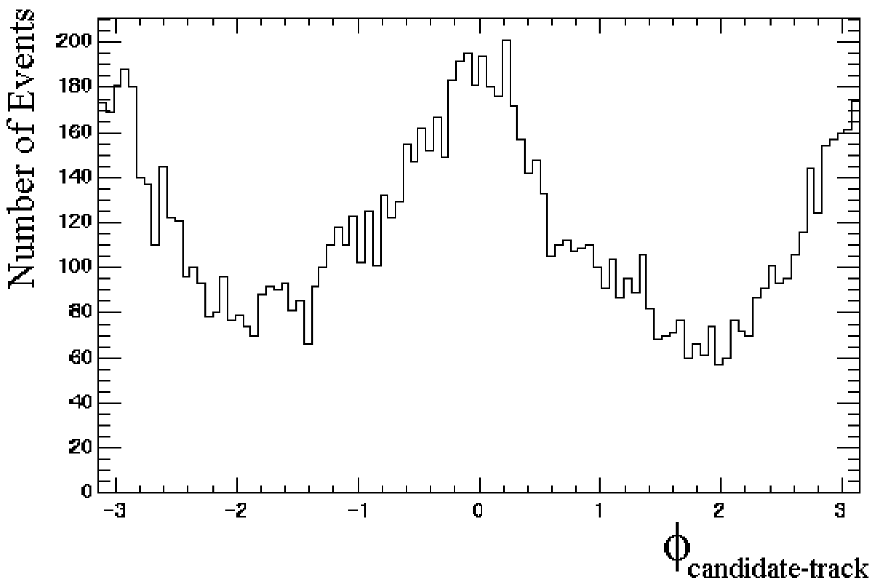

Figure 6.1: The ϕ of the candidate-tracks in all three charged-track events. The expected ϕ distribution of conversion daughter tracks is symmetric in ϕ, therefore, the peaks of Figure 6.1 at $\phi = 0$ and $\pm\pi$ imply the present of beam-induced backgrounds.

beam electrons or positrons showering in detector material and producing stray, low-energy electrons and positrons[26]. Beam-induced backgrounds are found in many events within my data sample and can be identified by their characteristic ϕ and θ distributions: beam-induced backgrounds are more likely to occur in the horizontal plane of the detector ($\phi = 0$, $\pm\pi$ rad and $\theta = 0$, π). These characteristic distributions should stand out since the angular distribution of conversion daughter tracks is expected to be symmetric. A plot of the ϕ distribution for the candidate-track in all three charged-track events is shown in Figure 6.1. Figure 6.1 shows a beam-induced background distribution on top of a symmetric conversion daughter track distribution.

One way to remove beam-induced backgrounds is to compare the direction of the candidate-track to the calculated direction of the converted photon. The normalized dot product between two tracks is equivalent to the cosine of the angle between the two tracks. If the two tracks are in the same direction, the normalized dot product will equal 1. By taking the normalized dot product of the two directions (Figure 6.2), we see there is both a constant signal and a large peak at 1, where the two directions are the same. Since beam-induced backgrounds are low-energy backgrounds that do not affect the Lab Frame distributions of tracks, they do not affect the calculated direction of the converted photon from Equation 5.3. Therefore, it is expected that constant signal of Figure 6.2 would contain the events in which the candidate-track is a beam-induced background. In contrast, it is expected that the peak in Figure 6.2 near 1 would contain the events in which the candidate-track is a conversion daughter track. To confirm these expectation, I examine the ϕ distributions of the candidate-track for different values of the normalized dot product as shown in Figure 6.3. In Figure 6.3 **(a)**, we indeed see that the source of the constant signal in Figure 6.2 has a characteristic beam-induced background distribution. In Figure 6.3 **(b)**, we can see that the large forward peak of Figure 6.2 is symmetric in ϕ as is expected for conversion daughter tracks.

To eliminate the constant beam-induced background signal shown in Figure 6.2, I have divided the figure into two halves: the events in which the normalized dot product shown in Figure 6.2 is greater than zero are subsequently considered to contain a conversion daughter track. The events in which the normalized dot product shown in Figure 6.2 is lower than zero will be used to remove the beam-induced background distributions in the events with a normalized dot product above zero. Since the beam-induced background signal is flat with respect to the normalized dot product shown in Figure 6.2, I can perform a bin by bin subtraction. Therefore, in Equation 6.3, the candidate-track energy spectrum for events with a normalized dot product below zero will be directly subtracted from the candidate-track spectrum for events with a normalized dot product above zero. In Equation 6.3, the variables for three charged-track events are:

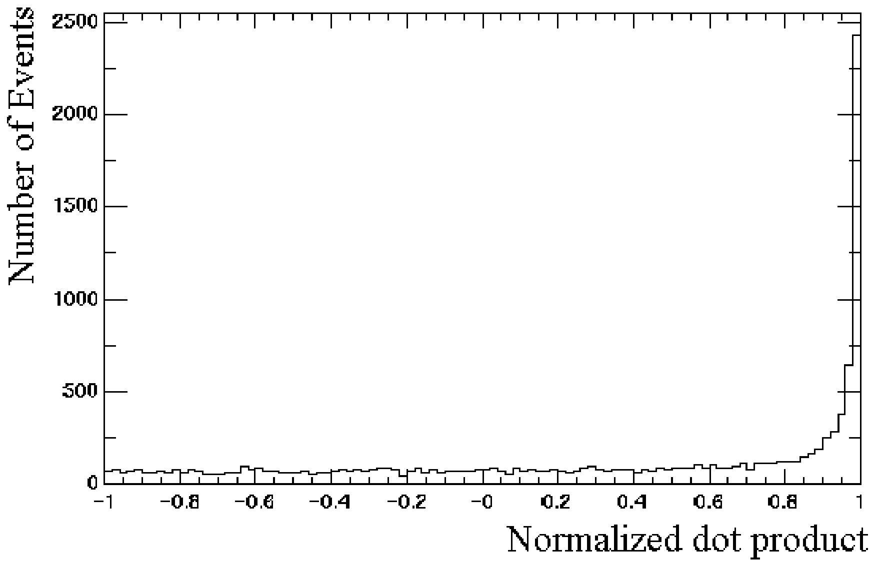

Figure 6.2: The normalized dot product of the directions of the candidate-track and the calculated direction of the converted photon, in all three charged-track events. The constant signal is likely due to events in which the candidate-track is a beam-induced background while the peak near 1 is likely due to events in which the candidate-track is a conversion daughter track.

- $N3_{ij}$ is the energy spectrum of candidate-tracks that have a normalized dot product of the candidate-track and the calculated direction of the converted photon above a value of zero, correlated to the energy spectrum of the calculated converted photon energy.

- $B3_{ij}$ is the energy spectrum of candidate-tracks that have a normalized dot product of the candidate track and the calculated direction of the converted photon below a value of zero, correlated to the energy spectrum of the calculated converted photon energy.

As mentioned briefly in Section 4.1.1, the PCF algorithm calculates the four-vector of a converted photon candidate through the vertexing of two charged-tracks input into it. Since there is, at most, only one conversion daughter track within a three charged

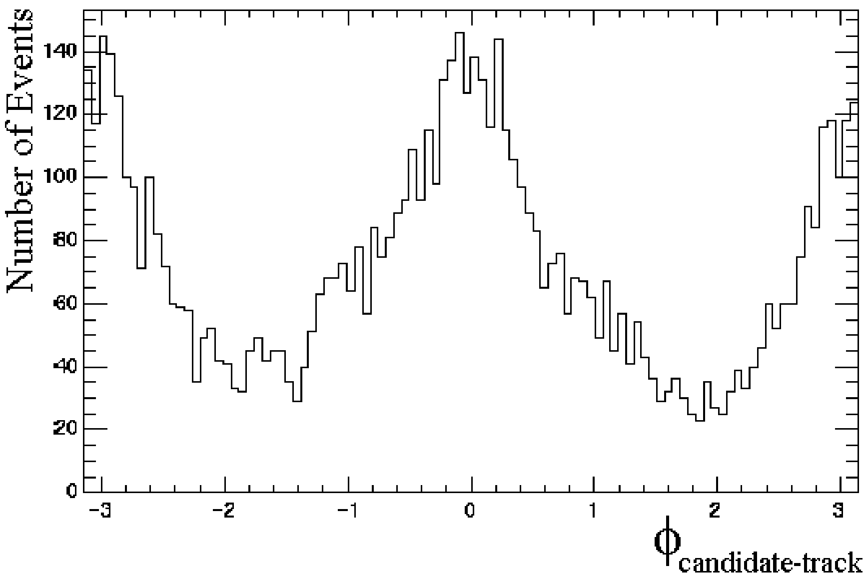

(a)

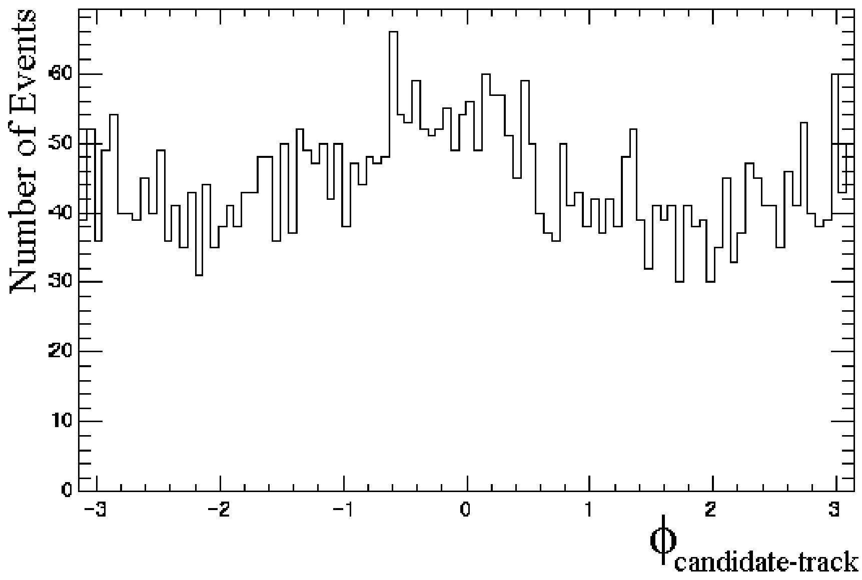

(b)

Figure 6.3: **(a)** is the ϕ distribution for the candidate-track in all three charged track events for events in which the normalized dot product shown in Figure 6.2 is below 0.85. **(b)** shows this ϕ distribution for events in which the normalized dot product shown in Figure 6.2 is above 0.85.

track event, I can not obtain a converted photon candidate for these events. In order to standardize the j energy bins of Equation 6.3, I will always use the calculated energy of the converted photon to correlate the energy spectrum of candidate-tracks to the energy spectrum of their parent converted photons. The calculated converted photon energy is used in Equation 6.3 because it can be calculated for both three and four charged-track events since it does not depend on the number of candidate-tracks within an event. One way to examine the validity of using the calculated converted photon energy is to compare it to the momentum of the candidate-track in all three track events. I expect that most events in which only one conversion daughter track was reconstructed will have the electron and positron from the conversion created with highly asymmetric energies (see Figure 4.13). Photonic Conversions that are highly asymmetric in the energy of the electron/positron pair will result in one of the conversion daughter tracks having a low energy. Since the BaBar detector has poor reconstruction efficiency at low energies, the low-energy conversion daughter track will most likely be the unreconstructed one. Conversely, the conversion daughter track carrying most of the original photon's energy will most likely be the one that is reconstructed in three charged-track events. Therefore, the ratio of the candidate-track's energy and the energy of the calculated converted photon, which is analogous to Figure 4.13, should peak slightly below 1 and decrease as the ratio decreases. A plot of this ratio in Figure 6.4 confirms this supposition. While there is no clear structure to Figure 6.4 **(a)**, the structure of Figure 6.4 **(b)** implies that events with a single reconstructed conversion daughter track are mostly due to the low-energy reconstruction inefficiencies of the BaBar detector on energy electron/positron pairs with highly asymmetric energies.

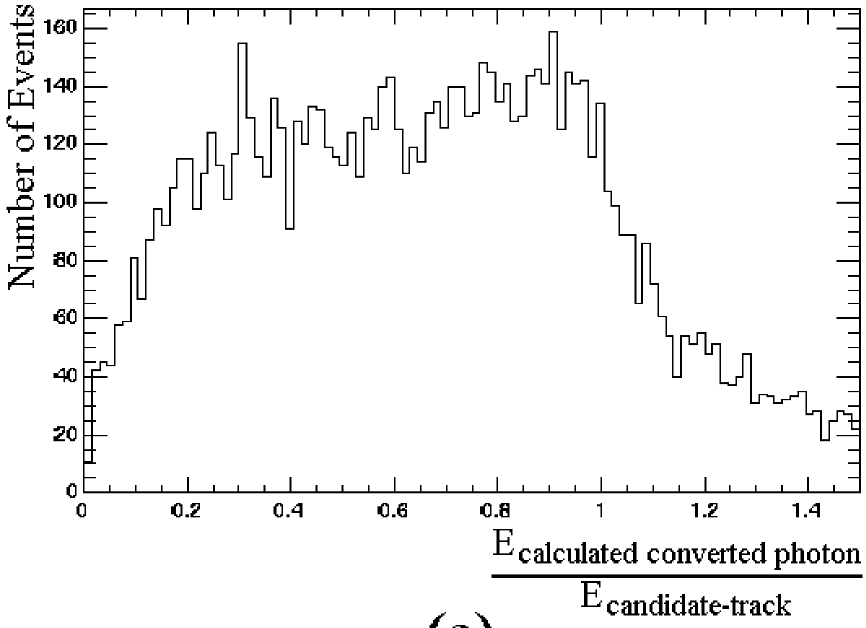

(a)

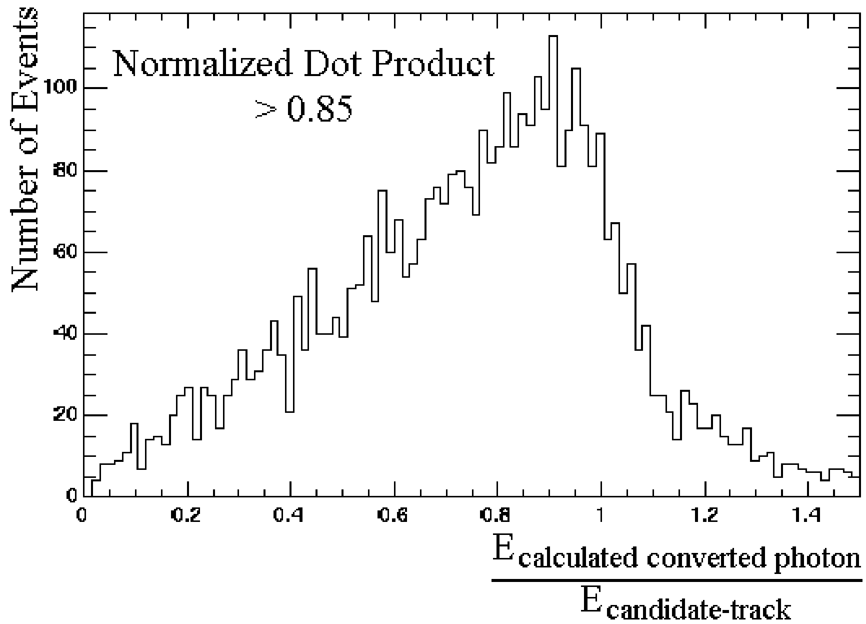

(b)

Figure 6.4: **(a)** is the ratio of calculated converted photon energy and the candidate-track energy for all three track events. **(b)** shows this ratio for events in which the normalized dot product of the candidate-track and the calculated converted photon (Figure 6.2) is above 0.85.

6.2.2 Four Charged-Track Events with No Net Charge

The BaBar PCF is able to construct a converted photon candidate in all four track events in which the two candidate-tracks that are input into the PCF are oppositely charged. If the converted photon candidate fails the PCF quality cuts listed in Section 4.1.2, the two candidate-tracks are considered unrelated. If the converted photon candidate passed the PCF quality cuts, the two tracks are considered to be identified as conversion daughter tracks. The method used in determining the background spectrum of candidate-tracks in four charged-track events is similar to the method used for three charged-track events. As in three track events, the major source of backgrounds is from beam-induced backgrounds. A near-identical procedure that was used for background subtraction in three charged-track events is also used to eliminate beam-induced backgrounds from four charged track events with no net charge. To eliminate the beam-induced backgrounds from four charged track events in which the converted photon candidate failed the quality cuts, I will observe the normalized dot product of the converted photon candidate and the calculated direction of the converted photon (Figure 6.5 **(a)**). Because I am calculating the normalized dot product with a converted photon candidate and not a conversion daughter track as in three charged-track events, the peak of Figure 6.5 **(a)** and **(b)** at 1 is sharper than the corresponding peak of Figure 6.2. The reason for the broader peak in Figure 6.2 is both because of the opening angle between the electron/positron pair created in a Photonic Conversion, and because of the magnetic field of the BaBar detector. This magnetic field causes a charged track's measured ϕ at the EMC to be different from its ϕ at the point of conversion (this difference is greater for lower-energy tracks). The reduced constant background signal of Figure 6.5 in comparison to Figure 6.2 supports the supposition that the majority of backgrounds in my data sample are due to beam-induced backgrounds since two oppositely charged beam-induced background tracks are much less likely to occur than only one.

To remove the beam-induced background distributions from those of the conversion daughter tracks, I divide Figure 6.5 **(a)** into two halves: the events in which the normalized dot product shown in Figure 6.5 **(a)** is greater than zero are subsequently considered to contain two conversion daughter tracks. The events in which the normalized dot product shown in Figure 6.5 **(a)** is lower than zero will be used to remove the beam-induced background distributions in the events with a value above zero. Since the beam-induced background signal is constant with respect to the normalized dot product shown in Figure 6.5 **(a)**, I can simply perform a bin by bin subtraction between the two halves. Therefore in Equation 6.3, the variables in the numerator used for four charged-track events with no net charge are:

- $N4fail_{ij}$ is the energy spectrum of both candidate-tracks for events in which the normalized dot product of the converted photon candidate that has <u>failed</u> the PCF quality cuts and the calculated converted photon is <u>above</u> a value of zero, correlated to the energy spectrum of the calculated converted photon energy.

- $B4fail_{ij}$ is the energy spectrum of both candidate-tracks for events in which the normalized dot product of the converted photon candidate that has <u>failed</u> the PCF quality cuts and the calculated converted photon is <u>below</u> a value of zero, correlated to the energy spectrum of the calculated converted photon energy.

The denominator of Equation 6.3 is defined as:

- $N4pass_j$ is the energy spectrum of the calculated converted photon for the events in which the converted photon candidate has <u>passed</u> the PCF quality cuts .

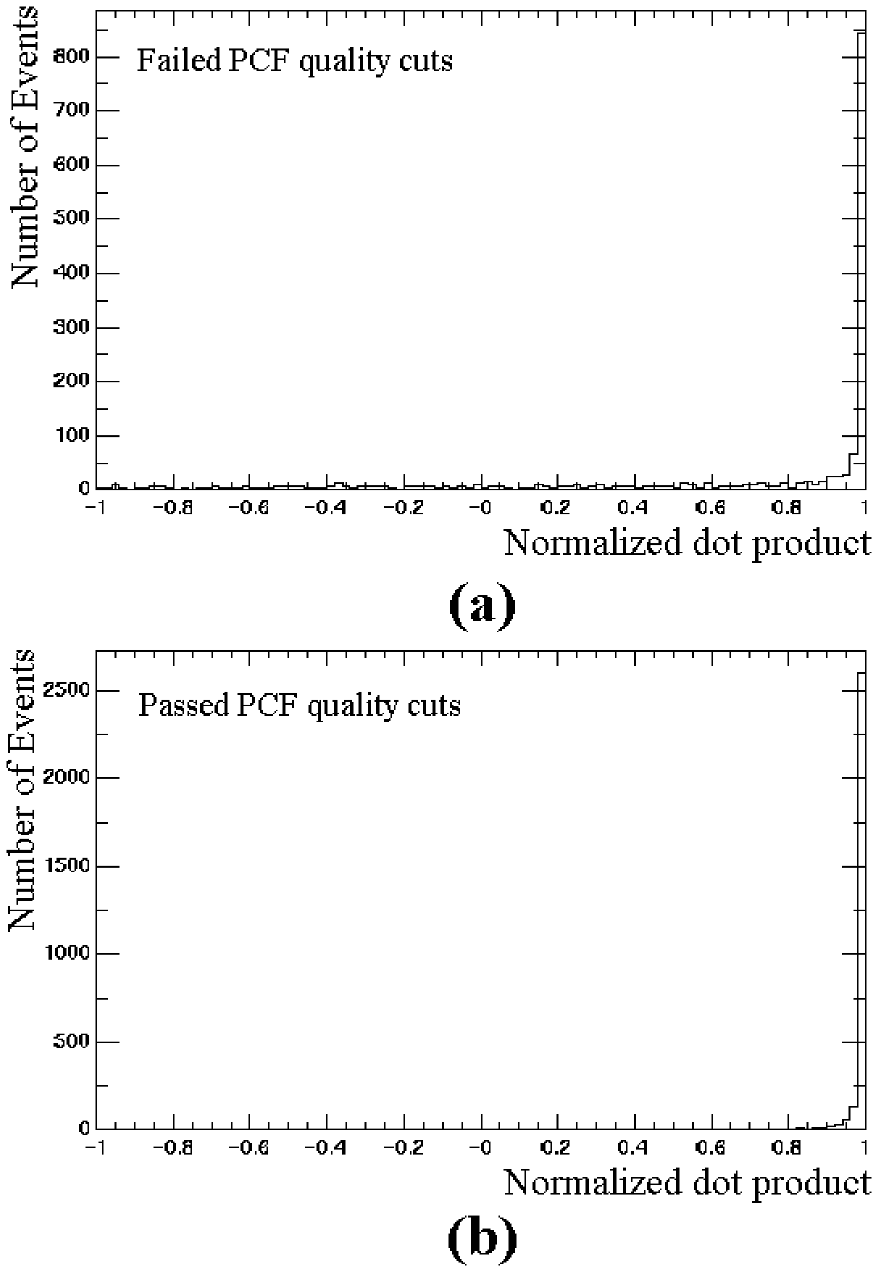

Figure 6.5: The normalized dot product of the calculated converted photon and the converted photon candidate in all four track events with no net charge. The peaks at 1 are due to conversion daughter tracks while the smaller constant signal in **(a)** is due to beam-induced backgrounds.

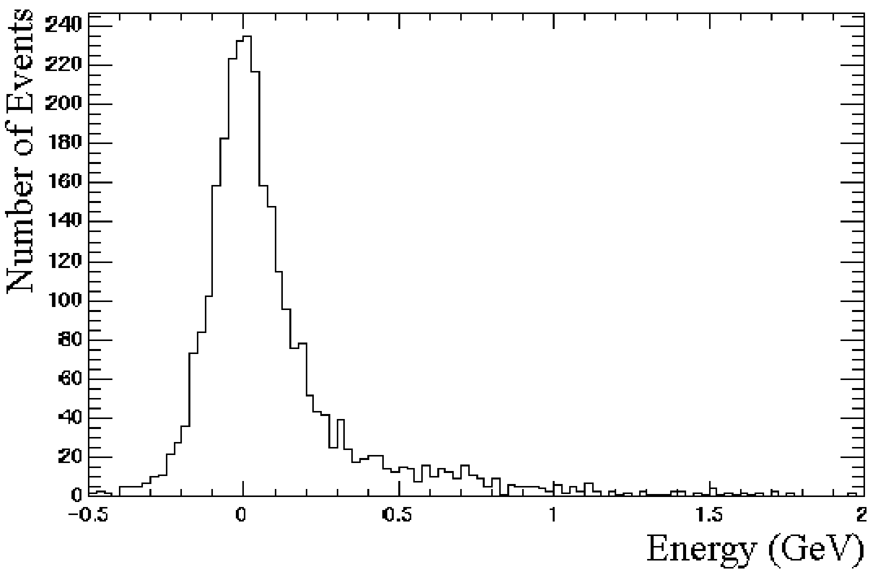

Figure 6.6: The energy difference between the calculated converted photon and the converted photon candidate for all events in which the candidate has passed the PCF quality cuts. The large peak centered on zero is what I use to determine the minimum j energy bin resolution of Equation 6.3. The long tail is due to events with unmeasured energy.

In Equation 6.3, the minimum resolution of the j energy bins will be determined by taking the differences between the energy spectra of the calculated converted photon and the converted photon candidates for events in which the converted photon candidate has passed the PCF quality cuts (Figure 6.6). For the purposes of this resolution, a converted photon candidate's energy is considered as exact when it has passed the PCF quality cuts.

The long tail of Figure 6.6 contains ~ 10 % of the total events and must be examined further. It is most likely that this long tail contains initial state radiation events in which either the primary electron or positron radiated before the beams interacted, often causing this radiation to go down the beam pipe. It should be possible to detect the initial state radiation in an event by observing the direction of any unmeasured momentum in the Lab Frame if we include a converted photon candidate's four-vector into Equation 5.3.

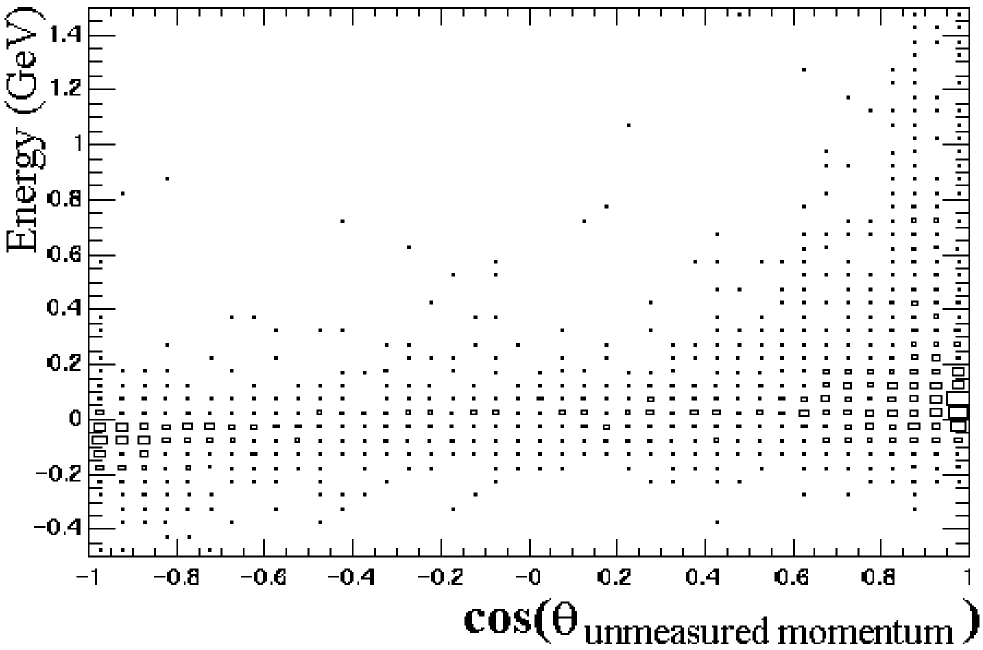

Figure 6.7: The scaled number of events per bin for the energy difference between an identified converted photon candidate and the calculated converted photon (this difference was plotted in Figure 6.6) versus $\cos\theta$ of any unmeasured momentum in the Lab frame. The unmeasured momentum is obtained by including a converted photon candidate's four-vector into Equation 5.3. The number of events in each bin is proportional to the area of the square.

A plot of the scaled number of events per bin for the energy differences shown in Figure 6.6, versus the angle of this unmeasured momentum can be seen in Figure 6.7. Even though almost all events within the long tail of Figure 6.6 are in the forward direction, there is no direct correlation between the direction of the unmeasured momentum and the differences in converted photon energies—even for events in which the unmeasured direction is outside the angular coverage of the BaBar detector. Since there is no practical means of removing the long tail of Figure 6.6, it has been included in obtaining the minimum j energy bin resolution of Equation 6.3.

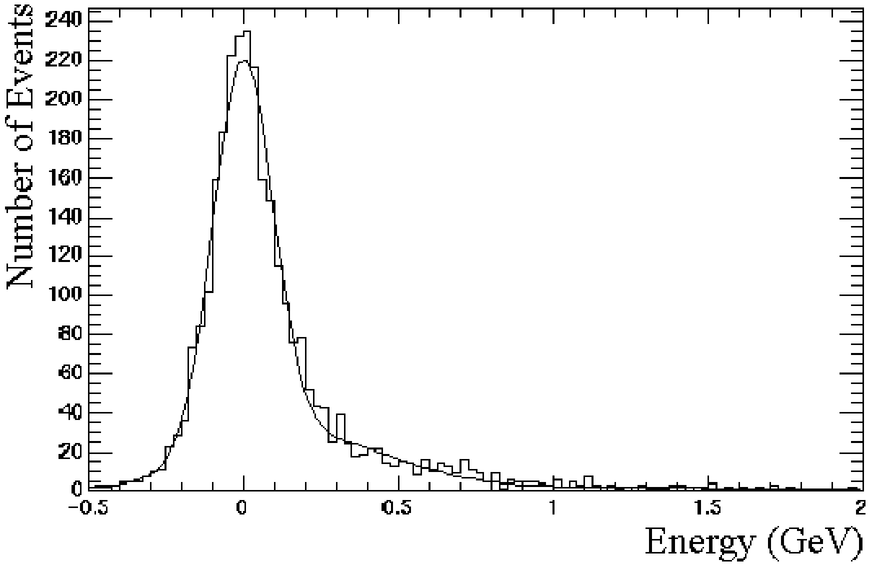

Figure 6.8: A double Gaussian equation with a 2^{nd} order polynomial background (as shown in Equation 6.7) is fit to the energy difference between the calculated converted photon and the converted photon candidate for all events in which the converted photon candidate has passed the PCF quality cuts. This energy difference is shown in Figure 6.6. The best result for the 9 parameters of this fit is shown in Table 6.1.

The primary peak centered on zero in Figure 6.6 is best described by a Gaussian peak while the long tail is best described by a Gaussian peak with a slight polynomial background. A double Gaussian equation with a 2^{nd} order polynomial background containing 9 fit parameters (shown in Equation 6.7) was fit to Figure 6.6. An overlay of this fit onto Figure 6.6 is shown in Figure 6.8. The results of this fit are shown in Table 6.1. The minimum resolution of the j energy bins in Equation 6.3 is obtained by taking twice the width of the primary Gaussian peak centered near zero—2 $\times$ element w_p from Equation 6.7 and Table 6.1. This gives a minimum resolution for the j energy bins of 190 $\pm$ 7 MeV.

$$a_p Exp^{-\frac{1}{2}(\frac{x-m_p}{w_p})^2} + a_s Exp^{-\frac{1}{2}(\frac{x-m_s}{w_s})^2} + p_0 + p_1 x + p_2 x^2 \tag{6.7}$$

Parameter	Value $\pm$ error (GeV)
a_p	199 ± 6
m_p	0.0007 ± 0.0030
w_p	0.0967 ± 0.0034
a_s	25.8 ± 3.0
m_s	0.192 ± 0.034
w_s	0.284 ± 0.027
p_0	1.5 ± 1.2
p_1	1.6 ± 1.4
p_2	-0.9 ± 0.7

Table 6.1: Results of a 9 parameter, double Gaussian equation with a 2^{nd} order polynomial background (Equation 6.7) fit to Figure 6.6. The large percentage errors in the polynomial parameters imply any terms beyond the double Gaussian peaks are likely superfluous. Twice the width of the primary Gaussian ($2 \times w_p$) determines the minimum resolution of the j energy bins in Equation 6.3 and gives a value of 190 $\pm$ 7 MeV.

Where x is the independent variable (the energy difference of Figure 6.6). With the primary Gaussian peak being the peak centered near zero, the parameters are labeled such that:

- a_p and a_s are the amplitudes of the primary and secondary Gaussian peaks.
- m_p and m_s are the means of the primary and secondary Gaussian peaks.
- w_p and w_s are the widths of the primary and secondary Gaussian peaks.
- p_0, p_1, and p_2 are the coefficients of the polynomial background.

6.2.3 Four Charged-Track Events with a Net Charge of $\pm$ 2e

In addition to the two Bhabha-tracks, there is either one conversion daughter track and one background track or two background tracks in every four charged-track event with a net charge of $\pm$ 2e. The main challenge in including four charge track events with a net charge of $\pm$ 2e into Equation 6.3 is to separate the conversion daughter track's distributions from the background distributions. The most obvious starting point for attempting this background separation is the method used for both three charged-track events and four charged-track events with no net charge. This method involves taking the normalized dot product of the candidate-track and the calculated converted photon (Figure 6.9). Both Figure 6.9 **(a)** and **(b)** show a peak at 1 that should contain all the conversion daughter tracks as well as a constant background that should contain all the beam-induced backgrounds.

These peaks indicates that at least one of the candidate-tracks is a conversion daughter track in many of these events. However, if we compare the normalized dot product of the calculated converted photon and the higher or the lower energy candidate-tracks within the same event (Figure 6.10) we have conflicting results. In Figure 6.10, the two forward peaks are represented by the uppermost row and rightmost column. The largest number of tracks appear in the upper-right most bin near (1,1). This bin contains events in which both the higher and the lower energy candidate-tracks are in the same direction as the calculated converted photon. There are also a large number of events in which the higher energy candidate-track is in the direction of the calculated converted photon while the lower energy candidate-track is not (the rightmost column). The reverse is not as common (the uppermost row).

In examining four charged-track events with no net charge, we found that both candidate-tracks' directions are also often highly correlated to the calculated direction of the converted photons. However, this correlation is expected because the two candidate-tracks are of opposite charge and can often be reconstructed into a converted photon candidate. In four charged-track events with a net charge of $\pm$ 2e, at least one candidate-track must always be background and it is not obvious which of the candidate-tracks are

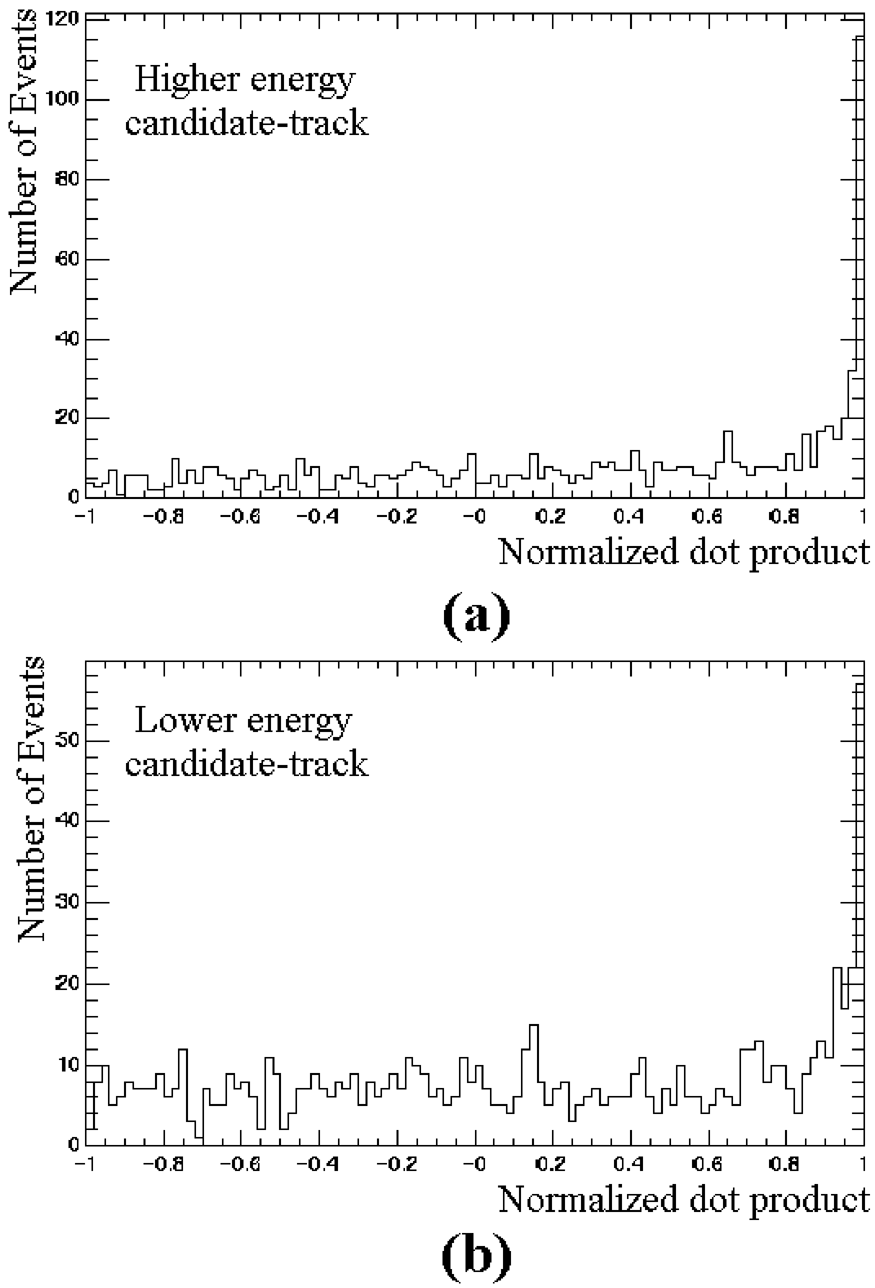

Figure 6.9: The normalized dot product of each candidate-track and the calculated direction of the converted photon in all four charged-track events with a net charge of $\pm$ 2e. **(a)** shows the normalized dot product of the higher energy candidate-track in each event while **(b)** shows the normalized dot product for the lower energy candidate-track.

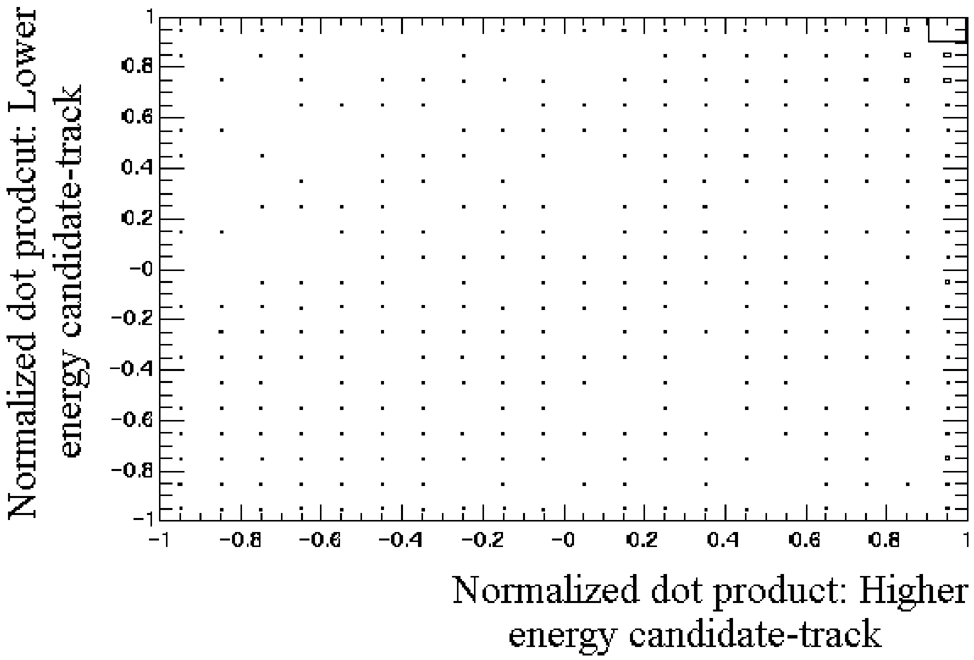

Figure 6.10: The relative number of events per bin for the normalized dot product of the calculated converted photon and both the higher and the lower energy candidate-tracks in four charged-track events with a net charge of ± 2e. The number of events in each bin is proportional to the area of the square. The bin with the most events is by far the one in the upper right near (1,1).

background from Figures 6.9 and 6.10. To resolve the issue of background separation, I must further examine the relationship between the two candidate-tracks. The isotropic flat distributions in Figure 6.9 indicate that there is a definite beam-induced backgrounds presence in four charged-track events with a net charge of $\pm$ 2e. However, the large peak at (1,1) in Figure 6.10 indicates the presence of another possible background.

By observing the normalized dot product of the candidate-tracks with the other, we see that in four charged track events with no net charge the normalized dot product peaks at 1 but has a definite decreasing distribution for lower values of the normalized dot product (Figure 6.11 **(a)**). In four charged-track events with a net charge of $\pm$ 2e, the normalized dot product also peaks at 1, but is has a much sharper roll-off (Figure 6.11 **(b)**). The fact that Figure 6.11 **(b)** is so much more peaked than Figure 6.11 **(b)** implies that the source of the large correlation in the peaks of Figure 6.10 is double-track reconstruction errors.

A double-track reconstruction error is the name given to the situation in which a single track's SVT and DCH hits are reconstructed into two, instead of only one, charged track. Each of the two reconstructed tracks is made form fits on different parts of the hit patterns, e.g., one from the SVT hits, one from the DCH hits. The two tracks are always the same charge and are almost always in very nearly the same direction since they are made from the same charged track's hits. A double-track reconstruction error indicates that the correlated forward peaks of Figure 6.10 is the result of only of one actual charged track in the direction of the calculated converted photon. To remove these double-track reconstruction errors tracks, I will include into Equation 6.3 only one of the two candidate-tracks within each four charged-track event with a net charge of $\pm$ 2e. I will choose higher energy candidate-track since, in an event with double-track reconstruction error, the higher energy candidate-track would have an energy closer to the

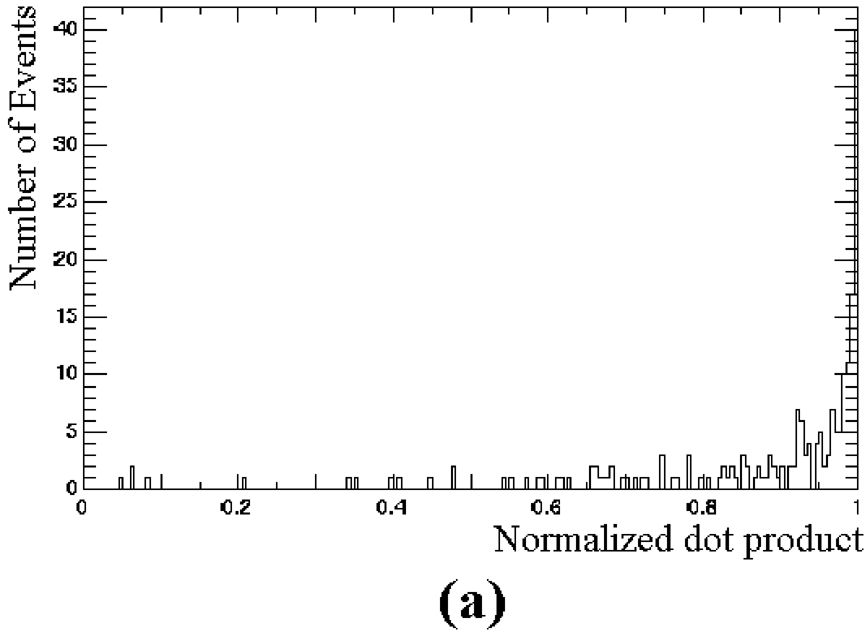

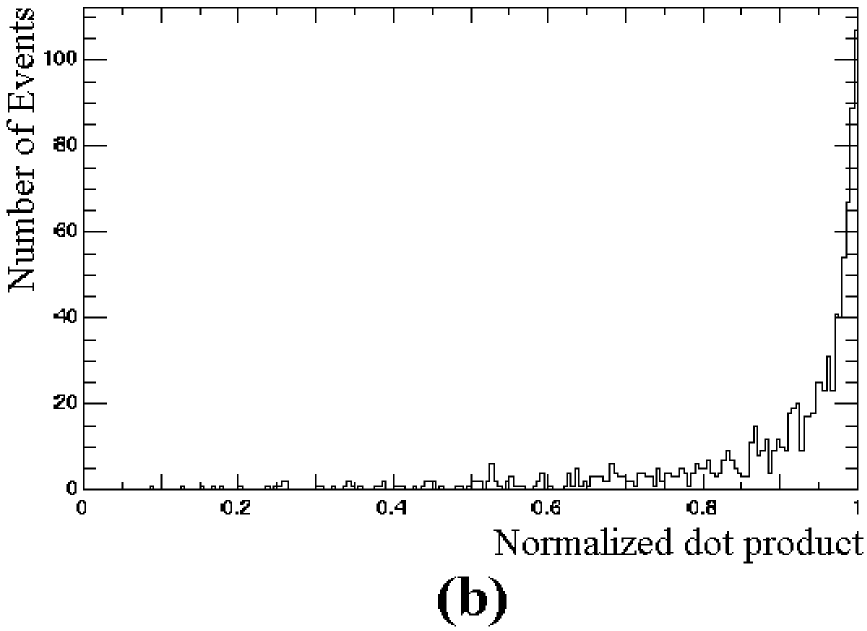

Figure 6.11: In every four charged-track event in which both tracks have a normalized dot product above zero, **(a)** shows the normalized dot product of the two candidate-tracks in all four charged-track events with no net charge while **(b)** shows this normalized dot product for all four charged-track event with a net charge of $\pm$ 2e. The difference in sharpness of the peaks implies that the peak in **(a)** is due to double-track reconstruction errors.

actual charged track's energy. Therefore, in Equation 6.3, the variables in the numerator used for four charged-track events with a net charge of ± 2e are:

- $N4sc_{ij}$ is the energy spectrum of higher energy candidate-track that has a normalized dot product of the candidate-track and the calculated direction of the converted photon above a value of 0, correlated to the energy spectrum of the calculated converted photon energy.

- $B4sc_{ij}$ is the energy spectrum of higher energy candidate-tracks that has a normalized dot product of the candidate-track and the calculated direction of the converted photon below a value of 0, correlated to the energy spectrum of the calculated converted photon energy.

The results for the background study are shown in Section 7.2.

6.3 Efficiency Study of the Photon Conversion Finder

In addition to the background study—which determins lepton contamination due to unidentified conversion daughter tracks within a data sample—I have also performed an efficiency study of the PCF's ability to correctly identify a converted photon candidate. This efficiency study will only measure the direct effectiveness of the PCF in determining if a converted photon candidate has been constructed either from two conversion daughter tracks or from two tracks that are not both from a converted photon. For the efficiency study of the PCF, I am only using four charged-track events with no net charge. Since all these events contain a converted photon candidate, I can use the converted photon candidate's energy to correlate the bins instead of the calculated converted photon's energy as in Equation 6.3. The PCF's ability to correctly identify a converted photon candidate is considered the percentage of converted photon candidates that pass the PCF quality cuts over the total number of converted photon candidates that are considered to be actual converted photons (Equation 6.8):

$$\text{PCF Efficiency}_j = \frac{\text{Identified candidates}_j}{\text{All candidates}_j \ - \ \text{backgrounds}_j} \tag{6.8}$$

Where

- j is the index for the bins, which for this efficiency study can be for either the energy, the θ angle, or the ϕ angle of the converted photon candidate.
- "PCF Efficiency$_j$" refers to the Efficiency of the PCF at identifying a converted photon candidiate in bin j
- "Identified candidates" refers to the number of converted photon candidates that pass the PCF quality cuts in bin j.
- "All candidates" refers to all converted photon candidates in my data sample in bin j that are considered to be converted photons.
- "Backgrounds" refers to the number of converted photon candidates in bin j that are considered background.

In Equation 6.8, I will use the same methods to subtract any background tracks from the failed converted photon candidate distributions as for the elements of Equation 6.3: I divide the normalized dot product of the failed converted photon candidate and the calculated converted photon (Figure 6.5 **(a)**) into two parts. The energy spectrum of unidentified converted photon candidates from events with a normalized dot product below zero are considered background (the element "Backgrounds" in Equation 6.8). These are subtracted from the events with a normalized dot product above zero (the element "All candidates" in Equation 6.8) to obtain the total number of converted photons.

The error of Equation 6.8 is determined by considering the fact that, neglecting a small amount of backgrounds, for every four charged-track event with no net charge an event's converted photon candidate can only be either identified or unidentified. Because there are only these two possibilities, I will use binomial errors for Equation 6.8. Since the efficiency of the PCF corresponds to the success rate, or p, of the binomial distribution, the error is be given by: $\sqrt{\frac{pq}{N}}$, or in terms of Equation 6.8, the error for every j bin is given by Equation 6.9:

$$\text{Error on Efficiency}_j = \sqrt{\frac{(\text{Efficiency}_j)(1 - \text{Efficiency}_j)}{\text{All candidates}_j \ - \ \text{backgrounds}_j}} \tag{6.9}$$

The results for the efficiency study of the PCF are shown in Section 7.1.

6.4 Results of the Bhabha Selector

To obtain the data sample for my efficiency studies, my Bhabha Selector was run over the appropriate prescale events from the "good runs" data sets of the 1999, 2000 and 2001 BaBar experimental runs. The number of events within my data sample corresponding to the various elements of Equation 6.3 and Equation 6.8 is shown in Table 6.2.

Terms in Equation 6.3	Number of Events
$N3$	8155
$N4fail$ (two per event)	1323
$N4sc$	540
$B3$	3507
$B4fail$ (two per event)	270
$B4sc$	268
Numerator	7026
$N4pass$	2912
Terms in Equation 6.8	**Number of Events**
Identified Candidates	2919
All Candidates	4242
backgrounds	272

Table 6.2: The number of events that have passed my Bhabha Selector for each term used in my efficiency calculations (Equation 6.3 and 6.8). Even though the number of "Identified Candidates" and $N\gamma c$ both give the number of identified converted photon candidates, the two numbers are slightly different due to the different variables used to bin the two. The same reason is behind the difference in the number of "Backgrounds" and $B4fail$.

Chapter 7

Results

7.1 Results for the Efficiency Study of the Photonic Conversion Finder

My efficiency study of the PCF, or more specifically the efficiency defined in Equation 6.8, has been evaluated with respect to the energy, θ angle, and ϕ angle of all converted photon candidates. The results are shown in Figure 7.1, 7.2, and 7.3 respectively, and are also listed in Tables 7.1, 7.2, and 7.3. For each of these efficiency studies, the bin width was kept as narrow as possible while keeping errors within acceptable limits. For the efficiency in energy and θ, this method resulted in a larger bin width for several bins due to a decrease in statistics.

Figure 7.1 shows that the PCF efficiency is relatively constant for all energy bins above 0.5 GeV, but has a lower efficiency below this energy. Because of lower efficiencies at low energy, the efficiency of the PCF in θ and ϕ has only been calculated for converted photon candidates within the PCF efficiency plateau above an energy of 0.5 GeV. Figures 7.2 and 7.3 indicate that above an energy of 0.5 GeV, the efficiency of the PCF is isotropic in both θ and ϕ.

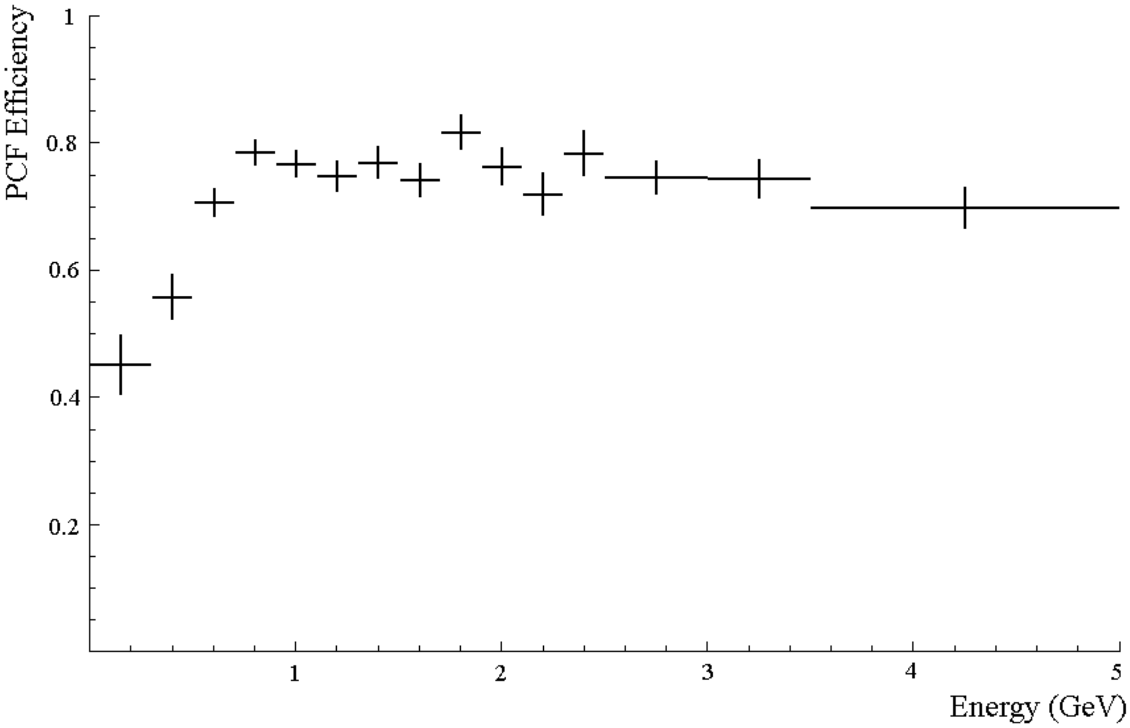

Figure 7.1: The results for the efficiency study on the PCF's ability to correctly identify a converted photon candidate as a function of the energy of the converted photon candidate. The efficiency is lower at lower energies, yet peaks and remains relatively steady above an energy of 0.5 GeV. The lower low-energy efficiencies of the PCF might be a result of the low-energy reconstruction efficiencies of the BaBar detector.

Energy Range (GeV)	Number of Events	Number Correctly Identified	Percent Efficiency
0 - 0.3	116	50	43 $\pm$ 5
0.3 - 0.5	292	166	56.8 $\pm$ 2.9
0.5 - 0.7	405	291	71.8 $\pm$ 2.2
0.7 - 0.9	427	335	78.5 $\pm$ 2.0
0.9 - 1.1	414	319	77.2 $\pm$ 2.1
1.1 - 1.3	321	241	75.1 $\pm$ 2.4
1.3 - 1.5	297	230	77.4 $\pm$ 2.4
1.5 - 1.7	272	206	75.7 $\pm$ 2.6
1.7 - 1.9	202	165	81.7 $\pm$ 2.7
1.9 - 2.1	218	167	76.6 $\pm$ 2.9
2.1 - 2.3	178	130	73.0 $\pm$ 3.3
2.3 - 2.5	138	109	79.0 $\pm$ 3.5
2.5 - 3.0	277	208	75.1 $\pm$ 2.6
3.0 - 3.5	208	157	75.5 $\pm$ 3.0
3.5 - 5.0	206	145	70.4 $\pm$ 3.2

Table 7.1: The results for the efficiency study on the PCF's ability to correctly identify a converted photon candidate as a function of the energy of the converted photon candidate.

Theta Range (Rad)	Number of Events	Number Correctly Identified	Percent Efficiency
0.410- 0.503	638	492	77.1 $\pm$ 1.7
0.503 - 0.597	763	559	73.3 $\pm$ 1.6
0.597 - 0.785	733	557	76.0 $\pm$ 1.6
0.785 - 0.974	281	206	73.3 $\pm$ 2.6
0.974 - 1.162	200	159	79.5 $\pm$ 2.9
1.162 - 1.540	291	210	72.2 $\pm$ 2.6
1.540 - 1.916	331	253	76.4 $\pm$ 2.3
1.916 - 2.457	331	268	81.0 $\pm$ 2.2

Table 7.2: The results for the efficiency study on the PCF's ability to correctly identify a converted photon candidate above and energy of 0.5 GeV as a function of the θ angle of the converted photon candidate. The larger bins at higher angles are due to a decrease in statistics.

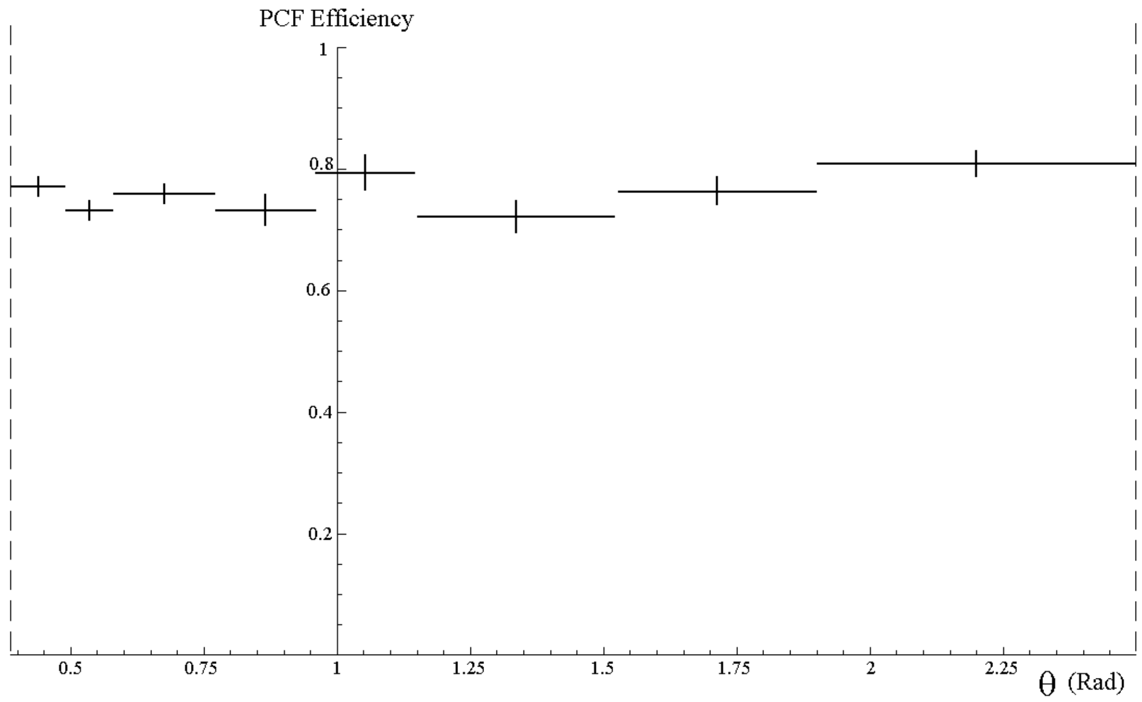

Figure 7.2: The results for the efficiency study on the PCF's ability to correctly identify a converted photon candidate above an energy of 0.5 GeV as a function of the θ angle of the converted photon candidate. The dotted lines at either end of the graph show the fiducial limits of the BaBar detector. The efficiencies appear within the limits obtained in the plateau of Figure 7.1.

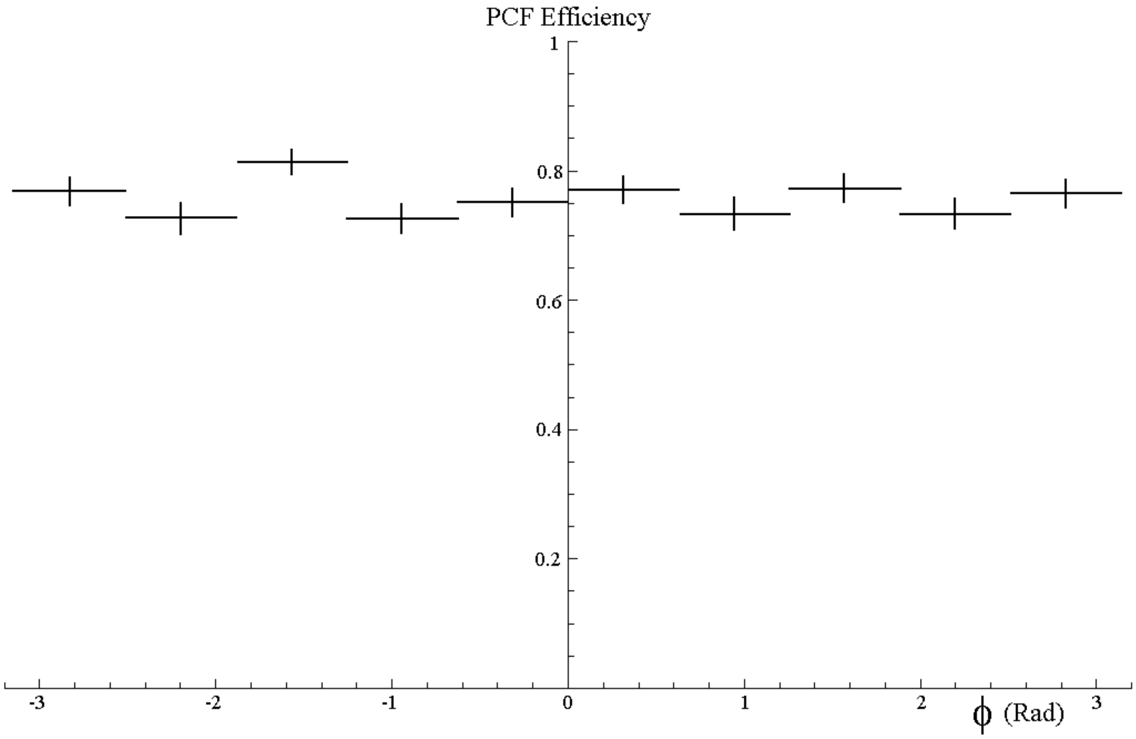

Figure 7.3: The results for the efficiency study on the PCF's ability to correctly identify a converted photon candidate above an energy of 0.5 GeV as a function of the ϕ angle of the converted photon candidate. The efficiencies appear within the limits obtained in the plateau of Figure 7.1.

Phi Range (Rad)	Number of Events	Number Correctly Identified	Percent Efficiency
-3.14 - -2.51	359	276	76.9 $\pm$ 2.2
-2.51 - -1.88	334	243	72.8 $\pm$ 2.4
-1.88 - -1.26	413	336	81.4 $\pm$ 1.9
-1.26 - -0.63	387	281	72.6 $\pm$ 2.3
-0.63 - 0	370	278	75.1 $\pm$ 2.2
0 - 0.63	367	283	77.1 $\pm$ 2.2
0.63 - 1.26	293	215	73.4 $\pm$ 2.6
1.26 - 1.88	348	269	77.3 $\pm$ 2.2
1.88 - 2.51	334	245	73.4 $\pm$ 2.4
2.51 - 3.14	362	277	76.6 $\pm$ 2.2

Table 7.3: The results for the efficiency study on the PCF's ability to correctly identify a converted photon candidate above an energy of 0.5 GeV as a function of the ϕ angle of the converted photon candidate.

7.2 Results for the Background Study

The results for my background study, measuring the background contamination due to unidentified conversion daughter tracks (Equation 6.3), are shown in Tables 7.4 to 7.7. There are 12 calculated converted photon energy bins, denoted by the j index of Equation 6.3, shown over four tables for ease of display, with widths determined by both statistical limitations and the limiting factors mentioned in Table 6.1. The bin width for both the higher and lower calculated converted photon energy bins of Tables 7.4 to 7.7 is larger due to a lack of statistics. There are 20 lepton energy bins, denoted by the i index in Equation 6.3, whose width was determined by statistics. All elements more than one entry below the i-j diagonal of Equation 6.3 have been omitted because they are all either zero or statistically insignificant.

The legend for Tables 7.4 to 7.7 is:

- $E_{\gamma c}$ refers to the j^{th} calculated converted photon energy bin of Equation 6.3.

- E_L refers the ith lepton energy bin of Equation 6.3.
- N_L is the value of the numerator in Equation 6.3. This is the total number of leptons in that bin that are considered to originate from a converted photon but are unidentified as such.
- $N_{\gamma c}$ is the value of the denominator ($N4pass_j$) in Equation 6.3. This is the number of identified converted photon candidates for each j energy bin.
- "ratio" refers to ratio$_{ij}$ in Equation 6.3. This is the ratio of number of leptons that are considered to originate from converted photons but are unidentified, to the number of identified converted photon candidates in energy bin i, j. For each bin, this ratio is equal to $N_L/N_{\gamma c}$.

7.3 Discussion of Results

The efficiency studies of the PCF using Equation 6.8 for energy (Figure 7.1) show that the PCF has an efficiency plateau for converted photon energies above 0.5 GeV. Within this efficiency plateau, the PCF is only able to properly identify a converted photon candidate between 70 to 80% of the time. Figures 7.2 and 7.3 show that this efficiency plateau is isotropic in both θ and ϕ.

When comparing the results for my efficiency studies on the PCF to the results obtained in previous Monte Carlo studies (Figure 4.7), we see that the two are similar. Within the Monte Carlo study, the PCF was able to correctly identify a converted photon candidate a very high percentage of the time only if both conversion daughter tracks were used. On the other hand, the lower efficiency plateau in the bottom half of Figure 4.7 was mostly due to the pairing of conversion daughter track with an unrelated track or the pairing of two unrelated tracks. While it is possible that this sort of mis-pairing

$E_{\gamma c}$ (GeV) $\rightarrow$ E_L (GeV) $\downarrow$	0.0 - 0.4	0.4 - 0.75	0.75 - 1.0
0.0 - 0.25 ($Nl \rightarrow$) (ratio $\rightarrow$)	1742 $\pm$ 89 12.3 $\pm$ 1.2	337 $\pm$ 32 0.79 $\pm$ 0.08	79 $\pm$ 14 0.23 $\pm$ 0.04
0.25 - 0.5	446 $\pm$ 36 3.1 $\pm$ 0.4	843 $\pm$ 31 1.97$\pm$ 0.12	157 $\pm$ 13 0.47 $\pm$ 0.05
0.5 - 0.75	51 $\pm$ 16 0.36 $\pm$ 0.12	403 $\pm$ 20 0.94$\pm$ 0.07	289 $\pm$ 17 0.87 $\pm$ 0.07
0.75 - 1.0	41 $\pm$ 10 0.29 $\pm$ 0.08	37 $\pm$ 7 0.087 $\pm$ 0.016	172 $\pm$ 13 0.51 $\pm$ 0.05
1.0 - 1.25			12 $\pm$ 4 0.036 $\pm$ 0.011
$N\gamma c \rightarrow$	142 $\pm$ 12	427 $\pm$ 21	334 $\pm$ 18

Table 7.4: The results for the first three j energy bins of Equation 6.3. This table covers converted photon energies below 1.0 GeV. All lepton energies more than one energy bin above the energy of the calculated converted photon (below the diagonal) have been omitted (except for in the first column) as they are either zero or statistically insignificant. Note that, due to a lack of statistics, the bin width of the columns is larger for lower calculated converted photon energies.

$E_{\gamma c}$ (GeV) $\rightarrow$ E_L (GeV) $\downarrow$	1.0 - 1.25	1.25 - 1.5	1.5 - 1.75
0.0 - 0.25 ($Nl \rightarrow$) (ratio $\rightarrow$)	41 $\pm$ 10 0.124 $\pm$ 0.032	50 $\pm$ 9 0.187 $\pm$ 0.035	25 $\pm$ 7 0.098 $\pm$ 0.026
0.25 - 0.5	87 $\pm$ 10 0.264 $\pm$ 0.032	52 $\pm$ 8 0.195 $\pm$ 0.031	38 $\pm$ 7 0.149 $\pm$ 0.028
0.5 - 0.75	86 $\pm$ 9 0.260 $\pm$ 0.032	56 $\pm$ 8 0.210 $\pm$ 0.031	36 $\pm$ 6 0.133 $\pm$ 0.024
0.75 - 1.0	169 $\pm$ 13 0.51 $\pm$ 0.05	57 $\pm$ 8 0.213 $\pm$ 0.031	35 $\pm$ 6 0.137 $\pm$ 0.025
1.0 - 1.25	95 $\pm$ 10 0.288 $\pm$ 0.034	114 $\pm$ 11 0.43 $\pm$ 0.05	45 $\pm$ 7 0.176 $\pm$ 0.029
1.25 - 1.5	9 $\pm$ 3.3 0.027 $\pm$ 0.010	72 $\pm$ 8 0.27 $\pm$ 0.04	57 $\pm$ 8 0.224 $\pm$ 0.033
1.5 - 1.75		9 $\pm$ 3.0 0.034 $\pm$ 0.011	41 $\pm$ 6 0.161 $\pm$ 0.027
1.75 - 2.0			4 $\pm$ 2.0 0.016 $\pm$ 0.008
$N\gamma c \rightarrow$	330 $\pm$ 18	267 $\pm$ 16	255 $\pm$ 16

Table 7.5: The results for the fourth to sixth j energy bins of Equation 6.3. This table covers converted photon energies between 1.0 and 1.75 GeV. All Lepton energies more than one energy bin above the energy of the calculated converted photon (below the diagonal) have been omitted as they are either zero or statistically insignificant.

$E_{\gamma c}$ (GeV) $\rightarrow$ E_L (GeV) $\downarrow$	1.75 - 2.0	2.0 - 2.25	2.25 - 2.5
0.0 - 0.25 ($Nl \rightarrow$) (ratio $\rightarrow$)	19 $\pm$ 6 0.091 $\pm$ 0.031	13 $\pm$ 5 0.070 $\pm$ 0.029	12 $\pm$ 4 0.075 $\pm$ 0.027
0.25 - 0.5	31 $\pm$ 6 0.145 $\pm$ 0.029	27 $\pm$ 5 0.145 $\pm$ 0.030	17 $\pm$ 4 0.106 $\pm$ 0.027
0.5 - 0.75	36 $\pm$ 6 0.173 $\pm$ 0.031	16 $\pm$ 4 0.086 $\pm$ 0.022	13 $\pm$ 4 0.081 $\pm$ 0.023
0.75 - 1.0	24 $\pm$ 5 0.115 $\pm$ 0.026	13 $\pm$ 4 0.070 $\pm$ 0.020	17 $\pm$ 4 0.106 $\pm$ 0.027
1.0 - 1.25	26 $\pm$ 5 0.125 $\pm$ 0.026	15 $\pm$ 4 0.081 $\pm$ 0.022	11 $\pm$ 3.3 0.069 $\pm$ 0.021
1.25 - 1.5	37 $\pm$ 6 0.178 $\pm$ 0.032	20 $\pm$ 4 0.108 $\pm$ 0.025	22 $\pm$ 5 0.138 $\pm$ 0.031
1.5 - 1.75	51 $\pm$ 7 0.25 $\pm$ 0.04	23 $\pm$ 5 0.124 $\pm$ 0.027	16 $\pm$ 4 0.100 $\pm$ 0.026
1.75 - 2.0	32 $\pm$ 6 0.154 $\pm$ 0.029	36 $\pm$ 6 0.19 $\pm$ 0.04	16 $\pm$ 4 0.100 $\pm$ 0.026
2.0 - 2.25	6 $\pm$ 2.4 0.029 $\pm$ 0.012	24 $\pm$ 5 0.129 $\pm$ 0.028	15 $\pm$ 4 0.094 $\pm$ 0.025
2.25 - 2.5		1 $\pm$ 1.0 0.005 $\pm$ 0.005	17 $\pm$ 4 0.106 $\pm$ 0.027
2.5 - 2.75			1 $\pm$ 1.0 0.006 $\pm$ 0.006
$N\gamma c \rightarrow$	208 $\pm$ 14	186 $\pm$ 14	160 $\pm$ 13

Table 7.6: The results for the seventh to ninth j energy bins of Equation 6.3. This table covers converted photon energies between 1.75 and 2.5 GeV. All Lepton energies more than one energy bin above the energy of the calculated converted photon (below the diagonal) have been omitted as they are either zero or statistically insignificant.

$E_{\gamma c}$ (GeV) $\rightarrow$ E_L (GeV) $\downarrow$	2.5 - 3.0	3.0 - 3.5	3.5 - 5.0
0.0 - 0.25 ($Nl \rightarrow$) (ratio $\rightarrow$)	15 $\pm$ 6 0.068 $\pm$ 0.026	8 $\pm$ 4 0.046 $\pm$ 0.024	1 $\pm$ 5 0.005 $\pm$ 0.023
0.25 - 0.5	23 $\pm$ 5 0.104 $\pm$ 0.024	7 $\pm$ 3.0 0.041 $\pm$ 0.018	13 $\pm$ 4 0.062 $\pm$ 0.020
0.5 - 0.75	20 $\pm$ 4 0.090 $\pm$ 0.021	15 $\pm$ 4 0.087 $\pm$ 0.025	11 $\pm$ 4 0.053 $\pm$ 0.018
0.75 - 1.0	13 $\pm$ 4 0.059 $\pm$ 0.017	13 $\pm$ 4 0.076 $\pm$ 0.022	9 $\pm$ 3.0 0.043 $\pm$ 0.015
1.0 - 1.25	25 $\pm$ 5 0.113 $\pm$ 0.024	4 $\pm$ 2.0 0.023$\pm$ 0.012	10 $\pm$ 3.2 0.048 $\pm$ 0.015
1.25 - 1.5	33 $\pm$ 6 0.149 $\pm$ 0.027	14 $\pm$ 4 0.081 $\pm$ 0.023	11 $\pm$ 3.3 0.053 $\pm$ 0.016
1.5 - 1.75	21 $\pm$ 5 0.095 $\pm$ 0.022	20 $\pm$ 4 0.116 $\pm$ 0.027	11 $\pm$ 3.3 0.053 $\pm$ 0.016
1.75 - 2.0	21 $\pm$ 5 0.095 $\pm$ 0.022	9 $\pm$ 3.0 0.052 $\pm$ 0.018	13 $\pm$ 4 0.062 $\pm$ 0.018
2.0 - 2.25	19 $\pm$ 4 0.086 $\pm$ 0.021	7 $\pm$ 2.6 0.041 $\pm$ 0.016	20 $\pm$ 4 0.096 $\pm$ 0.022
2.25 - 2.5	34 $\pm$ 6 0.153 $\pm$ 0.028	16 $\pm$ 4 0.093 $\pm$ 0.024	16 $\pm$ 4 0.077 $\pm$ 0.020
2.5 - 2.75	22 $\pm$ 5 0.099 $\pm$ 0.022	13 $\pm$ 4 0.076 $\pm$ 0.022	14 $\pm$ 4 0.067 $\pm$ 0.019
2.75 - 3.0	6 $\pm$ 2.4 0.027 $\pm$ 0.011	14 $\pm$ 4 0.081 $\pm$ 0.023	13 $\pm$ 4 0.062 $\pm$ 0.018
3.0 - 3.25	4 $\pm$ 2.0 0.018 $\pm$ 0.009	13 $\pm$ 4 0.076$\pm$ 0.022	13 $\pm$ 4 0.062 $\pm$ 0.018
3.25 - 3.5		7 $\pm$ 2.6 0.041 $\pm$ 0.016	10 $\pm$ 3.2 0.048 $\pm$ 0.016

Continued on next page

Continued from previous page			
3.5 - 3.75		0 ± 2.3 0 ± 2.3	8 ± 2.8 0.038 ± 0.014
3.75 - 4.0			4 ± 2 0.019 ± 0.010
4.0 - 4.25			0 ± 2.3 0 ± 2.3
4.25 - 4.5			0 ± 2.3 0 ± 0
4.5 - 4.75			0 ± 2.3 0 ± 2.3
4.75 - 5.0			0 ± 2.3 0 ± 2.3
$N\gamma c \rightarrow$	222 ± 15	172 ± 13	209 ± 14

Table 7.7: The results for the last three j energy bins of Equation 6.3. This table covers converted photon energies between 2.5 and 5 GeV. All Lepton energies more than one energy bin above the energy of the calculated converted photon (below the diagonal) have been omitted as they are either zero or statistically insignificant. Note that due to a lack of statistics the bin width of the columns increases for higher calculated converted photon energies.

could also explain the efficiency plateau in my results, it is not as likely since my data sample was a lot cleaner than that used in the Monte Carlo study. All events within my data sample had to pass both my Bhabha Selector and the directional requirements with respect to the calculated converted photon.

Other than mis-pairing, another possible explanation for the efficiency plateau might be reconstruction inefficiencies of the BaBar detector. The lower energy candidate-track belonging to a converted photon's electron/positron pair might often be so poorly reconstructed that the constructed converted photon candidate would fail the PCF quality cuts. However, in considering this explanation, one would expect the efficiency to rise for higher energies since the energy of the lower energy candidate-track of the electron/positron pair would also rise and escape this limitation.

Regardless of the underlying explanation, the efficiency plateau of Figure 7.1 implies that the PCF has an internal efficiency limit of between 70 and 80%. This finding implies that there will always be a considerable background of leptons from unidentified converted photon candidates.

Averaging the $ratio_{ij}$ in Equation 6.3 over all energies, there are approximately 2.4 background leptons originating from converted photons for every 2 leptons that are properly identified as originating from a converted photon. The entries in each calculated converted photon energy bin follow a general pattern of being smaller at low lepton energies, rising as the lepton energy rises, peaking slightly before the energy of the calculated converted photon, and then dropping off just afterwards. Also, there is sometimes a small lower energy peak appearing in the first few lepton energy bins. The values of these calculated converted photon energy bins is a result of the combination of three very different lepton energy spectrums from the first three elements of Equation 6.3. Insight can be gained into the relative values of Tables 7.4 to 7.7 by comparing a lepton's energy to its calculated converted photon energy in each event. This comparison was already shown for three charged-track events in Figure 6.4. Figure 6.4 shows that for three charged-track events, the results of Equation 6.3 should steadily rise for higher energies. Since three charged-track events dominate the entries for Equation 6.3 (66% of the total events after background subtraction), the source of Equation 6.3's steady rise versus calculated converted photon energy can be attributed to those events. Conversely, this same ratio in four charged-track events with no net charge looks like a flat plateau between 0.2 to 0.8 of the calculated converted photon energy, is slightly peaked at 0.2, and falls sharply on either side of the plateau (Figure 7.4 **(a)**). The main reason for the plateau of Figure 7.4 **(a)** is the internal efficiency limit of the PCF. The explanation for the shape of this ratio in four charged-track with a net charge of ± 2e, as shown in Figure 7.4 **(b)**, is the low energy reconstruction efficiencies of the BaBar detector as in three charged-track events. When adding the lepton spectrum from four charged-track events with no net charge to the lepton spectrum of three charged-track events, we get the two peaks found at both high and low energy for most calculated converted photon energy bins.

7.4 Monte Carlo Cross-Check

In order to increase confidence in the results of my efficiency studies, I conducted a small Monte Carlo study. Within this Monte Carlo study, the results of both the Bhabha Selector and the PCF algorithm on the Monte Carlo simulated data were cross checked with the expected results given the Monte Carlo truth tables. The Monte Carlo study was conducted on six hundred thousand $e^+e^- \longrightarrow e^+e^-\gamma$ events in which the γ's θ distribution was restricted to between 30° and 150° in the Center of Mass frame.

The Bhabha Selector was used on all Monte Carlo events within this sample and those that passed it were then classified with respect to the amount of candidate-tracks reconstructed in the event. If there were two candidate-tracks in the event, the PCF

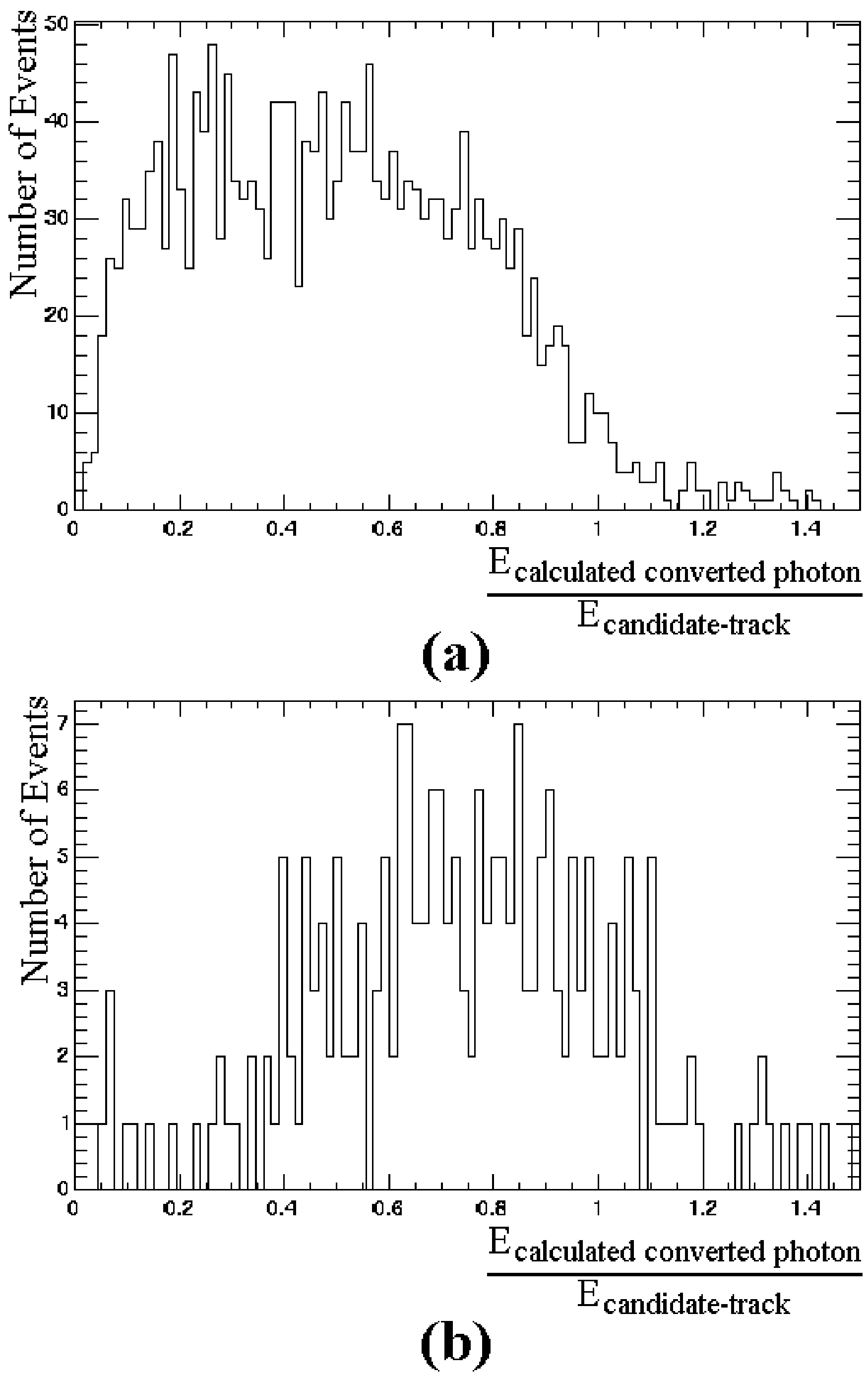

Figure 7.4: **(a)** is the ratio of calculated converted photon energy and the candidate-track energy for four charged-track events with no net charge which have a value of the normalized dot product of the converted photon candidate and the calculated converted photon above 0.8. **(b)** this same ratio but for four charged-track events with a net charge of $\pm$ 2e.

algorithm was then used to construct a converted photon candidate. For every event, the validity of the results for both the PCF quality cuts and the angular correlation between the calculated converted photon and either the candidate-track or the converted photon candidate was cross-checked using the Monte Carlo truth. These preliminary studies supported the analysis used in my efficiency studies. Within this Monte Carlo study, the majority of events with unreconstructed or unidentified Photonic Conversions contained a very low momentum (below 100 MeV/c) conversion daughter track.

Chapter 8

Summary and Conclusion

An accurate understanding of semi-leptonic B decays ($B^0 \rightarrow \ell^+\nu X$) is essential to the study of CP violation in the B system. One difficulty in the measurement of the semi-leptonic B decay spectra arises from lepton contamination due to lepton candidates that did not originate from the decay of the B meson. One source of this lepton contamination is Photonic Conversions. A Photonic Conversion is where, in the presence of an electromagnetic field, a photon changes into an electron/positron pair ($\gamma \rightarrow e^+e^-$). A Photonic Conversion Finder (PCF) has been written for the BaBar experiment with the purpose of identifying the electron/positron tracks resultant from Photonic Conversions. The PCF has only been tested previously on Monte Carlo simulated data. The purpose of this thesis is to perform a comprehensive efficiency study of the PCF using real BaBar data in order to better understand the lepton contamination due to unidentified converted photon daughter tracks in semi-leptonic B decays.

In order to understand the lepton contamination due to converted photons in B semi-leptonic decays, the efficiency studies of this thesis involve:

- Testing the PCF's ability to correctly identify a converted photon candidate.
- Measuring the energy spectrum of lepton tracks that originate from Photonic Conversions but are not identified by the PCF.

The energy spectrum of leptons unidentified as originating from Photonic Conversions will be correlated to the spectrum obtained for identified converted photon candidates so that in future analyses, the unidentified lepton spectrum can be obtained by a matching of the identified converted photon candidate spectrum.

The PCF is used to construct and test a converted photon candidate through the vertexing of two oppositely charged tracks. This vertexing involves finding the point of closest approach between two electron/positron tracks and calculating a converted photon candidate's four-vector at this point. Four characteristics of the converted photon candidate are evaluated by comparing them to predetermined cuts that test the probability of a converted photon candidate being an actual converted photon. If a candidate passes these cuts, the candidate's two daughter tracks are considered identified as originating from a Photonic Conversion whereas if it fails the cuts, the candidate is considered to be constructed from two unrelated tracks.

In order to conduct the efficiency studies of this thesis, it was determined that a data sample of Radiative Bhabha events should be used. In order to obtain an unbiased sample of Radiative Bhabha events, it is necessary to use "Prescale" event collections that have not gone through the complete BaBar trigger system. A "Bhabha Selector" algorithm has also been written to ensure the quality of my data sample by employing a set of increasingly restrictive cuts on an event's properties. The data sample obtained should consist of only Radiative Bhabha events that offer the possibility for Photonic Conversions and the subsequent measurement of their associated daughter tracks.

The data sample of Radiative Bhabha events is divided into three streams based on the number of charged tracks—called candidate-tracks—that might be from a converted photon.

- Events in which there is only one candidate-track—might contain a partially reconstructed converted photon.

- Events with two oppositely charge candidate-tracks—might contain a fully reconstructed converted photon.
- Events with two same charge candidate-tracks—might contain one Photonic Conversion daughter track and one background track.

In order to separate any background candidate-tracks from those originating from Photonic Conversions (also called conversion daughter tracks), the normalized dot product was taken between the direction of the candidate-tracks and the expected direction of a converted photon within each event. The expected direction of a converted photon is calculated by taking the Center of Mass four-vector and subtracting all tracks that are not part of the Photonic Conversion. In events with two oppositely charged candidate-tracks, the normalized dot product was taken between the expected direction of a converted photon and the direction of a converted photon candidate that was constructed from the two candidate-tracks. The normalized dot product distributions all peak at one and also contain a constant, isotropic signal that is attributed to beam-induced backgrounds. To separate the beam-induced backgrounds from the conversion daughter tracks, each normalized dot product was divided into two parts with the spectrum of tracks having a normalized dot product below zero being used for a one to one background subtraction on the spectrum of tracks with a normalized dot product above zero.

Further consideration was necessary in events containing two candidate tracks of the same-charge. A high angular correlation between the two candidate-tracks when the normalized dot product was near one indicated that several events contained two falsely reconstructed charged tracks that were from the detector hits of only one actual charged track. To eliminate this background, only the higher energy candidate-track was used in events with two candidate-tracks of the same charge.

The results of the efficiency study on the PCF's ability to properly identify converted photon candidates indicates that the PCF has a constant and isotropic efficiency of between 70-80% above an converted photon energy of 0.5 GeV, with slightly lower efficiencies at lower energies. This result indicates an internal efficiency limit of the PCF.

The overall results of the efficiency studies measuring the energy spectrum of leptons that are unidentified as originating from converted photons indicates that there are 2.4 such leptons for every 2 leptons properly identified as originating from a converted photon. The full energy spectrum of leptons that are unidentified as originating from converted photons as a function of the energy of identified converted photon candidates can be seen in Tables 7.4 to 7.7 of Section 7.2. 66% of these leptons are from events with only one candidate-track and 30% are from events with two candidate-tracks of opposite charge. The most likely result for the source of the events with only one candidate-track is the low energy reconstruction efficiencies of the BaBar detector that is expressed in events where the electron/positron pair of the conversion are highly asymmetric in energy. The source of the events with two candidate-tracks of opposite charge is the internal efficiency limit of the PCF.

Chapter 9

Glossary

Beam-induced backgrounds Backgrounds caused by the high-energy electron/positron beams at the BaBar experiment. Beams interacting with detector material and emitting low energy electrons and positrons are the predominant source of beam-induced backgrounds. A distinguishing characteristic of beam-induced backgrounds is that their θ and ϕ distributions are highly peaked in the horizontal plane ($\theta = 0, \pi$, and $\phi = 0$ and $\pm\pi$)

Bhabha Selector A computer algorithm that I have written to select Bhabha and Radiative Bhabha events from the BaBar experimental data sets, which contain every type of event produced in the BaBar experiment.

Bhabha-track(s) One or both of the (usually) high-energy electron/positron tracks that are part of the primary electron/positron pair always present in a Bhabha event. The Bhabha-tracks are part of the original reaction at the interaction point.

Bremsstrahlung A type of electromagnetic radiation caused by the change in velocity of an electromagnetic particle, such as when an electron collides with material.

Bremsstrahlung event(s) A type of Radiative Bhabha event that contains a track that has undergone Bremsstrahlung radiation.

Calculated converted photon If I assume that all radiated but unconverted photons in an event with significant energy have been measured by the EMC, Equation 5.3

gives the four-vector for any photon that has converted in a Radiative Bhabha event, and is therefore referred to as the calculated converted photon. The calculated converted photon has the direction and magnitude that a converted photon would have if it were to account for all the momentum in an event that is not contained in either the primary e^+e^- pair or measured photons.

Candidate-tracks The label given to all tracks within a Bhabha or Radiative Bhabha event that are not part of the primary electron/positron pair (Bhabha-tracks) of the event. Within a four charged-track event, there would be two candidate-tracks, while within a two charged-track event, there would be none. One of the purposes of this thesis is to test whether candidate-tracks are conversion daughter tracks or background tracks.

Center of Mass frame The inertial frame of a physical reaction where the net momentum of all products involved is zero (before and after). In relation to the BaBar detector, the Center of Mass frame is the inertial frame in which the electron and positron beams have zero net momentum and so are at the same energy and in opposite directions. All Bhabha events in the Center of Mass frame originally have two back to back Bhabha-tracks with equal energy.

Conversion daughter track(s) One or both of the electron/positron pair that is created in a Photonic conversion.

Converted photon A photon which, in the presence of an electromagnetic field, converted into an electron/positron pair ($\gamma \rightarrow e^+e^-$). It should be noted that since a photon can only convert in the presence of an electromagnetic field and because the electromagnetic field inside matter is so much larger than the field outside, photons typically convert inside matter.

Converted photon candidate A converted photon track which has been reconstructed by the Photon Conversion Finder algorithm from vertexing two oppositely charged e^+e^- tracks. The likelihood of the converted photon candidate being an actual converted photon is determined by testing the candidate's properties with respect to the ideal values of converted photons. This testing is done by using the quality cuts of the PCF: if the candidate passes, the e^+e^- tracks used to make the converted photon candidate are considered identified as originating from a converted photon (they are considered as conversion daughter tracks) whereas if the candidate fails, these e^+e^- tracks are considered unrelated.

DCH The Drift Chamber: Detector component of the BaBar experiment that measures charged particle momenta through the drift of ionized gas. The Drift Chamber is the main tracking component of the BaBar detector and can provide particle identification through a particle's energy loss over its track path ($\frac{dE}{dx}$).

DIRC The Detector of Internally Reflected Cerenkov light: Detector component of the BaBar experiment that measures particle velocities by their emitted angle of Cernekov light in a quartz barrel. Since the particle mass can be obtained by dividing the particle's momentum by its velocity, the DIRC is the main source of charged particle identification for the BaBar experiment.

EMC The Electromagnetic Calorimeter: Detector component of the BaBar experiment that measures the energy of charged and neutral particles through calorimetry. The Electromagnetic Calorimeter is the only detector component able to detect photons.

Fiducial region The region of measurement in a given detector for which we are confident that tracks are both well measured and well contained, implying there are no support structures in front of the detector, nor are there any detector edges in the region. In regards to the BaBar detector, the Fiducial region covers the areas of the Electromagnetic Calorimeter with a low amount of material between it and the Interaction Point. In the Lab frame of the BaBar detector, the fiducial region is $-0.78 \leq \cos\theta \leq 0.92$.

Four charged-track event An event within the data sample containing exactly four charged tracks with no restrictions on the number of neutral tracks. Two of the charged-tracks are considered Bhabha-tracks while the other two (most often the two lowest energy tracks) are candidate-tracks.

Good runs The name given to experimental runs of the BaBar experiment that pass a set of quality restrictions placed on the data. Only good runs have been used in creating this project's data sample.

IFR The Instrumented Flux Return: Detector Component of the BaBar experiment used to create the axial magnetic field throughout the BaBar detector. The IFR is instrumented to measure cosmic rays, muons and K_L for the BaBar experiment.

IP The Interaction Point: The point of the BaBar detector where the electron and positron beams cross each other. The interaction point varies by a few millimeters from the origin of the BaBar coordinate system, which is taken as the expected point that the e^+e^- beams would collide if the BaBar magnetic field was turned off.

Lab frame The inertial frame of the BaBar detector. For the BaBar experiment, the Lab frame is boosted by a $\beta\gamma$ of 0.56 with respect to the Center of Mass frame, as the incident positron and electron beams do not have the same energy.

non-Radiative Bhabha-track The track from the primary electron/positron pair in a simple Radiative Bhabha event that has not undergone a significant radiation. The non-Radiative Bhabha-track can be easily identified since it has the higher Center of Mass energy of the two primary e^+e^- tracks in the Radiative Bhabha event.

Normalized Dot Product The normalized dot product is the cosine of the angle between two tracks.

Partially reconstructed converted photon The name given to the situation where only one of the conversion daughter tracks has been reconstructed by the BaBar detector. Since only one conversion daughter track has been reconstructed, the Photonic Conversion Finder can not be used to create a converted photon candidate. Within this project's efficiency studies, kinematic restrictions are used to confirm the identify of a partially reconstructed converted photon.

PCF The Photon Conversion Finder: A computer algorithm used in the BaBar experiment to reconstruct a converted photon candidate from two daughter electron/positron tracks. The general purpose of the Photon Conversion Finder is to properly identify two conversion daughter tracks as being from a Photonic conversion. The identification of converted photon candidates is based on using the quality cuts of the PCF to compare their properties to those expected for Photonic Conversions.

Photonic Conversion A reaction in which, in the presence of an electromagnetic field, a photon converts into an electron/positron pair. It should be noted that since a photon can only convert in the presence of an electromagnetic field and because the electromagnetic field inside matter is so much larger than the field outside, photons typically convert inside matter.

Point of conversion The point where a photon converts into an electron/positron pair.

PMT Photomultiplier tube: measurement device used to detect electromagnetic radiation. Photomultiplier tubes are used to measure the angle of Cerenkov radiation within the Detector of Internally Reflected Cerenkov light of the BaBar detector.

Quality cuts (of the PCF) The name given to a set of cuts that, when applied to a converted photon candidate, are used to determine the probability that the candidate was really a converted photon. Both a "loose" and a "tight" set of quality cuts have been determined but only the "loose" cuts are used within my efficiency studies.

Radiative Bhabha-track The track from the primary electron/positron pair in a simple Radiative Bhabha event that has undergone a significant radiation. The Radiative Bhabha-track can be easily identified since it has the lower Center of Mass energy of the two primary e^+e^- tracks in the Radiative Bhabha event.

Reconstructed converted photon The name given to a converted photon candidate that is reconstructed from two conversion daughter tracks. Since the PCF algorithm is only used to test the identity of a converted photon candidate, whether a converted photon candidate is a reconstructed converted photon must be determined by methods such as the Monte Carlo truth or kinematic restrictions on the direction of a converted photon.

SSD Silicon strip detectors: Detectors used to measure charged particle information by detecting an electron/hole pair that is produced whenever the charged particle passes through a silicon strip. Silicon strip detectors are used with the Silicon Vertex Tracker of the BaBar detector.

SVT The Silicon Vertex Tracker: Detector component of the BaBar experiment used for precision measurements of particle trajectories near the Interaction Point. The Silicon Vertex Tracker is the first instrument radially outwards from the beam pipe of the BaBar experiment and is the only source of very low-energy particle tracking information. Combined with the Drift Chamber, the Silicon Vertex Tracker makes up the tracking system of the BaBar experiment.

Three charged-track event An event within the data sample containing exactly three charged-tracks with no restrictions on the number of neutral tracks. Two of the charged-tracks are considered Bhabha-tracks while the third (most often the lowest energy) is a candidate-track.

Two charged-track event An event within the data sample containing exactly two charged tracks with no restrictions on the number of neutral tracks. The two charged-tracks are considered to both be Bhabha-tracks.

Vertexing The act of swimming two or more track's trajectories, each based on its five fit track parameters, back to a point where they fit a common vertex. With respect to the Photon Conversion Finder algorithm, vertexing swims an electron and positron track back to the "point of conversion", the slopes of the tracks are tangent to each other.

Bibliography

[1] B. Aubert et al. A study of time dependent cp-violating asymmetries and flavor oscillations in neutral b decays at the upsilon(4s). 2002.

[2] K. Abe et al. Observation of large cp violation in the neutral b meson system. *Phys. Rev. Lett.*, 87:091802, 2001.

[3] Q. R. Ahmad et al. Measurement of the charged of current interactions produced by b-8 solar neutrinos at the sudbury neutrino observatory. *Phys. Rev. Lett.*, 87:071301, 2001.

[4] M. Kobayashi and T. Maskawa. CP violation in the renormalizable theory of weak interaction. *Prog. Theor. Phys.*, 49:652–657, 1973.

[5] D. E. Groom et al. Review of particle physics. *Eur. Phys. J.*, C15:1–878, 2000.

[6] L. Wolfenstien. Parametrization of the Kobayashi-Maskawa matrix. *Phys. Rev. Let.*, 51:1945, 1983.

[7] D. Griffiths. *Introduction to Elementary Particles.* Wiley, 1987.

[8] C. S. Wu, E. Ambler, R. W. Hayward, D. D. Hoppes, and R. P. Hudson. Experimental test of parity conservation in beta decay. *Phys. Rev.*, 105:1413–1414, 1957.

[9] Murray Gell-Mann and A. Pais. Behavior of neutral particles under charge conjugation. *Phys. Rev.*, 97:1387–1389, 1955.

[10] J. H. Christenson, J. W. Cronin, V. L. Fitch, and R. Turlay. Evidence for the 2 pi decay of the k(2)0 meson. *Phys. Rev. Lett.*, 13:138–140, 1964.

[11] ed. Harrison, P. F. and ed. Quinn, Helen R. The babar physics book: Physics at an asymmetric B factory. Papers from Workshop on Physics at an Asymmetric B Factory (BaBar Collaboration Meeting), Rome, Italy, 11-14 Nov 1996, Princeton, NJ, 17-20 Mar 1997, Orsay, France, 16-19 Jun 1997 and Pasadena, CA, 22-24 Sep 1997.

[12] A. D. Sakharov. Violation of CP invariance, C asymmetry, and baryon asymmetry of the universe. *Pisma Zh. Eksp. Teor. Fiz.*, 5:32–35, 1967.

[13] Yosef Nir and Helen R. Quinn. Learning about the CKM matrix from CP asymmetries in b0 decays. *Phys. Rev.*, D42:1473–1476, 1990.

[14] Useful Drawings form PEP II. March, 2001. BaBar. Jan, 2002. <http://www.slac.stanford.edu/BFROOT/www/doc/public/babar_plots/PEPII/drawings/pep_ii_drawings.htm>.

[15] B. Aubert et al. The babar detector. 2001.

[16] Mark Schwarb. Characterization of Silicon Strip Detectors using ru106. Master's thesis, U.C.S.C., 1994. Home Page. Jan. 2002. <http://www.nde.lanl.gov/staff/schwab/thesis/sdetect.htm>.

[17] Patrick Robbe. Photonic Conversion Finder. 1998. BaBar internal web page. Jan. 2002 <http://www.slac.stanford.edu/∼robbepa>.

[18] Wouter Verkerke. Charm production in deep inelastic scattering: The Conversion finder. 1999. ZEUS. Jan. 2002 <http://www.nikhef.nl/pub/experiments/zeus/theses/wouter_verkerke/latex2html/ node55.html>.

[19] Dan Azzapardi. Conversion background study. 1999. BaBar internal webpage. Jan. 2002 <http://www.slac.stanford.edu/∼desva>.

[20] Cut-based Electron Selectors. Mar. 2001. BaBar internal web page. Feb. 2002. <http://www.slac.stanford.edu/BFROOT/www/Physics/Tools/Pid/Electrons/cutbasedSelector.html>.

[21] Candidate lists and maps in the Micro database: Run time lists. BaBar internal web page. Jan. 2002 <http://www.slac.stanford.edu/BFROOT/www/doc/workbook/nanomicro/v8.8/Micro/CandLists.html>.

[22] Wouter Verkerke. Charm production in deep inelastic scattering: Conversion finding efficiency. 1999. Zeus. Jan. 2002 <http://www.nikhef.nl/pub/experiments/zeus/theses/wouter_verkerke/latex2html/node58.html>.

[23] Yung-Su Tsai. Pair production and bremsstrahlung of charged leptons. (erratum). *Rev. Mod. Phys.*, 49:421–423, 1977.

[24] Trigger Information in the Nano(Tag) Database. BaBar internal web page. Jan 2002 <http://www.slac.stanford.edu/BFROOT/www/doc/workbook/nanomicro/v8.8/Nano/TriggerFlags.html#L3info>.

[25] Georges Vasseur. BaBar data sets. Dec. 2001. BaBar internal web page. Jan. 2002 <http://www.slac.stanford.edu/BFROOT/www/Physics/BaBarData/GoodRuns/dataSets.html>.

[26] Backgrounds and remediation at BaBar . Dec. 2001. BaBar internal web page. Jan. 2002. <http://www.slac.stanford.edu/BFROOT/www/Detector/Backgrounds/back.html>.